



NTNU – Trondheim
Norwegian University of
Science and Technology

Dynamic load on High Head Francis turbines during start/stop

Sigurd Tangerud Haga

Master of Energy and Environmental Engineering

Submission date: June 2014

Supervisor: Torbjørn Kristian Nielsen, EPT

Norwegian University of Science and Technology
Department of Energy and Process Engineering

EPT-M-2014-45

MASTER THESIS

for

Student Sigurd Tangerud Haga

Spring 2014

Dynamic load on High Head Francis turbines during start/stop

*Dynamisk belastning på høytrykks Francis turbin ved start/stopp***Background and objective**

When starting and stopping Francis turbines, the dynamic load on the turbine runner will be higher, and of another nature than for steady state operation. In his project work, measurements of the transient pressure during start/stop have been done in the test rig at Waterpower Laboratory. However, it is room for improvements regarding how to perform such measurement in the laboratory, both regarding methods and instrumentation.

The dynamic load will imply increased structural strain for the turbine runner; hence it is of interest to identify the structural effect of the transient pressure on the runner with respect to fatigue. A model runner is, relative to a prototype, much stiffer. Therefore, strain gauge measurement on the runner blades will probably have no purpose. However, by using rapid prototype methods, replacement of the runner blades of the Tokke is a possibility. The blades can then be produced in a material that increases the compliance of the runner, giving more significant displacement to be measured by strain gauges.

The objective is to address fatigue issue on the runner caused by repeating start/stop and how this effects the life time of the runner.

The following tasks are to be considered:

- 1 Suggest method for identify pressure oscillation on the runner as a cause for fatigue
- 2 Suggest improved instrumentation for measuring transient load on the runner during start/stop
- 3 Perform measurements on a runner in the test rig
- 4 Analyse the structural behaviour of the runner with respect to fatigue
- 5 If possible, use rapid prototyping to replace the runner blades and do simultaneous pressure and strain gauge measurement.

Within 14 days of receiving the written text on the master thesis, the candidate shall submit a research plan for his project to the department.

When the thesis is evaluated, emphasis is put on processing of the results, and that they are presented in tabular and/or graphic form in a clear manner, and that they are analyzed carefully.

The thesis should be formulated as a research report with summary both in English and Norwegian, conclusion, literature references, table of contents etc. During the preparation of the text, the candidate should make an effort to produce a well-structured and easily readable report. In order to ease the evaluation of the thesis, it is important that the cross-references are correct. In the making of the report, strong emphasis should be placed on both a thorough discussion of the results and an orderly presentation.

The candidate is requested to initiate and keep close contact with his/her academic supervisor(s) throughout the working period. The candidate must follow the rules and regulations of NTNU as well as passive directions given by the Department of Energy and Process Engineering.

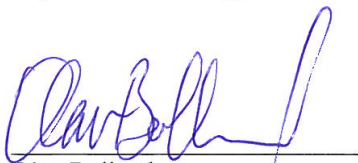
Risk assessment of the candidate's work shall be carried out according to the department's procedures. The risk assessment must be documented and included as part of the final report. Events related to the candidate's work adversely affecting the health, safety or security, must be documented and included as part of the final report. If the documentation on risk assessment represents a large number of pages, the full version is to be submitted electronically to the supervisor and an excerpt is included in the report.

Pursuant to “Regulations concerning the supplementary provisions to the technology study program/Master of Science” at NTNU §20, the Department reserves the permission to utilize all the results and data for teaching and research purposes as well as in future publications.

The final report is to be submitted digitally in DAIM. An executive summary of the thesis including title, student's name, supervisor's name, year, department name, and NTNU's logo and name, shall be submitted to the department as a separate pdf file. Based on an agreement with the supervisor, the final report and other material and documents may be given to the supervisor in digital format.

- Work to be done in lab (Water power lab, Fluids engineering lab, Thermal engineering lab)
 Field work

Department of Energy and Process Engineering, 14. January 2014


Olav Bolland
Department Head


Torbjørn K. Nielsen
Academic Supervisor

Research Advisor: Ole Gunnar Dahlhaug

Acknowledgements

This master thesis was written during the 2014 spring semester for the Waterpower Laboratory in the department of Energy and Process engineering, at the Norwegian University of Science and Technology. The objective of the master thesis was to address fatigue issues on the runner regarding start and stop procedures. This consisted of work and measurements performed in the Waterpower laboratory. I experienced that when working in the laboratory, it is often more time consuming due to unexpected scenarios and measurements being postponed. In this thesis pressure measurements were performed on the Francis runner to identify pressure oscillations during the start and stop procedures. I have learned a lot from running the Francis rig and I hope this thesis can help the issues related to start and stop procedures as well as improving the instrumentation used to measure these issues.

I would like to thank my supervisor Professor Torbjørn K. Nilsen and research advisor Professor II Ole Gunnar Dahlhaug for all guidance and interesting conversations regarding my thesis. I would also like to thank Bård Aslak Brandåstrø for answering any question regarding the Francis rig. A big thank you to the doctoral students Peter Joachim Gogstad and Bjørn Winther Solemslie who has always been accommodating if questioned. I would also like to thank Joar Grilstad and the other people working in the laboratory for any help regarding measurement equipment to faults in the rig.

I would like to thank the other master students at the Waterpower Laboratory for a good and social study environment.



Sigurd Tangerud Haga

Trondheim, 10. June 2014

Abstract

Pressure measurements were performed on the Francis runner in the Waterpower laboratory at NTNU. These measurements were divided into start and stop procedures, with the generator on or off. The suggested method that was used to identify the pressure oscillations during the start and stop procedures consisted of finding curves that fit the performed pressure measurements. The MATLAB application Curve Fitting Tool was used to find the curves that fit to the performed pressure measurements. A FFT analysis was then performed on the difference between the measurements and the fit curve to identify the pressure oscillations experienced during the measurements in the laboratory. The FFT analysis showed few signs of interference from the suggested method.

The results from the FFT analysis showed that the largest frequency experienced was the blade passing frequency and it was observed during the start and stop procedures, as well as for BEP and part load operation. The guide vane frequency was not observed, this is due to the lack of functioning transducer in the runner blades. The Rheingan frequency had higher peak values during the stop sequence compared to startup. The reason for this is believed to be the chaotic flow pattern experienced in the draft tube cone during the startup sequence. The runner frequency was not observed during the performed procedures. For the occurring frequencies the part load operation resulted in larger pressure amplitudes compared to the start and stop procedures. Elastic oscillations were experienced both upstream and downstream of the turbine. To determine the structural behavior of the runner during the start and stop procedures proper instrumentation in the runner is needed. Improving the instrumentation is strongly advised to further analyze the structural behavior of the runner during the start and stop procedures.

By improving the instrumentation on the Francis rig it is possible to perform transient load measurements on the runner during start and stop procedures. There is especially a need to perform measurements along the runner blades to further analyze the effect of the dynamic load on the runner. This can be done by replacing the current defect runner blade transducers, and with a slight modification of the transducer cables to make them stick to epoxy. It is also possible to locate more pressure transducers at the upper draft tube cone. This is to perform more measurements on the chaotic flow that was experienced in the draft tube cone during the runner startup. The usage of accelerometers are suggested to determine the occurrence of vibration and cavitation. By installing the accelerometer on top of the guide vane trunnion it is possible to determine the wake and cavitation bubbles occurring from the guide vanes and traveling into the runner. Attaching

an accelerometer on the ball-bearings to measure the wear on the ball-bearings while experimenting on how the guide vane angle during startup procedures effects the stress fluctuations on the runner. Strain gauges can also be used simultaneously with pressure transducers along the blade to determine both the pressure and strain occurring along the runner blades. Simultaneous pressure and strain gauge measurements were not performed due to the lack of rapid prototyped runner blades. With the suggested improved instrumentation it is possible to perform these measurements for both the original and rapid prototyped runner blades.

Sammendrag

Trykkmålingene som ble utført på Francis løpehjulet på Vannkraftlaboratoriet på NTNU ble delt inn i ulike segmenter. Disse segmentene beskrev om det var en start eller stopp prosedyre, og om generatoren var på eller av. Videre ble en metode utarbeidet for å identifisere trykkpulsasjoner fra start og stopp sekvensene. Trykkmålingene ble prosessert og videre behandlet i MATLAB der applikasjonen "Curve Fitting Tool" ble benyttet. Denne applikasjonen finner en kurve som følger trykkvariasjonene til den utførte målingen. For å indentifisere trykkpulsasjoner ble FFT benyttet på differansen mellom trykkmålingene og denne kurven. Den foreslåtte metoden viste få tegn til støy etter FFT analysen av start og stopp sekvensene.

Resultatene fra FFT analysen viste at bladpasseringsfrekvensen var frekvensen med størst amplitude. Denne ble observert i omdreieningshulrommet under start og stopp prosedyrene, i tillegg til kjøring ved BEP og dellast. Ledeskovelfrekvensen ble ikke observert under målingene, dette er grunnet mangel på fungerende trykksensorer langs løpehjulsskivene. Rheingan frekvensen hadde en større amplitude under stopp sekvensen enn start sekvensen. Grunnen til dette er den kaotiske strømmingen av vann og luft som ble erfart i sugerørskonusen under oppstart. Løpehjulsfrekvensen ble ikke erfart under noen driftspunkt. Kjøring med dellast resulterte i de høyere frekvenser av bladpassering og Rheingan frekvensen sammenlignet med resultatene fra start og stopp prosedyrene. Trykkstøtsfrekvensen ble erfart både oppstrøms og nedstrøms av turbinen under start og stopp målingene. De utførte trykkmålingene viste at kjøring ved dellast har den største påvirkningen på løpehjulets mekaniske struktur, noe som kan føre til materialtretthet over tid. Ved å forbedre instrumenteringen i Vannkraftlaboratoriet er det mulig å gjøre mer nøyaktige målinger med hensyn på løpehjulets mekaniske struktur og materialtretthet under start og stopp sekvenser.

For å kunne gjennomføre målinger på den dynamiske belastningen som oppstår under start og stopp prosedyrer, er det viktig å ha riktig instrumentering i løpehjulet, i tillegg til før og etter. Laboratoriet har per dags dato ingen fungerende trykksensorer langs løpehjulsskivene, noe som er en viktig del for å kartlegge hvordan start og stopp prosedyrene påvirker løpehjulet. I tillegg kan flere trykksensorer bli festet i øvre sugerørskonus for å gjennomføre målinger med tanke på det kaotiske strømningsbildet som ble erfart under oppstart. Ved å benytte seg av et akselerometer så er det mulig å måle forekomsten av kavitasjon og vibrasjoner. Et akselerometer kan installeres på ledeskovelstappen for å måle tilstedeværelsen av vaker og kavitasjonsbobler som oppstår ved ledeskivene og beveger seg inn i løpehjulet. Det kan festes

et akselerometer på kulelageret for å måle lagerslitasje under oppstartsprosedyrer med varierende ledeskovelåpninger. Grunnen til dette er at en mindre åpning på ledeskovelene under oppstart kan redusere spenningsvariasjonene på løpehjulet, men kan føre til en økt slitasje på kulelageret. Strekkklapper kan benyttes samtidig med trykksensorer for å måle belastninger som oppstår langs løpehjulsbladene. Det ble ikke utført strekkklapp- og trykkmålinger på løpehjulsskovler produsert ved hjelp av 3D-printing, grunnet uferdig skovelproduksjon. Ved å benytte seg av den foreslåtte instrumenteringen vil det være mulig å gjennomføre disse strekkklapp- og trykkmålingene, og videre kartlegge om de originale ledeskovelene kan erstattes med de printede bladene.

Table of Contents

1	Introduction	1
1.1	Background	1
1.2	Previous Work	2
2	Theory	3
2.1	Francis runner	3
2.2	Fracture and fatigue	4
2.2.1	Stress and strain	4
2.2.2	Crack initiation	5
2.2.3	Cyclic stresses & fatigue	7
2.3	Turbine lifetime	8
2.3.1	Estimated load cycles for turbine	9
2.3.2	Turbine state analysis	9
2.3.3	Material of Francis runners	10
2.4	Pressure oscillations	11
2.4.1	Guide vane frequency	11
2.4.2	Runner vane frequency	12
2.4.3	Runner frequency	13
2.4.4	Rheingan frequency	13
2.4.5	Elastic oscillations	13
2.4.6	Reducing pressure oscillations	14
2.5	Frequency analysis	15
2.5.1	Discrete sampling and time-varying signals	15
2.5.2	Fast Fourier Transform	16
2.6	Deviation and error	18
3	Measurement preparations	21
3.1	Laboratory setup	21
3.2	Calibration	24
3.3	Execution of pressure measurements	25
4	Results	27
4.1	Expected frequencies	27
4.2	Pressure measurements analysis	29
4.3	Method for identifying pressure oscillations	31
4.3.1	Execution of method	31
4.3.2	Error and uncertainties in suggested method	34

4.4	FFT results	37
4.4.1	Inlet transducer	37
4.4.2	First and second vaneless transducers	38
4.4.3	Upper draft tube cone transducer	40
4.4.4	Lower draft tube cone transducer	41
4.4.5	Downstream draft tube transducer	42
5	Discussion	43
5.1	Post measurement experience	43
5.2	Pressure oscillation frequencies	44
5.2.1	Expected frequencies	44
5.2.2	Unexpected frequencies	46
5.2.3	Comparing different procedures and operational loads	49
5.3	Suggested method of identification	50
5.4	Structural behavior of runner	51
5.5	Runner blade replacement	53
5.6	Improving Instrumentation	54
5.6.1	Pressure transducers	54
5.6.2	Accelerometer	56
5.6.3	Strain gauges	57
6	Conclusion	59
7	Further Work	61
A	Francis runner measurements	I
A.1	FFT analysis BEP and part load	I
A.1.1	BEP - Best efficiency point	I
A.1.2	Part load	II
A.2	Start & stop pressure measurements and pressure difference	III
A.2.1	Inlet sensor	III
A.2.2	First Vaneless sensor	IV
A.2.3	Second Vaneless sensor	V
A.2.4	Upper draft tube cone sensor	VI
A.2.5	Lower draft tube cone sensor	VII
A.2.6	Downstream draft tube sensor	VIII
B	MATLAB application Curve Fitting Tool	IX
C	Running the Francis rig	XI
D	Draft tube cone during stop & start	XIII
E	Runner rotational speed measurements	XV
F	Calculation of bending stresses during the stop and start procedures	XIX

F.1	Graphical result of the calculated bending stresses	XIX
F.2	Equations to calculate the bending stresses	XX
G	Calibration	XXI
G.1	Pressure transducers attached on Francis rig	XXI
G.1.1	Pressure transducer Druck PTX1400 at inlet	XXI
G.1.2	Pressure transducer PTX1400 in upper draft tube cone	XXIV
G.1.3	Pressure transducer PTX1400 in lower draft tube cone	XXVII
G.1.4	Pressure transducer PTX1400 at downstream draft tube	XXX
G.1.5	First pressure transducer Kuliter XTL-190-7BARA in vaneless space	XXXIII
G.1.6	Second pressure transducer Kuliter XTL-190-3.5BARA in vaneless space	XXXVII
G.2	Internal pressure transducers in Francis rig	XL
G.3	Weighing tank	XLVI
G.4	Flowmeter	XLVII
G.5	Friction torque	XLVIII
G.6	Generator torque	LI
H	Risk Assessment	LV

List of Figures

2.1.1	Francis runner with runner- (grey), guide- (yellow), and stay vanes (blue) [31]	3
2.1.2	Fatigue related areas on a Francis runner: blade & T-joint [1]	4
2.2.3	Elastic or plastic deformation regarding stress & strain	5
2.2.4	Crack growths showed in a Paris' diagram [30]	6
2.2.5	An analysis of the Wöhler curve [27]	7
2.4.6	Flow through guide vanes [16]	11
2.4.7	Pulse created when runner blade passes guide vane [23]	12
2.4.8	Hub extension to reduce pressure oscillations [14]	14
2.5.9	Higher frequency aliases	16
2.5.10	Fundamental frequency with its half and second harmonics	17
2.5.11	Applying a Hann window to the original signal [11]	17
3.1.1	Francis rig closed loop show as the blue circuit with green valves	21
3.1.2	IEC60193 Pressure transducer placement [10]	22
3.1.3	Pressure transducer placement on Francis rig at NTNU	23
3.1.4	Setup for transducer equipment	24
4.2.1	Dividing pressure measurement into the different procedures	30
4.2.2	Variation of the guide vane angle during the different procedures	30
4.3.3	Upper draft tube cone measurements, BEP and stop & start	31
4.3.4	A curve fit to the pressure measurements at upper draft tube cone	32
4.3.5	Pressure difference between measured values and estimated curve	33
4.3.6	Fourier transform performed on the pressure difference	33
4.3.7	Fit curve and pressure difference, startup with generator off & on	34
4.3.8	Values for goodness of fit for startup. Upper cone measurements	35
4.3.9	Values for error measurements	36
4.4.10	Frequency peaks at inlet transducer	37
4.4.11	Frequency peaks at first vaneless transducers	38
4.4.12	Frequency peaks at second vaneless transducers	39
4.4.13	Frequency peaks at upper draft tube cone transducers	40
4.4.14	Frequency peaks at lower draft tube cone transducers	41
4.4.15	Frequency peaks at downstream draft tube transducers	42
5.2.1	Wakes hitting the runner blades [23]	45
5.5.2	Rapid prototyped turbine model	53
5.6.3	Pressure transducers located at runner blade [8]	54
5.6.4	Procedure to attach pressure transducers along the blade [23]	55

5.6.5	An example of an accelerometer and placement	56
A.1.1	Frequency peaks at BEP	I
A.1.2	Frequency peaks at Part load	II
E.0.1	Turbine rotational speed for measured rpm & averaged rpm	XV
E.0.2	Disc installed at rig to measure rpm, 1 pulse per revolution	XVI
E.0.3	Created pulse per revolution with used & installed disc	XVII
E.0.4	Created pulse per revolution with new & recommended disc	XVII

List of Tables

2.3.1	Mechanical properties for possible runner material	10
3.1.1	Pressure transducers used in the measurement	23
3.1.2	Instruments used to process signal from transducers	24
3.2.3	Calibration instruments	25
4.1.1	Calculation of the expected elastic oscillations	27
4.1.2	BEP operation	28
4.1.3	Expected frequencies	29
4.2.4	Measurements divided into dynamic procedures	29
A.1.1	Part load operation	II

Nomenclature

a	crack size	m
N	Number of load cycles	—
C	material constant	—
m	material constant	—
K	Stress intensity factor	$\text{MPa}\sqrt{m}$
f(g)	Crack figuration factor	—
g	Tyngdeakselerasjon	$\frac{m}{s^2}$
c	Sound wave propagation speed	$\frac{m}{s}$
t	time	s
T	hours of operation	hours per year
E	Modulus of elasticity	Pa
E_w	Elasticity of water	Pa
E_p	Elasticity of pipe material	Pa
H	Head	m
e	Pipe thickness	m
D	Pipe diameter	m
L	Length	m
H	Head	m
Q	Flow	$\frac{m^3}{s}$
α	Opening angle of guide vanes	°
n_{runner}	Runner speed	$\frac{m}{s}$
$n_{generator}$	Generator speed	$\frac{m}{s}$
n_{pump}	Pump speed	$\frac{m}{s}$
n_{ED}	Dimensionless speed	—
Q_{ED}	Dimensionless flow	—
Z_{rv}	Number of runner vanes	—
Z_{gv}	Number of guide vanes	—
$Z_{impeller}$	Number of impeller vanes	—

f_n	Runner frequency	$Hz = \frac{1}{s}$
f_{rv}	Runner vane frequency	$Hz = \frac{1}{s}$
f_{gv}	Guide vane frequency	$Hz = \frac{1}{s}$
f_R	Rheingan frequency	$Hz = \frac{1}{s}$
f_{wh}	Water hammer frequency	$Hz = \frac{1}{s}$
f_{mass}	Mass oscillation frequency	$Hz = \frac{1}{s}$
f_{pump}	Pump frequency	$Hz = \frac{1}{s}$
f_s	sampling frequency	$Hz = \frac{1}{s}$
f_m	measured signal frequency	$Hz = \frac{1}{s}$
p	Pressure	Pa
bar g	Gauge pressure	bar
bar abs	Absolute pressure	bar
P	Effekt	Watt
V	Volt	Volt
A	Ampere	Ampere
y_i	measured value	—
w_i	weighted value	—
\hat{y}	predicted value	—
\bar{y}	averaged value	—

Greek letters

ρ	Water density	$\frac{kg}{m^3}$
ϵ	strain	—
σ	stress	Pa
σ_{maks}	maximum stress	Pa
σ_{min}	minimum stress	Pa
ω	frequency	$\frac{1}{s}$

Abbreviations

NTNU	Norwegian University of Science and Technology
BEP	Best Efficiency Point
rpm	revolutions per min
N/A	Not applicable
RSI	Rotor Stator Interaction
SSE	Sum of Squares due to Error
SSR	Sum of Squares of the Regression
SST	Total Sum of Squares
RMSE	Root Mean Square Error
NDT	Non-Destructive Tests
FFT	Fast Fourier Transform
PVC	Poly Vinyl Chloride

Sub- and superscripts

n	runner
R	Rheingan
rv	Runner vanes
gv	Guide vanes
wh	water hammer
w	water
p	pipe
s	sampling
m	measured
i	Position i of numeric variables

Chapter 1

Introduction

1.1 Background

Norway introduced a new energy legislation in the beginning of the 1990s which affected the energy market and hydropower operation. Before this legislation the operational pattern of the hydropower turbines in Norway was focusing on constant operation at BEP with few stops or start ups. The turbine is designed to operate and withstand load experienced during BEP operation, and is therefore causing minimal damages to the runner. By operating turbines with regard to economical profit and varying the turbine operation with the energy prices, the turbine is experiencing an increased dynamic load. This load increase and operation outside of BEP result in a larger wear on the turbine, shortening the turbines lifetime by enhancing issues related to fatigue. These issues are common for high head Francis turbines, resulting in increased maintenance costs or shortening the runner lifetime. The effect the dynamic load has on the runner in a high head Francis is still not known in detail and therefore an important field of study. Francis turbines also experience a varying load during the start and stop procedures and this load is believed to enhance the fatigue issues of the runner. It is therefore beneficial to investigate how this dynamic load affects the runner and how issues regarding fatigue are occurring on a high head Francis turbine.

The material used to make runners have evolved since the large hydropower expansion in Norway during the 1900th century. Before computer and CFD analysis was utilized in runner blade optimization the runner blades were designed with safety factors to eliminate wear of the runner. The CFD optimized runner blades of today have a reduced thickness and amount of blade material compared to previous runners. It is questionable if this computer optimization is causing the runner to more rapidly experience issues regarding fatigue. One objective in my thesis is to perform pressure and strain gauge measurements on rapid prototyped runner blades. To perform these measurements I was dependent on another master student that was designing and producing a rapid prototyped runner.

1.2 Previous Work

Pressure oscillations have been a field of interest for a long period of time, and still hydropower plants experience issues related to pressure pulsations and reduced turbine lifetime. The result of this is a broad field of research to determine and find methods to prevent the occurrence of these oscillations. W. J. Rheingan was one of the first to study oscillations located in the draft tube in the 1940s. In 1966 I. Oftebro og A. Lønning from Kværner published the coincidence between pressure pulsations and Francis runner operation. Norwegian companies within hydropower started in the early 2000s to finance projects focusing on the dynamic load experienced during start and stop procedures, as well as the cost of varying runner operation. The interest of the dynamic load and pressure pulsations experienced during start and stop procedures is still an important issue that is desired to solve. The Waterpower laboratory at NTNU has had a lot of students writing theses focusing on pressure pulsations, but this is mainly static load operation. Some examples of previous master students are Kari Haugan (2007), Jo Solberg (2008), Julie Hovland (2013), Ingeborg Lassen Bue (2013) and Einar Kobro (2006). Einar Kobro continued with the same topic in his doctoral thesis. Since all of these involved steady state operation then a less explored researched field was measuring the dynamic load during start and the stop procedures. Only one previous master student at NTNU, Anders Tørklep (2012), had written about pressure oscillations during start and stop procedures in Francis turbines. Hovland's and Bue's theses also involved measuring stress in high head Francis turbines. Hans-Jörg Huth wrote his doctoral thesis involving fatigue design of hydraulic turbine runners for the Department of Engineering Design and Materials.

Chapter 2

Theory

2.1 Francis runner

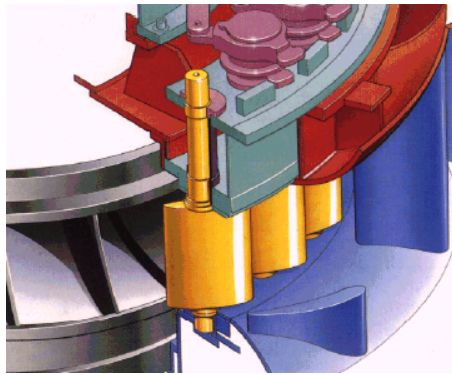


Figure 2.1.1: Francis runner with runner- (grey), guide- (yellow), and stay vanes (blue) [31]

Hydropower was and still is important for power generation in Norway. The operation of a hydropower plant has developed and changed due to financial maximization instead of optimal power generation. When operating a turbine outside of its ideal operational point, BEP, it has an effect on the runner lifetime. The turbine is experiencing dynamic load caused by pressure and material stress oscillations when operating in part load and over load [5]. These oscillations may cause fatigue issues, a shortened lifetime and an increased need for maintenance. Statkraft employee Jens Ragnvald Davidsen presented a tripling in start and stop procedures between 1993 and 2000, and a further doubling between 2001 and 2003 [19]. Thomas Welte stated during a speech that there is no significant increase, only a weak trend in more start and stop procedures [35]. He further indicated that hydropower companies have different figures regarding this trend, and stated that it is important to look at each turbine individually regarding turbine lifetime and fatigue issues.

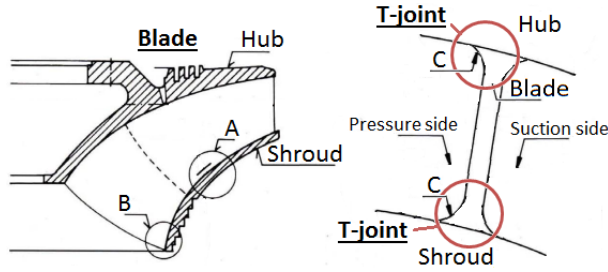


Figure 2.1.2: Fatigue related areas on a Francis runner: blade & T-joint [1]

The runner is experiencing a load during the startup procedure equivalent to several years of BEP operation [33]. The load is a result of the runner not being capable to accelerate fast enough during startup. Hence the incoming masses of water are causing high stress amplitudes in addition to dynamic pressure [33]. The areas with the largest stresses are occurring along the runner hub and shroud at the T-joints [17]. Figure 2.1.2 shows these high stress areas (A, B and C) on a Francis runner and where cracks are likely to occur. Areas A & B are along the blade, but C is along blade and are the the stress areas at the T-joints.

2.2 Fracture and fatigue

2.2.1 Stress and strain

Fatigue is a serious issue for hydropower turbines since they occur suddenly and without any warning they often result in serious damages to the turbine. Fatigue is a result of stress and strain that causes a deformation to an object, and exposed areas are mainly the guide vanes and runner vanes. Stress is defined as the force added to the material, while strain is the materials reaction to the given stress. There are two types of deformation or strains: elastic and plastic deformation. The elastic deformation is based on Hooke's law, equation (2.2.1), where σ is the applied stress, E the modulus of elasticity and ϵ is the applied strain. This deformation is resulting in a non-permanent change when the load decreases and causes the object to return back to its original shape [38]. Plastic deformation is the opposite of this, causing a permanent change or deformation to the object. Most materials have both deformations, starting at elastic and proceeding to plastic deformation. The elastic to plastic transition is often defined as the yield strength. This transition is shown in figure 2.2.3 and is valuable knowledge regarding material behavior due to the permanent deformation. When performing material tests it is also preferable to obtain the tensile strength, which is the maximum stress a structure can be sustained in tension [38].

$$\sigma = E \cdot \epsilon \quad (2.2.1)$$

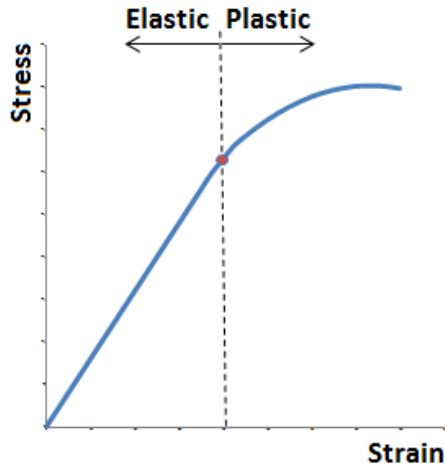


Figure 2.2.3: Elastic or plastic deformation regarding stress & strain

2.2.2 Crack initiation

There are different types of fractures that can occur to materials and they are based on the materials' vulnerability for plastic deformation. The two types of fractures are ductile and brittle. Ductile materials can often have high energy absorption and withstand substantial plastic deformation before they fracture. While brittle materials have low energy absorption and can only withstand little or no plastic deformation. A ductile fracture is preferred because it is easier to detect due to the plastic deformation, and preventive methods can be performed when these types of cracks are detected [38]. Ductile materials are often tougher because more strain energy is required to induce a ductile fracture. A brittle fracture occurs suddenly and often without any warning due to the rapid crack propagation, therefore the consequences can be catastrophic if occurring in hydropower plants. During any progression of a fracture there are two different stages, either an occurrence of crack formation or propagation of an existing crack. Whether the crack is determined as stable or unstable depends on the material properties and stress controlled growth [30]. A stable crack is determined as ductile with a slow proceeding plastic deformation, and this type of crack does not increase unless further stress is applied. An unstable crack is rapidly spreading and once started it has spontaneous growth regardless of the applied stress. These cracks are characterized with very little plastic deformation.

$$\frac{da}{dN} = C \cdot \Delta K^m \quad (2.2.2)$$

Equation (2.2.2) is the Paris' equation and it is used to calculate crack growth in materials. Where the crack size is determined as a , N is the number of load cycles,

C and m are the material constants and ΔK is the range of the stress intensity factor. The ΔK is given by equation (2.2.3), where $\Delta\sigma$ is the stress amplitude and $f(g)$ is the crack configuration (geometry) factor. This equation is used further and represented in equation (2.2.4). This equation shows the number of load cycles that result in a crack increase between the two sizes, a_1 to a_2 [30].

$$\Delta K = \Delta\sigma\sqrt{\pi a} \cdot f(g) \tag{2.2.3}$$

$$\Delta N = \frac{1}{C \cdot (\Delta\sigma\sqrt{\pi} \cdot f(g))^m \cdot (\frac{2-m}{2})} (a_2^{(\frac{2-m}{2})} - a_1^{(\frac{2-m}{2})}) \tag{2.2.4}$$

The Paris' equation is often used to sketch a Paris' diagram, shown in figure 2.2.4. The Paris' diagram illustrates the logarithmic ratio between crack growth and stress intensity factor. It can further be divided into three parts. Due to different crack conditions the Paris' law is only applicable in region II, where there is crack propagation. The ideal region for turbines is region I due to the non-propagation of fatigue cracks, while region II is for crack propagation. Region III is for larger and rapid crack growths, often crack instability and rest fracture. The stress ratio is defined as the ratio between the minimum and maximum stress amplitudes, $R = \frac{\sigma_{min}}{\sigma_{max}}$ [30]. The stress ratio is also an important variable regarding turbine lifetime because a higher stress ratio lowers the amount of cycles before fatigue occurring [7].

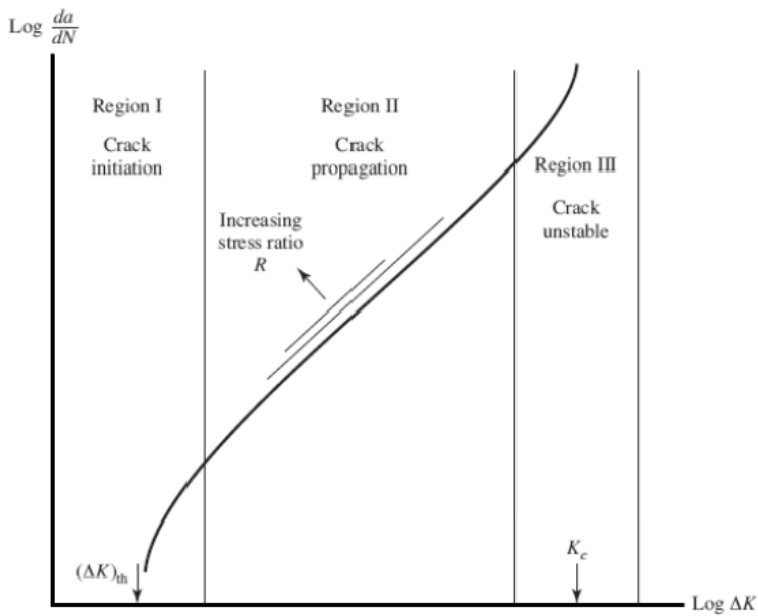


Figure 2.2.4: Crack growths showed in a Paris' diagram [30]

2.2.3 Cyclic stresses & fatigue

Fatigue is defined as a structural failure due to repeating, dynamic or fluctuating stresses. These cyclic stresses may result in fatigue occurrence on stress levels lower than the yield and tensile strength. This is because these stress levels are found during static load conditions. Fatigues normally occur after a longer time period of repeated load conditions with varying stress and strains. About 90% of all metallic failures are related to fatigue, causing it to be the single largest cause of failure in metals [38]. Issues regarding fatigue are often sudden and without any warning, causing it to be similar to a brittle fracture because it has little or non-existing plastic deformation. The stress direction is perpendicular to the fracture surface and can be defined as axial (tension & compression), flexural (bending) or torsional (twist). The fatigue related stresses can be either one or all three of these [38].

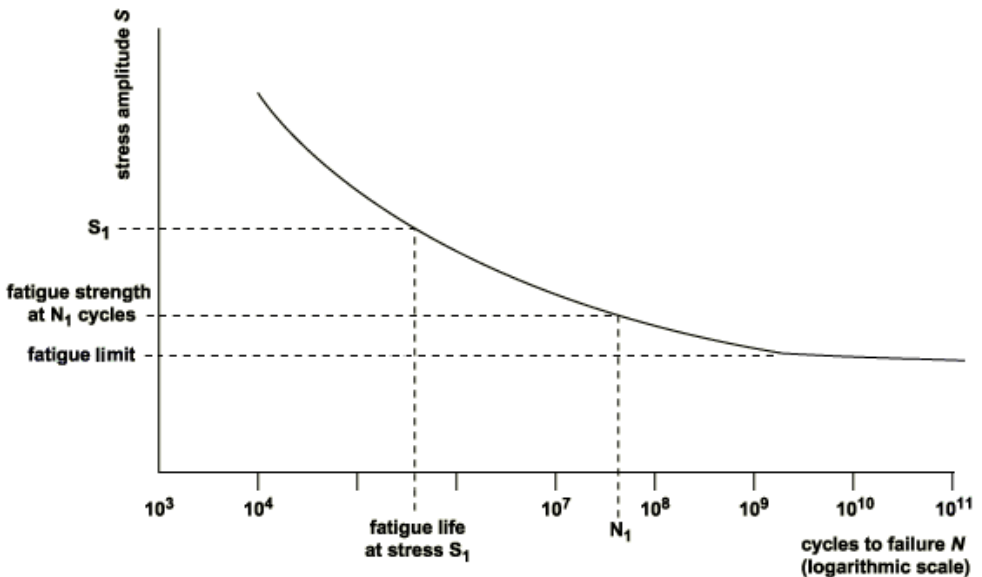


Figure 2.2.5: An analysis of the Wöhler curve [27]

A Wöhler curve, seen in figure 2.2.5, is often referred to as a S-N curve because it shows the ratio between the stress amplitudes and the number of load cycles. The fatigue limit is the largest fluctuating value that will not cause failure for an infinite number of cracks. Fatigue strength is defined as the stress level where failure will occur for a specific number of cycles. The fatigue life is the number of cycles to cause failure at a specific stress level. The cyclic fatigue stresses can be divided into high cycle and low cycle fatigue. High cycle fatigue are for lower stress levels and need a large number of cycles to cause failure, above $10^4 - 10^5$ cycles. The deformation occurring during these cycles are elastic [38]. Low cycle fatigue are occurring at a higher stress level where the fatigue life is shorter, under $10^4 - 10^5$

cycles. The large stresses are typically related to startup procedures, and the high loads under these conditions produce both elastic and plastic strain during each cycle. As mentioned earlier cracks are either initiating or propagating, and for fatigue failures small cracks are initiated at high stress points, often on the surface. These high stress points are often due to cyclic loading that produce microscopic surface discontinuities on the surface enhancing the increase in stress. While for propagation terms the crack advances incrementally with each stress cycle. Before a final failure occurs when the crack has reached its critical size. There are some methods to increase the fatigue life, either by increasing the mean stress levels, performing surface treatment or improving the design [38].

2.3 Turbine lifetime

Determining and predicting the turbine lifetime is difficult due to several factors that can affect this lifetime. Turbines are consisting of several components that experience individual wear and tear during operation, and the sustainability of these components may vary on type of load. Some of the main causes for turbine damage which may result in a shortened lifetime are fatigue, material defects, cavitation, and erosion [20]. These are well known issues for high head turbines due to the high pressure and the pressure variation under dynamic load. It is important when evaluating the runner lifetime to bear in mind that hydropower plants and turbines need to be analyzed independently. A reason for this is that some hydropower plants have base load turbines that have long time in operation at a constant speed, often at BEP. While the peak load turbines are often started or stopped to counter the increase or reduced energy demand. These peak load turbines are often run outside of BEP at part load or overload, and experiencing many load variations during time in operation. During the start and stop procedures an increase in pressure pulsations is a concern regarding the dynamic load and lifetime of the runner. Many companies have their own model for determining turbine condition and estimating time for inspection, maintenance and replacing turbine components. Since no weld can be defined as perfect there is always a chance of material defects occurring [20]. Therefore the "Leakage before rupture"-criteria is an important criteria for materials used in a hydropower plant [30]. This is to ensure the safety on site and prevent catastrophic events from occurring, such as rupture of inlet pipe. The reason for this criterion is that a leakage is possible to detect through a thorough inspection. This inspection may prevent a rupture from occurring, since a rupture is sudden and often without warning. Regarding the high pressure in the water conduit of a high head turbine it can lead to destruction of the hydropower plant if a rupture occurs.

2.3.1 Estimated load cycles for turbine

The amount of load cycles a turbine is exposed to through a year have an impact on a turbine's lifetime. As mentioned in chapter 2.2.3 the fatigue is dependent on the number of cycles and the amplitudes of these cycles. Equation (2.3.5) calculates the number of load cycles experienced by a runner vane. Where N equals the load cycles, n is the turbine rotational speed, Z_{rv} is the amount of runner vanes and T is the hour of operation.

$$N = n_{runner} \cdot Z_{rv} \cdot T \cdot 60 \quad (2.3.5)$$

By inserting representative values in the previous equation it may give a perspective of the amount of load cycles that an operating turbine experiences through a year of operation. The values used are 30 runner vanes, 7884 hours of operation (10% downtime of a total 8760 hours of operation per year) and 320 runner revolutions per min.

$$N = 320 \cdot 30 \cdot 7884 \cdot 60 = 4.54 \cdot 10^9 \quad (2.3.6)$$

This results in approximately $5 \cdot 10^9$ load cycles, which leads to a lot of load fluctuations on the turbine during a year. The many load cycles in addition to high load fluctuations due to peak load operation may therefore have serious impact on fatigue and runner lifetime. Since not all turbines have the equal amount of operating hours the equation may be expressed as load cycles per hour of operation by dividing on the variable T . By using the same values this leads to around $6 \cdot 10^5$ load cycles per hour of operation. It can be stated that model turbines usually have a higher rotational speed compared to prototypes. This may imply that model turbines would experience more load cycles and be more exposed to crack initiation and fatigue. But the hours of operation are much smaller compared to operational turbines, and this should result in a reduced risk of fatigue occurrence on model turbines.

2.3.2 Turbine state analysis

Performing measurements to determine the condition of the turbine may increase the lifetime of the runner, as well as minimize the probability for failure. Some examples are governor testing, efficiency, vibration, and guide vane measurements as well as performing non-destructive tests on the turbine [15]. When performing a non-destructive test (NDT) it is to determine the condition of the turbine regarding maintenance and lifetime. The NDT consists of multiple methods from visual inspection to using different devices. The competence needed to fully understand and analyze the result increases with instrumentation technique [30]. The visual inspection is the easiest of the methods and is used to look for surface cracks, cavitation damage or indication of corrosion. By further using penetrants it is

easier to find surface cracks, but these penetrants are less certain due to paint and humidity. Magnetic powder tests are also a method used regarding surface cracks and require a paint film less than 50 micrometer. Depending on the surface the flourishing method is for smooth surfaces and black powder is used for rough surfaces. If using a swirl current it is possible to detect crack depths up to two - three millimeters. An advantage of using this method is that it can be used through painting. To determine internal cracks a method utilizing acoustic devices are used, but this method demands experience and high competence [32].

2.3.3 Material of Francis runners

Stainless steel is the material that is most commonly used on a high head Francis runners in hydropower plants. Mainly the 13Cr 4Ni alloy steel is used in Francis runners, but other combinations like 13Cr 1Ni, 16Cr 5Ni and 18Cr 8Ni may also be used [6]. There are slight differences between these combinations, for instance the 16Cr 5Ni show better resistance regarding cavitation compared to the normally casted 13Cr 4Ni [7]. The installed Francis runner at the Waterpower Laboratory is made out of different bronze material. The runner vanes are made of cast tinbronze JM 3 – 15 (also called SS 5465 – 15), while the hub and ring are made of bronze JM-7. The main concern for the blades is to withstand the different temperature and pressure so it does not deform during operation. For the runner model at NTNU the benefits of using bronze are also due to financial reasons in addition to the material properties regarding deformation. When evaluating other materials for the runner blades it is important to look at the different characteristics to avoid fatigue, deformation and crack occurrence. Rapid prototyping have several advantages due to the high heat resistance and tough material properties, while the disadvantage may be the granulated surface [4]. A material called DuraForm HST is considered when looking at replacing the runner vane material with rapid prototyped blades. The DuraForm HST material are characterized by a high specific stiffness and elevated thermal resistance [2]. Some of the material properties of the three runner materials are presented in table 2.3.1. The bronze is the current material in the model, steel is the often used material in prototype runners and Duraform HST is the rapid prototyped material.

Table 2.3.1: Mechanical properties for possible runner material

Material type	JM 3 – 15 [25]	13Cr 4Ni [3]	DuraForm HST [2]
Tensile strength	275 - 320 MPa	930 MPa	48 - 51 MPa
Yield strength	145 - 170 MPa	899 MPa	N/A
Elongation	6 - 15 %	14 %	4.5 %

2.4 Pressure oscillations

Pressure oscillations are a concern for the turbine and are related to operation of the hydropower plant. The increase in turbine operation outside of BEP is a result of operation being controlled by maximum profit, and is causing increased problems regarding pressure pulsations. These oscillations are always present when the turbine is operating, but the impact and size of the pressure pulsations can be reduced to prevent wear and tear on the runner. The impacts of the pressure oscillations are also dependent of the operational state. The different operational states can be divided into dynamic and steady states. The steady state is defined as stable operation at given operational point, this could either be at BEP, part load or overload. The dynamic state is defined by changing between different steady states over a time period, in addition to start and stop procedures.

The pressure pulsations are based on different oscillations. It can either be rotational oscillations, from the turbine rotation, or elastic oscillations. The elastic oscillations are a result of system inequity, due to the motion of the masses of water. There are primarily four areas on the turbine that result in the rotational oscillations; guide vanes, runner vanes, runner and draft tube. The elastic oscillations are a result of the flow changing through the turbine and causing a dynamic pressure difference, either an acceleration or retardation of the flow. This pressure wave will travel through the plants waterways and is dependent on the adjustment of valves or vanes.

2.4.1 Guide vane frequency

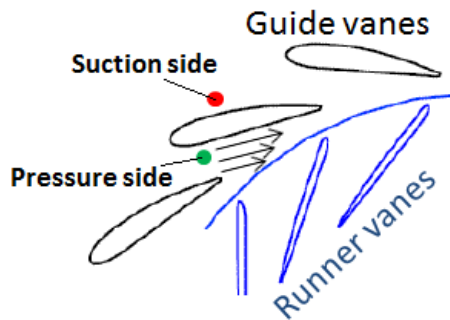


Figure 2.4.6: Flow through guide vanes [16]

The guide vane frequency is shown in equation 2.4.7, and it is a result of an inhomogeneous flow field between the guide vanes [26]. This flow field result in a pressure

difference over the guide vane, creating a pressure and suction side seen in figure 2.4.6. A wake is being formed at the tail of the guide vane due to this pressure difference, and a pulse is created when a runner vane hits the wake. There are two essential parameters to reduce the size of this pulse; the guide vane geometry and the distance between the guide and runner vanes. In addition to wakes the guide vane frequency will increase if a runner vane is damaged or there are equal number of runner vanes, and guide vanes. The need for unequal number of runner blades and guide vanes equation, (2.4.8), is to prevent the runner vanes to pass the guide vanes at the same time at different locations in the turbine runner [31]. The guide vane frequency can be characterized by high amplitudes at part load operation and low amplitude at BEP.

$$f_{gv} = \frac{n}{60} \cdot Z_{gv} \tag{2.4.7}$$

$$\frac{Z_{gv}}{Z_{rv}} \neq \text{integer} \tag{2.4.8}$$

2.4.2 Runner vane frequency

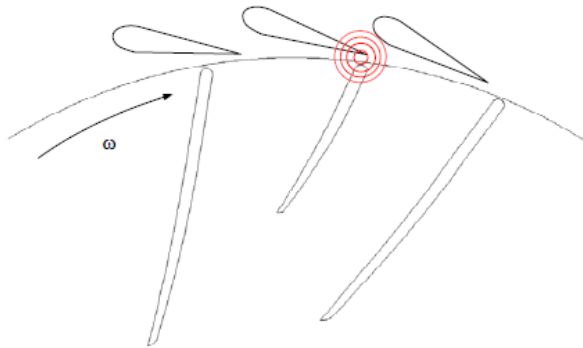


Figure 2.4.7: Pulse created when runner blade passes guide vane [23]

The runner vane frequency, equation 2.4.9, is occurring every time a runner vane passes a guide vane. This is because a pulse is produced whenever this passing happens, therefore it is also called the blade passing frequency, illustrated in figure 2.4.7. Since there are a lot of blade passings turbine during operation this may result in wear and tear of the runner, even at low amplitudes. This frequency is usually the dominant frequency during steady state operation, and the turbine produces a lot of noise when high amplitudes of this frequency occur. Similar to

the guide vane frequency the runner vane frequency is also dependent of the distance between the guide and runner vanes. This conjunction between the runner and guide vanes are often described as the runner stator interaction, abbreviated as RSI. The guide vane frequency is also a part of this runner start interaction.

$$f_{rv} = \frac{n}{60} \cdot Z_{rv} \quad (2.4.9)$$

2.4.3 Runner frequency

Equation 2.4.10 represents the runner frequency and is caused by the turbine rotation. This frequency is characterized by normally being at low amplitude, but if high amplitudes it can indicate severe issues to the runner. Some of the issues may be defect runner vanes, the runner is unsymmetrical or the flow field through the runner is rotosymmetrical [32].

$$f_n = \frac{n}{60} \quad (2.4.10)$$

2.4.4 Rheingan frequency

The Rheingan or draft tube frequency is due to a rotation of the flow field in the draft tube, which may create a swirl. This frequency, equation 2.4.11, is always present during turbine rotation. During operation at BEP this frequency is characterized by low amplitudes without swirl existence. The highest amplitudes are found to be between 50% to 70% of BEP [22]. High amplitudes indicate a negative pressure in the draft tube, which may result in cavitation and a swirl. Large noises may occur from the draft tube when operating outside of BEP due to the swirl "whipping" the draft tube wall.

$$\frac{f_n}{3,6} \leq f_R \leq \frac{f_n}{3,0} \quad (2.4.11)$$

2.4.5 Elastic oscillations

The elastic oscillations are a result of system inequity and due to the moving masses of water, they are often categorized as mass oscillations or water hammer oscillations. The mass oscillations are caused from the moving masses of water, both before and after the turbine. Equation (2.4.12) expresses these oscillations where L is the length between the pressure tank to the turbine or between the turbine and the surge tank. The water hammer pulsations are from pressure waves created

when a flow is experiencing a change in pressure. This acceleration or retardation in flow are causing oscillations both upstream and downstream of the turbine. The water hammer oscillations are determined by Joukowski and is expressed in equation (2.4.13) [12]. In this equation the propagation speed is the variable c and is expressed by equation (2.4.14), which usually is around $1\,000 \frac{m}{s}$.

$$f_{mass} = \frac{1}{2\pi} \sqrt{\frac{2 \cdot g}{L}} \tag{2.4.12}$$

$$f_{wh} = \frac{c}{4 \cdot L} \tag{2.4.13}$$

$$c = \sqrt{\frac{\frac{E_w}{\rho}}{1 + \left(\frac{E_w}{E_p} \cdot \frac{D}{e}\right)}} \tag{2.4.14}$$

2.4.6 Reducing pressure oscillations

Pressure oscillations will always exist when a turbine is operating, but measures can be executed to reduce the effect of these oscillations. By reducing the pressure pulsations it may reduce the fatigue occurrence and increase the lifetime of the turbine. There are different procedures that can be executed depending on the location of these pulsations. Issues related from guide or runner vane pulsations are often due to spacial reasons. If the distance between the guide vanes and the runner (vaneless space) is too small then it could result in higher amplitudes for the blade passing and guide vane frequency, due to the flow and wake iteration. One of the main reasons that large pressure oscillations are occurring is operation outside of BEP. This resulting in the best method to reduce pressure pulsations is to operate the turbine in or close to BEP. The design of the runner inlet being unoptimal regarding the turbine operation is another reason for the occurrence of these pulsations.

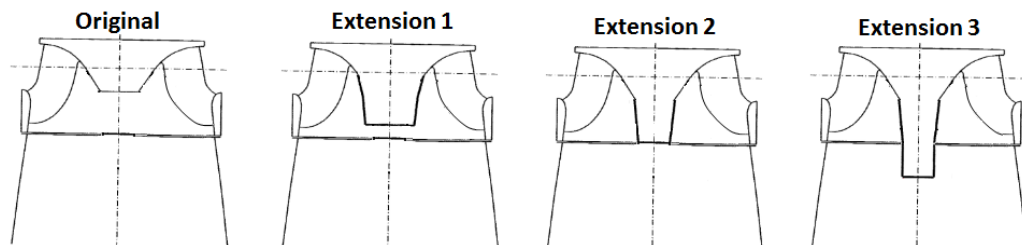


Figure 2.4.8: Hub extension to reduce pressure oscillations [14]

If issues regarding pulsations are occurring in the draft tube, then preventive methods can be proceeded. An injection of air or water can be performed to dampen

and lower the amplitude of the oscillations. Injection of air is a common method where air goes through the center of main shaft and runner into the draft tube. If too much air is injected into the draft tube the flow might change into axial flow, which is undesirable. An extension of the hub is also a method to reduce the pressure pulsations in the draft tube. This method can be seen in figure 2.4.8 and pulsations are reduced because a longer hub length extends the flow further into the draft tube making it more difficult for a swirl to be produced. Even though the hub extension is resulting in smaller pressure pulsations the efficiency of the turbine at BEP is also becoming reduced [13].

2.5 Frequency analysis

Frequency analysis is often used to find a pattern in numerous amount of information. This is done by searching for and categorizing repeating combinations. The reason for performing a frequency analysis on pressure oscillations is to determine the amplitudes of different frequencies. A Fourier transform is often used when performing a frequency analysis. The Fourier transform function is defined in equation (2.5.15) and is a continuous complex valued function [36]. More mathematical derivation and equations regarding the Fourier transform can be found in books about signal analysis [36] and engineering mathematics [24].

$$\hat{f}(\omega) = \int_{-\infty}^{\infty} f(t) \cdot e^{-j\omega t} dt \quad (2.5.15)$$

2.5.1 Discrete sampling and time-varying signals

Digital data-acquisition systems record signals at a discrete timeframe, opposed to the analog recording systems who record continuously. A consequence of this timeframe recording is a small gap between the timeframes, and the information in this gap is lost. The sampling rate is an important parameter, and a badly chosen sampling rate may lead to misleading results. These results are also called aliases and are false frequencies [36]. To prevent misleading results a recommendation on the sampling rate is given, this is known as the sampling-rate theorem (equation 2.5.16). This theorem states that the sampling rate must be greater than twice the size of the highest expected or known signal frequency [36]. The sampling-rate theorem is essential to correctly reconstruct the original waveform, but filtering may be necessary due to higher frequency aliases. An example of higher frequency aliases can be seen in figure 2.5.9 where the original 10 Hz signal and a 30.1 Hz signal is compared. The green dots are places where data is consistent of both the 10 Hz and 30.1 Hz signal. This may cause false frequency peaks at approximately 30 Hz and filtering is needed if the sampling rate theorem is fulfilled.

$$f_s > 2f_m \quad (2.5.16)$$

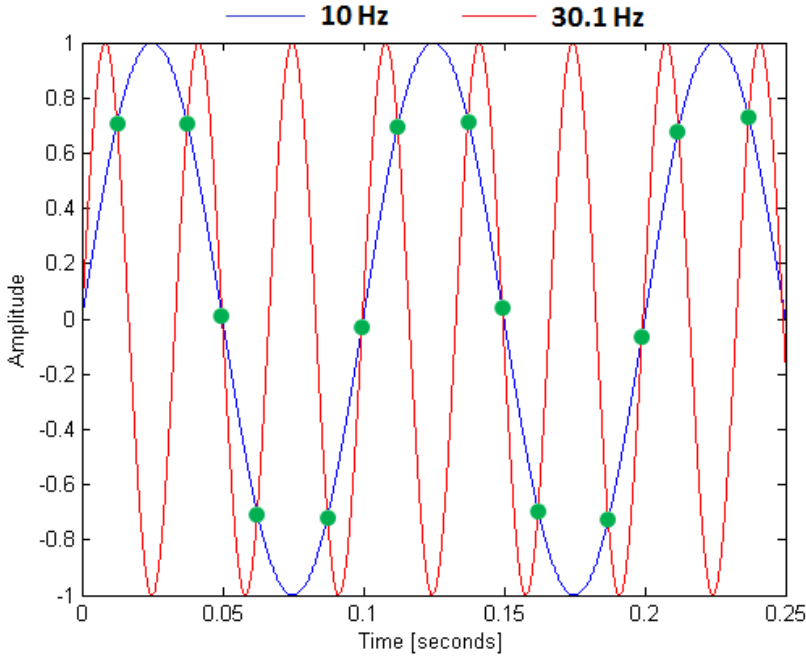


Figure 2.5.9: Higher frequency aliases

2.5.2 Fast Fourier Transform

A Fourier transform is used to find repetitive periodic signals, and these signals are often sine or cosine functions. Since a time-varying signal also consists of sine and cosine waves with different frequencies, a Fourier transform is therefore commonly used as a method to analyze and decompose these signals. By performing a FFT it transforms the signal from time domain to frequency domain. The frequency amplitudes show the different harmonic frequencies existing in the analyzed signals. The highest and lowest frequencies are defined as the fundamental or first harmonic frequency, and are often followed by the second and third harmonic frequency. Figure 2.5.10 shows the ratio between the pressure amplitude and the frequency relative to runner rpm, $\frac{f}{f^n}$. The fundamental frequency is located at 29.99, while 15 is the half harmonic frequency and 59.99 is the second harmonic frequency.

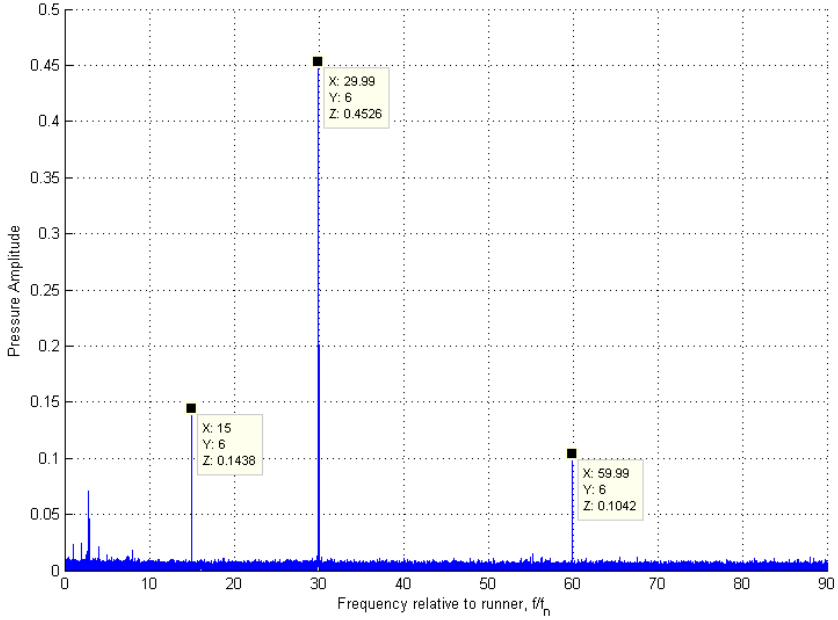


Figure 2.5.10: Fundamental frequency with its half and second harmonics

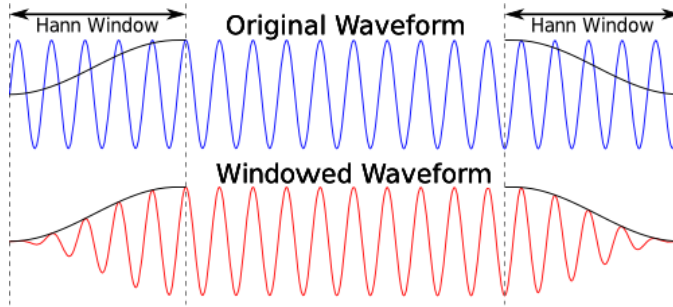


Figure 2.5.11: Applying a Hann window to the original signal [11]

A frequency analysis is sensitive to interference and vibrations. Interference will result in a dispersed signal over several frequencies, resulting in lower amplitudes. This is determined as spectral leakage, and may result in misleading results. Spectral leakage is often a result of incomplete cycles at the end of the sampling period. Windows are a useful contraceptive tool and by overlapping these windows they can remove this type of leakage [36]. As explained previously the recorded signals can be determined as multiple timeframes, and windows may be used to connect these

timeframes by overlapping multiple windows. The disadvantages of using windows are the loss of information and altered amplitudes that may occur. This is because pressure oscillations have large inconsistencies and windows may not include the whole peak. This will result in correct frequency, but with lower amplitude. Figure 2.5.11 shows how an original signal is affected by applying a hanning window. Using a smaller size on windows and a large overlap percentage will result in a more accurate analysis, but the disadvantages of having a higher accuracy is longer time consumption. MATLAB was used as a program to process the pressure measurements and perform the frequency analysis. MATLAB consists of different tools to help with the frequency analysis, and the chosen function for the FFT was the power spectral density. The used MATLAB script returns the root mean squared (rms) values of the pressure amplitudes for the different frequencies. There are also different types of window functions available in MATLAB. In this thesis the Hanning, also called Hann, window is used. One of the benefits of using the Hann window is that it results in very low aliasing, but the disadvantage is a broaden base at the frequency peak.

2.6 Deviation and error

To get a reliable result with a low uncertainty it is important to evaluate the goodness of the data. This evaluation is relevant when identifying and validating the results. Some of the variables that characterize a curve with a good fit are used later and presented in the equations below. The sum of squares due to error (SSE) measures the total deviation between the input (measured) values and the values of the fit curve. The R-square indicate at which extent the curve fits the variation of the measured values. A curve that is a good fit to the measured values is characterized with a SSE value close to zero, because this value indicates how small the random error component is [29]. For the value of R-square it is desired to obtain a value close to one, since it shows how much of the total variance that is included in the model. The standard deviation of the random component is defined as the Root Mean Square Error (RMSE). The SSE, SSR (Sum of Square of the Regression), SST (total sum of square), R-square, adjusted R-square and RMSE are given by the equations (2.6.17),(2.6.18),(2.6.19), (2.6.20), (2.6.21) and (2.6.22). The measured data value defined as y_i and w_i represents the weighting applied to each data point, often equal to one. The predicted value of the fitted curve is determined as \hat{y} , while \bar{y} is the averaged values from the observed data. To calculate the RMSE and adjusted R-square the variable v is necessary. The variable v is determined as the number of independent pieces of information regarding the data points (n) that are needed to calculate the sum of squares[29].

$$SSE = \sum_{i=1}^n w_i (y_i - \hat{y})^2 \quad (2.6.17)$$

$$\text{SSR} = \sum_{i=1}^n w_i (\hat{y}_i - \bar{y})^2 \quad (2.6.18)$$

$$\text{SST} = \sum_{i=1}^n w_i (y_i - \bar{y})^2 \quad (2.6.19)$$

$$\text{R - square} = \frac{\text{SSR}}{\text{SST}} = 1 - \frac{\text{SSE}}{\text{SST}} \quad (2.6.20)$$

$$\text{adjusted R - square} = 1 - \frac{\text{SSE}_{(n-1)}}{\text{SST}_{(v)}} \quad (2.6.21)$$

$$\text{RMSE} = \sqrt{\frac{\text{SSE}}{v}} \quad (2.6.22)$$

Chapter 3

Measurement preparations

3.1 Laboratory setup

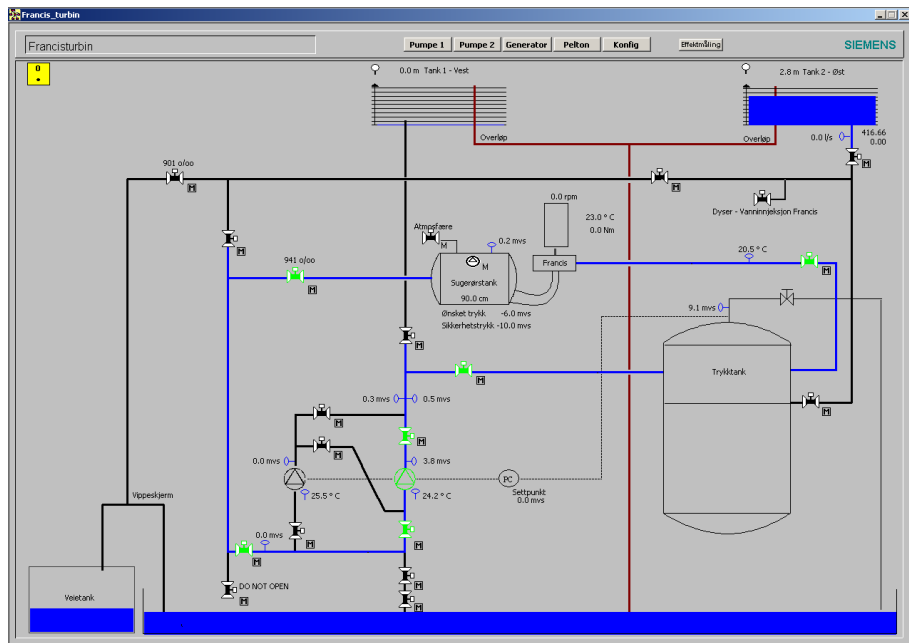


Figure 3.1.1: Francis rig closed loop show as the blue circuit with green valves

The Waterpower laboratory at NTNU consists of several test rigs for different types of turbines, but for this thesis the Francis test rig was the only rig operated. The Francis turbine in the test rig is designed by Professor Ole Gunnar Dahlhaug at the Waterpower laboratory, and is a modified replica of a 107.5 MW turbine installed at Tokke power plant. The Francis turbine consists of 14 stay vanes, 28 guide vanes and 30 runner vanes, where 15 of the runner vanes are split blades. The runner is connected to a 352 kW generator by a vertical shaft and a transparent draft tube cone is installed downstream of the runner. To transport the water

around in the rig one of total two basement pumps was used in the laboratory. The Francis test rig consists of two different loops, a closed and open loop, where I chose to perform my measurements using the closed loop (figure 3.1.1). The reason for this is because of the ability to control different parameters on the rig during operation, for example the head. The loop was setup to follow the international standard (IEC60193) with equipment calibrated and located accordingly.

As seen in figure 3.1.1 the closed loop consists of pumps, a pressure tank, turbine and a draft tube tank. Essential parameters for the closed loop are monitored and controlled by computers found in the laboratory control room. Several transducers are placed both in front, in and at the end of the turbine. Figure 3.1.2 shows the recommended location of the transducers according to the international standard. The standard strongly recommends that for pressure measurements the transducers should be placed at inlet and in draft tube cone, shown in figure 3.1.2 as p1, p2 and p3 [10]. If possible then transducers could also be placed in the vaneless space, further downstream and upstream of the turbine: p5, p4, p7 and p6. The chosen localization and types of transducers for the performed measurements are explained in table 3.1.1. According to the international standard the draft tube cone transducers are preferred located between 0.3 and 1.0 diameters from the low pressure side of the runner. After measuring on the Francis rig the upper cone transducer was located approximately 0.37 diameters from the runner, while the lower cone transducer was located approximately 1.08 diameters from the runner.

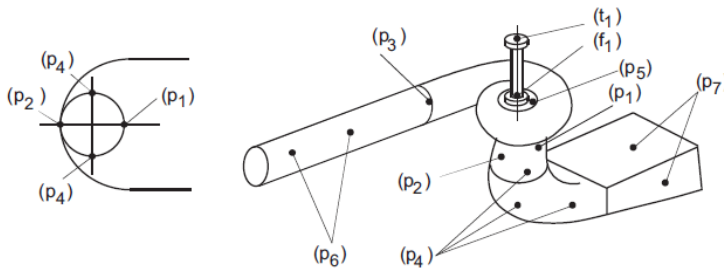


Figure 3.1.2: IEC60193 Pressure transducer placement [10]

Table 3.1.1: Pressure transducers used in the measurement

Transducer type	Pressure interval	Placement	Placement in figure 3.1.3
Druck <i>PTX1400</i>	0 – 10 bar g	Inlet, before spiral casing	1
Kulite <i>XTL</i> –190M – 7BARA	0 – 7 bar abs	First vaneless placement	2
Kulite <i>XTL</i> –190M – 3.5BARA	0 – 3.5 bar abs	Second vaneless placement	3
Druck <i>PTX1400</i>	0 – 4 bar g	Upper draft tube cone	4
Druck <i>PTX1400</i>	0 – 2.5 bar g	Lower draft tube cone	5
Druck <i>PTX1400</i>	0 – 10 bar g	Draft tube	6

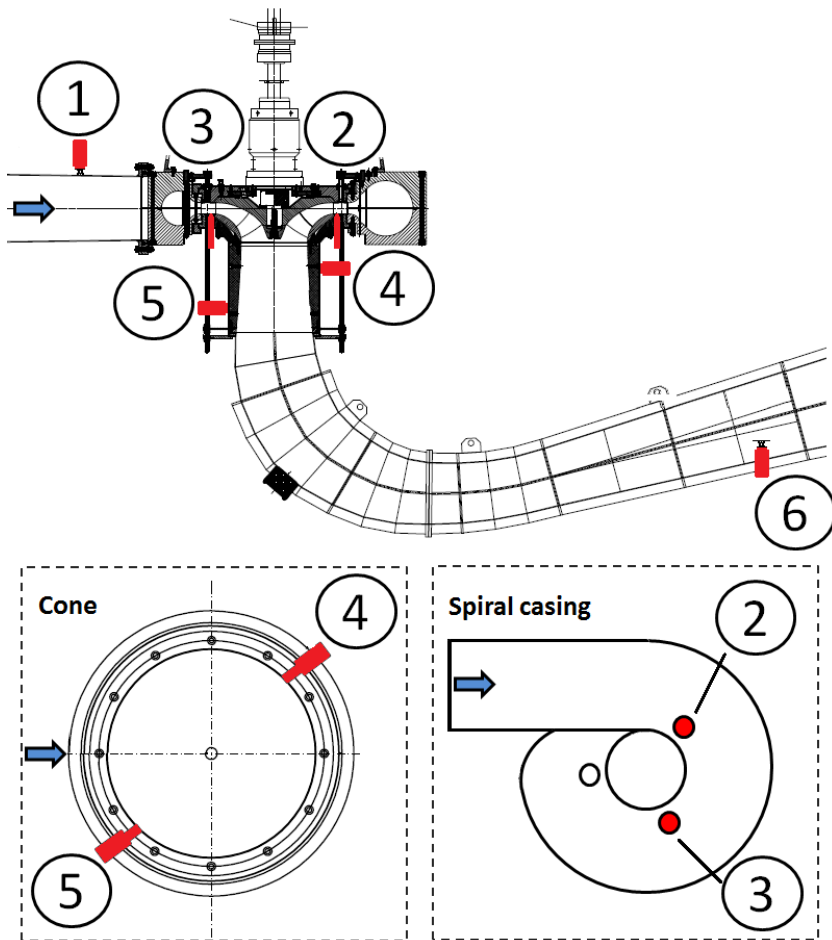


Figure 3.1.3: Pressure transducer placement on Francis rig at NTNU

It is necessary to connect different devices or programs to be able to analyze the signal from the pressure transducers. The laboratory setup is shown in figure 3.1.4 where the Druck pressure transducers are connected directly to a National Instrument DAQ USB log device. The Kistler pressure transducers are connected to an amplifier before connecting to the same DAQ device. This DAQ log device is then connected to a separate computer with a log program made in LabVIEW. Details about the different devices and programs are explained in table 3.1.2. As mentioned earlier the control room consists of multiple computers that monitor different operational values. In my measurements some of the most important are the head, guide vane angle, efficiency, rotational speed, generator torque, inlet pressure and differential pressure. During the pressure measurements both the stationary computers in the controlroom and a separate computer was used.

Table 3.1.2: Instruments used to process signal from transducers

Instrument	Type
Computer with LabVIEW	Dell Latitude E6540
National Instruments LabVIEW	Version 2012
Amplifier	Hottinger Baldwin Messtechnik DA12
National Instruments USB log box	NI-USB6211

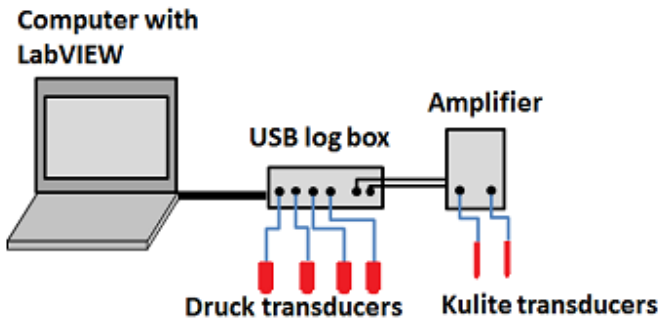


Figure 3.1.4: Setup for transducer equipment

3.2 Calibration

Calibration of the used equipment is necessary before any proceeded measurements, and every calibration in this thesis is performed on and with equipment found at the Waterpower laboratory at NTNU. Table 3.2.3 shows the different instruments used during the calibrations, where the calibration documents are located in Appendix G. To calibrate the different instruments a calibration program made by a previous master student at NTNU, Håkon Hjort Francke, was used.

Table 3.2.3: Calibration instruments

Calibration instruments	Instrument type	Interval	Output signal
Hydraulic deadweight tester	GE Sensing <i>P3223 – 1</i>	1 – 350 bar g	2 – 10 V
National Instruments USB log box	<i>NI – USB6211</i>	4 – 20 mA +/- 10 V	
Weighing instrument for pressure tank	Hottinger Baldwin Messtechnik <i>AB22A</i>		
Calibrated equipment	Instruments used	Programs used	Appendix reference
Pressure transducers	Hydraulic deadweight tester	LabVIEW	G.1 & G.2
Weighing tank	Manual weights & Weighing instrument for pressure tank	LabVIEW	G.3
Flowmeter	Weighing tank & Weighing instrument for pressure tank	LabVIEW	G.4
Friction torque	Manual weights	LabVIEW	G.5
Generator torque	Manual weights	LabVIEW	G.6

3.3 Execution of pressure measurements

There are some differences between a hydropower plant and the Waterpower laboratory at NTNU. Hydropower plants use both guide vanes and the main valve regularly to control the inflow to the turbine, and a diversion valve is needed to equalize the pressure on both sides of the main valve. The Waterpower laboratory uses mainly pumps to control, and change the flow and pressure throughout the conduit. Excitation of the generator is often used during plant startup and when the rotational speed of the runner is 90% of synchronous speed. Synchronous speed is achieved when the rotor of the machine rotates at the same speed as the magnetic field [9]. Since the laboratory needs pumps to transport the water around in the loop and create the head this leads to a different startup procedure at the laboratory and before the measurements. Therefore the rig is started according to laboratory procedures made by previous master student Andrea Stranna [34] and can be seen in Appendix C. The measured start and stop procedures are performed later when the accordingly conditions are achieved. The start and stop measurements of the Francis turbine test rig are performed with the basement pump running constantly to maintain a head in the water conduit.

The total time period to execute the stop and start measurements was determined to 240 seconds and the measurement interval was set to 60 second with a sampling rate of 1 000. The used LabVIEW script has a continuously loop function to prevent the loss of pressure values during the total log time. The result of this was four

files with measurement data consisting of 60 000 pressure values per transducer for each file.

Since the Francis rig is running at BEP before the measurements were proceeded the sequence was to perform a stop procedure followed by system stabilization and then a start procedure. This performed sequence was based on conversations with doctoral student Joakim Gogstad and Statkraft's Erik Wiborg. The logging series is started with operation at BEP before guide vanes are slowly reduced; this is to prevent large water hammer effects. The guide vanes are closed until the generator produces 0 MW, this is when the amount of water through the turbine is equal the amount of water that is needed to keep the runner at synchronous speed. The generator is then switched off before guide vanes are being fully closed. If the generator is running while the guide vanes are continued to close the generator would use power from the grid to maintain the balanced rotational speed. This is an unfavorable situation both for the runner and economically. When closing the guide vanes completely the rotational speed of the runner is reduced to zero rpm, gradually stopping the turbine. The stabilization of the turbine lasts for about 30 seconds to ensure a stabilization of the system. After this stabilization the startup procedure can be initiated by slowly opening the guide vanes, and as a result of this the runner slowly starts to rotate. During the opening of the guide vane the generator would be switched on when synchronous speed is achieved. After the generator is switched on a short stabilization is performed for a couple of seconds before continuing to open the guide vanes until BEP is achieved.

The performed stop and start procedure is listed below to shortly describe the different steps done during the measurements.

Stop & start procedure of model Francis turbine

1. Turbine operation at BEP
2. Closing guide vanes slowly until the generator produces 0 MW
3. Switching off the generator
4. Fully closing the guide vanes
5. Stabilization of the turbine and water conduit
6. Opening the guide vanes slowly
7. Switching on the generator at synchronous rpm
8. A short stabilization of the turbine
9. Opening the guide vanes until BEP is achieved
10. Turbine stabilization at BEP

Chapter 4

Results

4.1 Expected frequencies

Table 4.1.1: Calculation of the expected elastic oscillations

Variable	Value	Comment
Elasticity of water, E_w	$2.19 \cdot 10^9$ Pa	Source of value: [37]
Elasticity of pipe material, E_p	$2.10 \cdot 10^{11}$ Pa	Source of value: [18]
Pipe diameter, D	0.35 m	
Water density, ρ	$998.4 \frac{kg}{m^3}$	Source of value: [37]
Pipe thickness, e	0.004 m	
Calculation	Value	Comment
Propagation speed, c	$1070.95 \frac{m}{s}$	
Upstream water hammer frequency, f_{wh-up}	15.21 Hz	
Downstream water hammer frequency, $f_{wh-down}$	38.25 Hz	
Mass oscillation frequency, f_{mass}	0.17 - 0.27 Hz	Upstream & downstream

The elastic oscillations and equation for calculating the propagation speed was introduced in section 2.4.5. The values listed in table 4.1.1 are used to calculate the propagation speed in equation (2.4.14). There are many uncertainty factors regarding these values due to different assumptions made regarding the Francis rig. It is assumed that the pipe thickness and diameter is constant through the rig and the water density and elasticity stays constant during turbine operation. Equation (2.4.13) also includes the variable L, which is the length from the point where change in pressure is initiated to the closest free water surface. In the Francis rig this is the pressure tank located upstream of the turbine or the surge tank located downstream of the turbine. The distance between the pressure tank and runner was estimated to be approximately 17.6 m and the distance between the runner and surge tank is approximately 7 m. This estimation was done by measuring parts of the Francis rig with measuring tape and with laboratory sketches

in the program Inventor. These values are therefore subject to uncertainty. By inserting these values in equation (2.4.13) the calculated values are presented in table 4.1.1. During the start and stop procedures the water level in these tanks are varying and therefore changing the previously known length. To account for this variation an interval of uncertainty is added resulting in a frequency interval between 14.55 - 15.56 Hz upstream and 33 - 41 Hz downstream of the turbine. The length independency is also a reason for the mass oscillation frequency interval, but due to nearby frequency peaks they are combined into an interval between 0.17 and 0.27 Hz.

Table 4.1.2: BEP operation

Type	Value	Unit
$n_{generator}$	320	rpm
n_{runner}	320	rpm
n_{pump}	440	rpm
n_{ED}	0.184	-
Q_{ED}	0.154	-
$\alpha_{guide\ vanes}$	10.371	°
H_{model}	10.4	m
$H_{prototype}$	408	m
Q_{model}	0.189	$\frac{m^3}{s}$
$Q_{prototype}$	33.6	$\frac{m^3}{s}$

As mentioned earlier the stop and start sequences are proceeded from operation at BEP. Table 4.1.2 shows the different values measured at BEP operation. These values are essential in calculating the expected frequencies and further analyzing the FFT results. The pressure pulsations that are expected during the start and stop operation are the pulsations presented in Chapter 2.4 and the frequency of these oscillations are listed up in table 4.1.3. During the stop and start procedure the rotational speed of the runner varies. Since some of the expected frequencies are dependent on the runner speed they are also varying, this is making it more difficult to locate the expected frequencies. This is a result of the connection between the generator speed controlling the runner speed when it is switched on. When the generator is switched off the frequencies in table 4.1.3 are expected to be reduced or disappear.

Table 4.1.3: Expected frequencies

Frequency [Hz]	Type of frequency	Expected peak location
5.33	Runner frequency	Close to runner
160	Runner vane frequency	Vaneless space
149.33	Guide vane frequency	Runner or vaneless space
1.48 - 1.78	Rheingan frequency	Draft tube cone
14.55 - 15.56	Upstream water hammer frequency	Upstream runner
33 - 41	Downstream water hammer frequency	Downstream runner
0.17 - 0.27	Mass oscillation frequency	Water conduit

4.2 Pressure measurements analysis

Before using the chosen method for identifying the pressure oscillations it was necessary to divide the pressure measurements into different parts. The reason for this is to minimize the possibility for interference, obtain reliable results and separate the start and stop procedure. The pressure measurements were divided into four parts regarding the different dynamic procedures. These four parts are firstly start and stop, and further into if the generator is switched on or off (abbreviated gen on / off). Table 4.2.4 and figures 4.2.1 and 4.2.2 show how the pressure measurements were divided into the different procedures. Since the pressure measurements went from a stop procedure to a start procedure the order of the results from the FFT analysis is: stop with the generator, stop with generator off, start with generator off to start with the generator on. It is only these four parts that are used and analyzed further, a separate steady state measurement at BEP and part load was also executed to compared results, these are found in Appendix A.1.

Table 4.2.4: Measurements divided into dynamic procedures

Procedure	Time interval beginning [ms]	Time interval ending [ms]	Number in figure 4.2.1
BEP	0	30 000	1
Stop gen on	30 000	71 500	2
Stop gen Off	73 000	94 000	3
Stabilization	94 000	140 000	4
Start gen Off	140 000	161 000	5
Start gen On	162 000	210 000	6
BEP	210 000	240 000	7

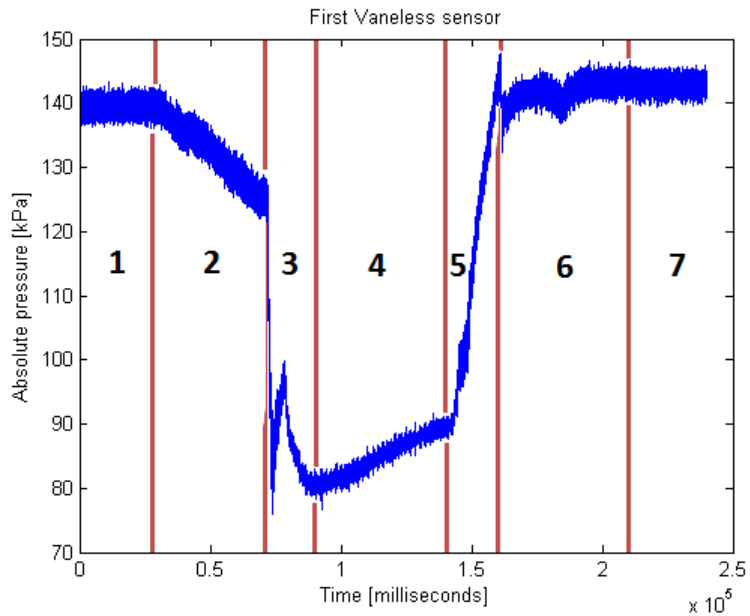


Figure 4.2.1: Dividing pressure measurement into the different procedures

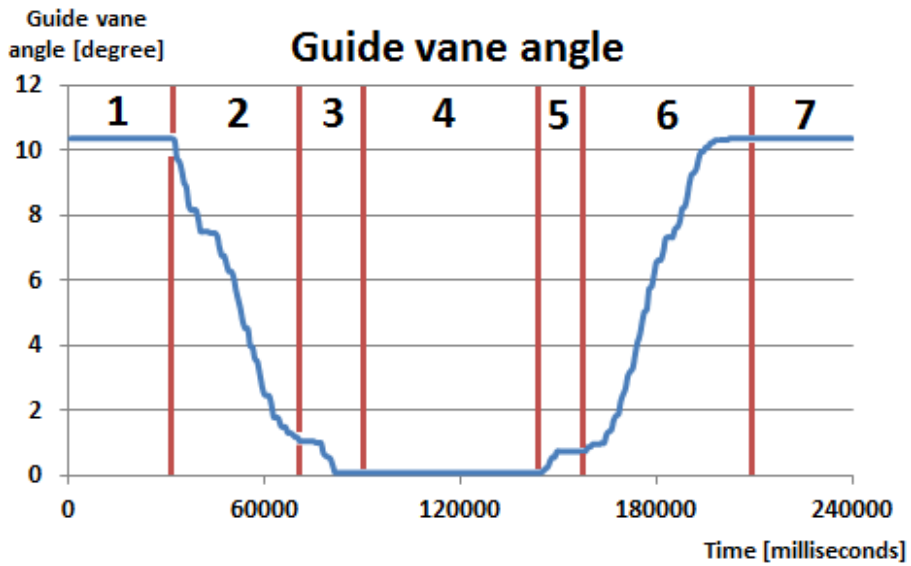


Figure 4.2.2: Variation of the guide vane angle during the different procedures

4.3 Method for identifying pressure oscillations

4.3.1 Execution of method

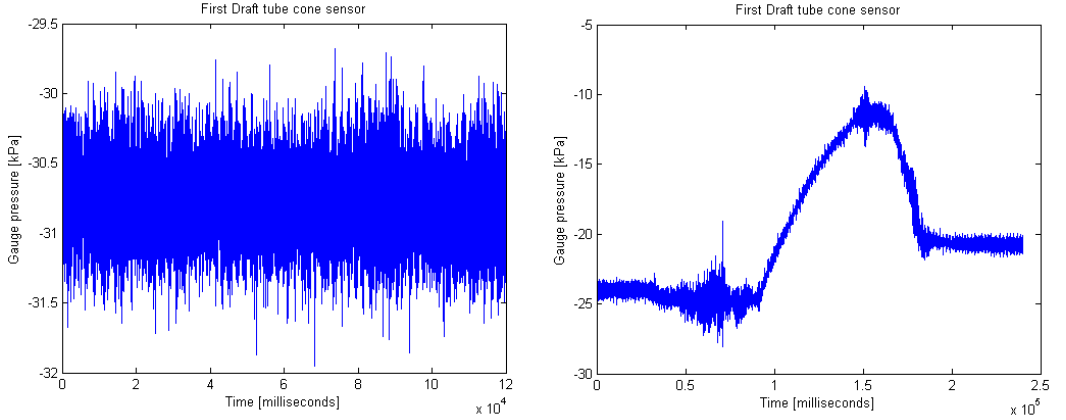


Figure 4.3.3: Upper draft tube cone measurements, BEP and stop & start

The pressure measurements during static load conditions are different to dynamic load conditions, where the main difference is the gradient or total change in pressure. This can clearly be seen in the measured figure 4.3.3 which is the pressure measurement during BEP operation (left figure) compared to a stop and start operation (right figure). There are considerable differences when comparing these two pressure measurements, where the dynamic pressure result in challenges regarding a FFT-analysis. An important aspect to perform a FFT-analysis successfully is the desire for a small pressure gradient, as seen during BEP operation. Since the start and stop procedures does not fulfill this requirement, a FFT-analysis is performed on these pressure values will only result in large interference.

To be able to identify pressure oscillations from the FFT-analysis the suggested method focused on creating small pressure gradients similar to BEP operation. Firstly the method consists of creating a curve that fits the pressure measurements by using the MATLAB application Curve Fitting Toolbox. A picture of the Curve Fitting Toolbox application is found in Appendix B. This application provides a function for fitting curves to given input data and different linear and nonlinear regression models can be utilized [28]. In addition to the fit curve the Curve Fitting Toolbox also shows the magnitude of error between the two curves, the different parameters of error are mentioned in section 2.6. An example of a fit curve from the Curve Fitting Toolbox is shown in figure 4.3.5, where the measured pressure is shown in blue and the red line is the fit curve.

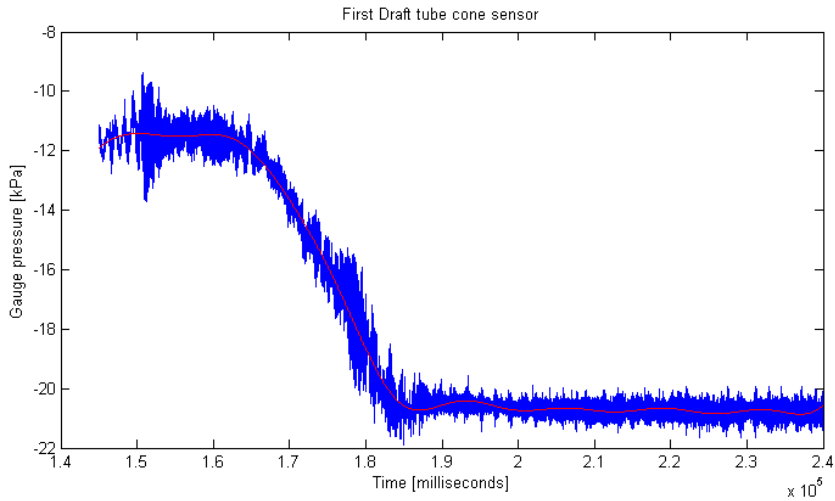


Figure 4.3.4: A curve fit to the pressure measurements at upper draft tube cone

After finding a suitable curve that fits the pressure measurements the difference between them was calculated to obtain a small pressure gradient. This was done by subtracting the measured pressure with the estimated curve. This resulted in a fairly small pressure gradient and a FFT-analysis may now be executed. An example of the pressure difference between the measured values and the found curve is shown in figure 4.3.5. By performing a Fourier transform on this pressure difference it is possible to identify different pressure oscillations that occur during the start and stop sequences. Figure 4.3.6 shows the result of the FFT-analysis with multiple frequency peaks and pressure amplitudes for the transducer located at the upper draft tube cone.

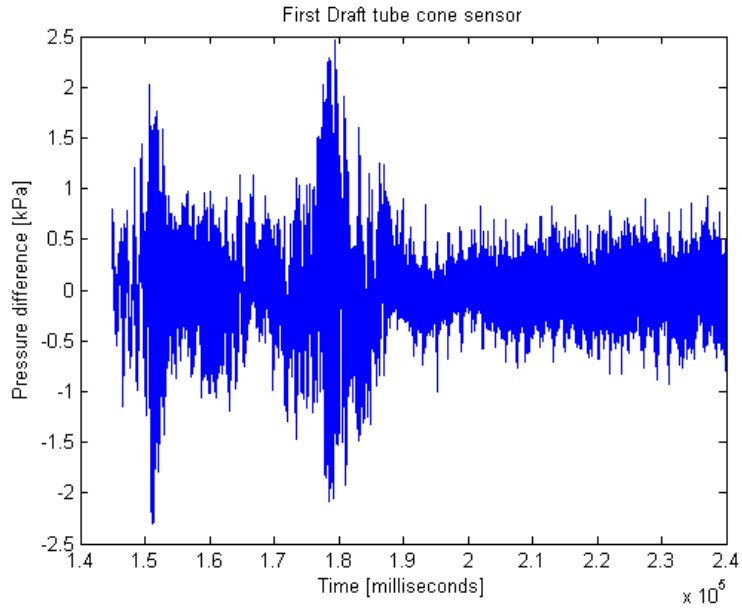


Figure 4.3.5: Pressure difference between measured values and estimated curve

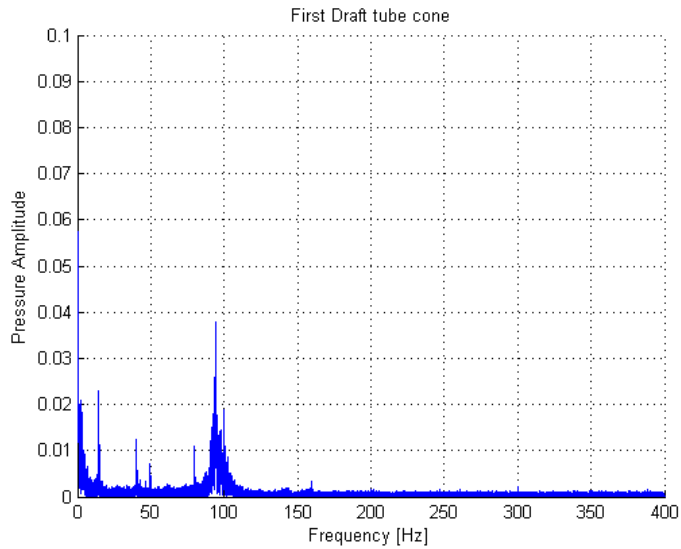


Figure 4.3.6: Fourier transform performed on the pressure difference

4.3.2 Error and uncertainties in suggested method

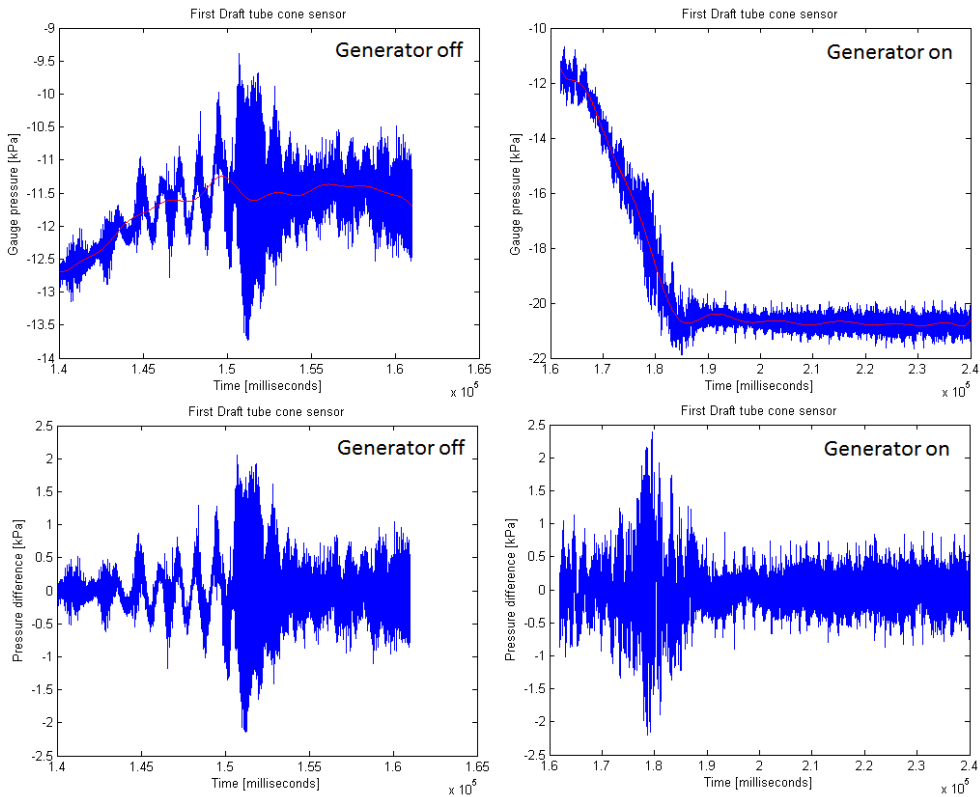


Figure 4.3.7: Fit curve and pressure difference, startup with generator off & on

When the method for identifying pressure oscillations was performed the error between the measured pressure and the fit curves was determined. From chapter 2.6 the different measures of error are presented in addition to the desired value for a estimated curve with a goodness of fit [29]. Due to the large variation regarding the pressure fluctuations there were some differences on how each estimated curve fits the measured pressure fluctuations. It is important to consider the error values related to goodness and not only the visual aspect of how well the curve fits. An example of this can be seen in figure 4.3.7. These figures shows the pressure measurement and the fit curve of the startup procedure at the upper draft tube cone transducer with the generator on or off, with the pressure difference presented below. By visual inspection the estimated curve for the generator on has a better fit because it follows the pressure gradient compared to when the generator is switched off. Further looking at the pressure difference of the values with the generator on have larger maximum and minimum values compared to when the generator was

off. Figure 4.3.8 charts the error values measured by the Curve Fitting Toolbox. An interesting observation is that the sum of squares due to error (SSE) is largest when generator is on and therefore applying worst fit for the visually best fitted curve. By closer inspection the R-square and adjusted R-square for when the generator is on has a value very close to one. This indicates that most of the total variance is accounted for by the model and that it is a good fit [29]. The RMSE is preferred to be as close to zero as possible and figure 4.3.8 show that the curve has a better fit when the generator is switched on compared to when it is off.

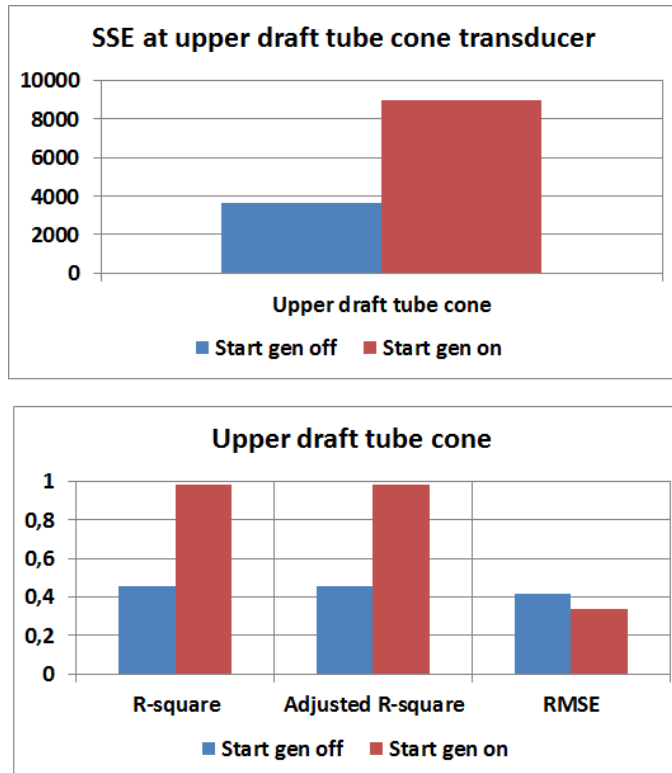


Figure 4.3.8: Values for goodness of fit for startup. Upper cone measurements

Figure 4.3.9 charts all values of SSE, R-square, adjusted R-square and RMSE for every transducer and for all the different procedures (stop & start and generator on & off). There are some uncertainties regarding the goodness of the found curves since most transducers have large SSE values and this value is preferred close to zero. The largest value of SSE is at 1 047 000 and is downstream the draft tube during the start up with the generator switched on. The lowest value of SSE is 807.4 and is the lower draft tube cone during stop procedure when the generator is switch off. Both these values are very large and above the optimal zero value. By looking at the R-square, adjusted R-square and RMSE it is clear

that the draft tube transducer has worst values among all the estimated curves and therefore having the worst fit. For some procedures the inlet, vaneless and cone transducers have good R-square and adjusted R-square values, but the cone transducers are the only one that stand out regarding low RMSE value (smaller than 0.5). Since every transducer have varying goodness of fit regarding the type of error and procedure in focus it is important to bear this in mind regarding uncertainties in the FFT-analys. The suggested method for identifying pressure oscillations is further discussed in section 5.3.

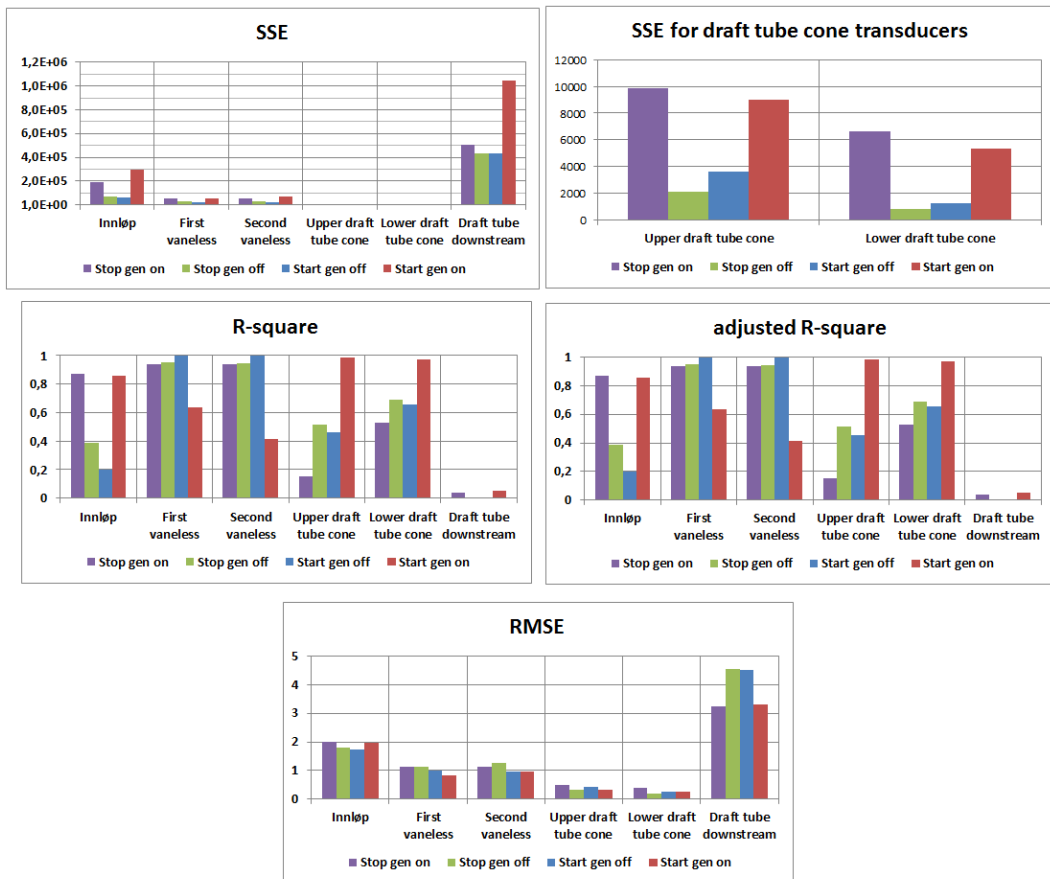


Figure 4.3.9: Values for error measurements

4.4 FFT results

The FFT results are presented in a waterfall plot with the frequency on the x-axis, rms values of the pressure amplitude (unit kPa) on the z-axis and the different dynamic procedures as y-axis. The different procedures are marked in different colors for each procedure. The measured frequency peaks are presented by transducer and is further discussed in section 5.2. Pressure measurements during BEP was also performed and Fourier transformed, the results from this FFT are located in Appendix A.

4.4.1 Inlet transducer

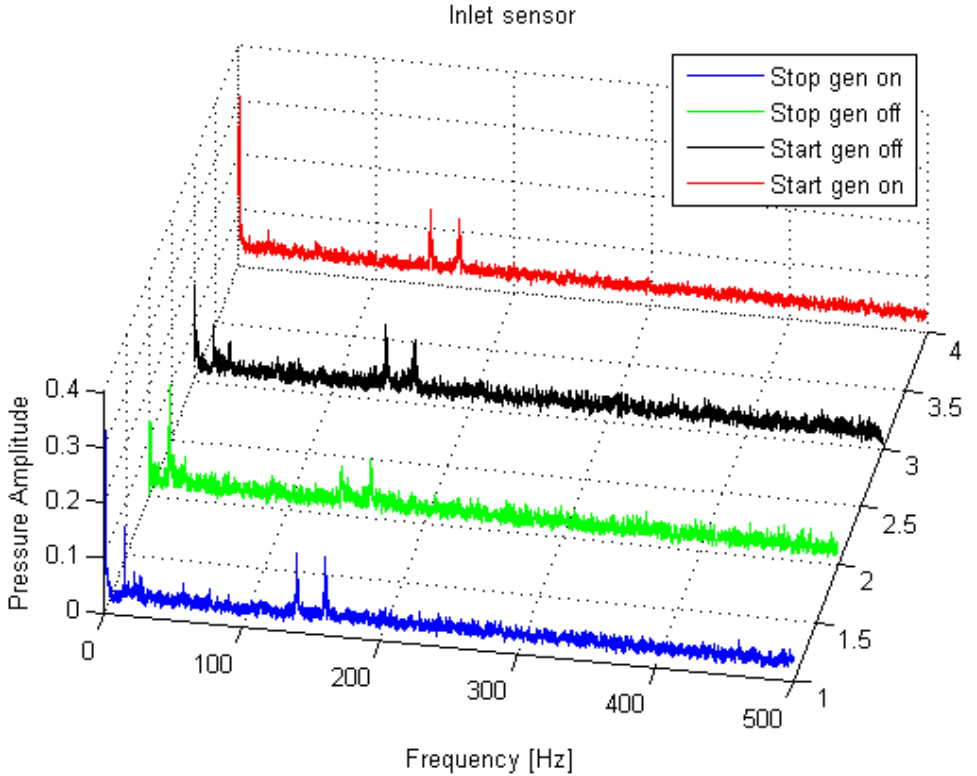


Figure 4.4.10: Frequency peaks at inlet transducer

There are some frequencies that was experienced from the inlet sensors. Frequencies related to transducer interference with pronounced peaks at 139 Hz & 160 Hz during the stop and start sequence. These frequencies were also observed during BEP and part load operation. There was a peak observed at 14.7 Hz, this frequency was

smaller during the startup sequence. Some other peaks observed are 21, 56 and 75 Hz when generator was on and 26 Hz during both stop procedures and startup when generator was off. Frequencies below 1 Hz occurred during the measurements, and these frequencies are related to high uncertainty and are often neglected. None of these low frequencies were due mass oscillations. However figure 4.4.10 shows that these low frequencies results in the highest pressure amplitudes at the inlet when generator was on. This may indicate an unoptimal fit curve due to level of interference.

4.4.2 First and second vaneless transducers

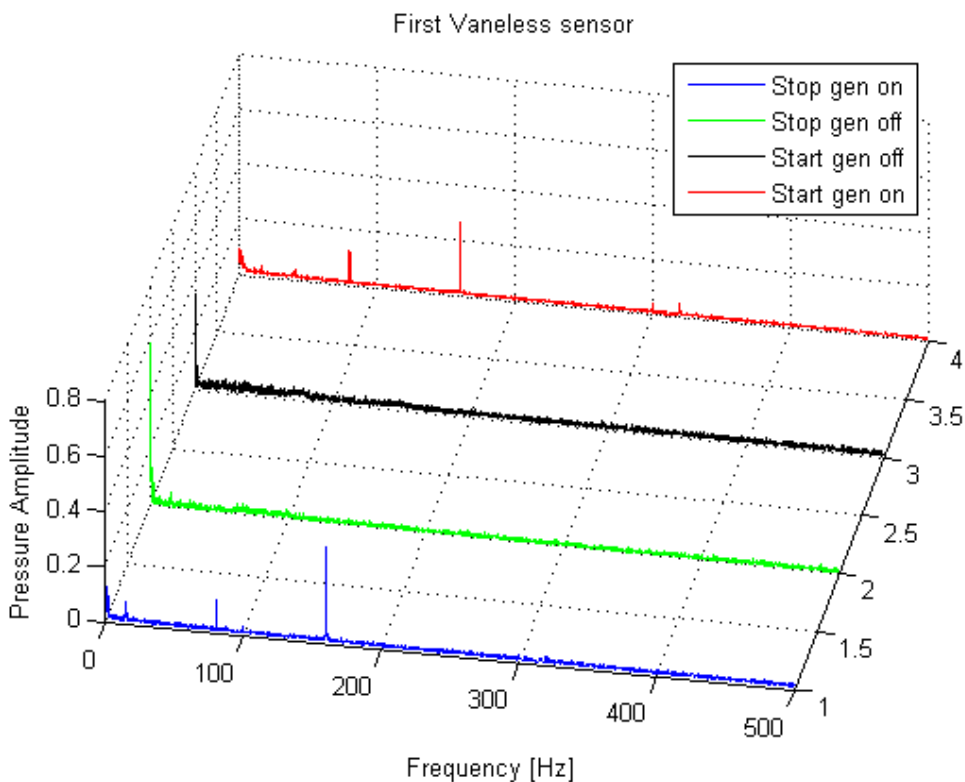


Figure 4.4.11: Frequency peaks at first vaneless transducers

The most significant frequency seen from the vaneless sensors was the runner vane frequency at approximately 160 Hz. The frequency peak at 80 Hz was the half harmonic runner vane frequency, while the small peak at 319.5 Hz was the second harmonic runner vane frequency. Both the second and half harmonic had larger amplitude during the start procedure compared to the stop sequence. Other fre-

frequencies were the 14.7 Hz frequency as well as the low frequencies. During the stop procedure the Rheingan frequency was experienced. Some smaller amplitudes was observed at 7.333 and 300 Hz as well as between 33 - 41 Hz. The FFT results for the vaneless transducers show similarity regarding frequency peaks. The only difference when comparing the amplitude for the two vaneless sensors is that the frequencies measured at the second vaneless sensor is larger or equal to the first vaneless sensor.

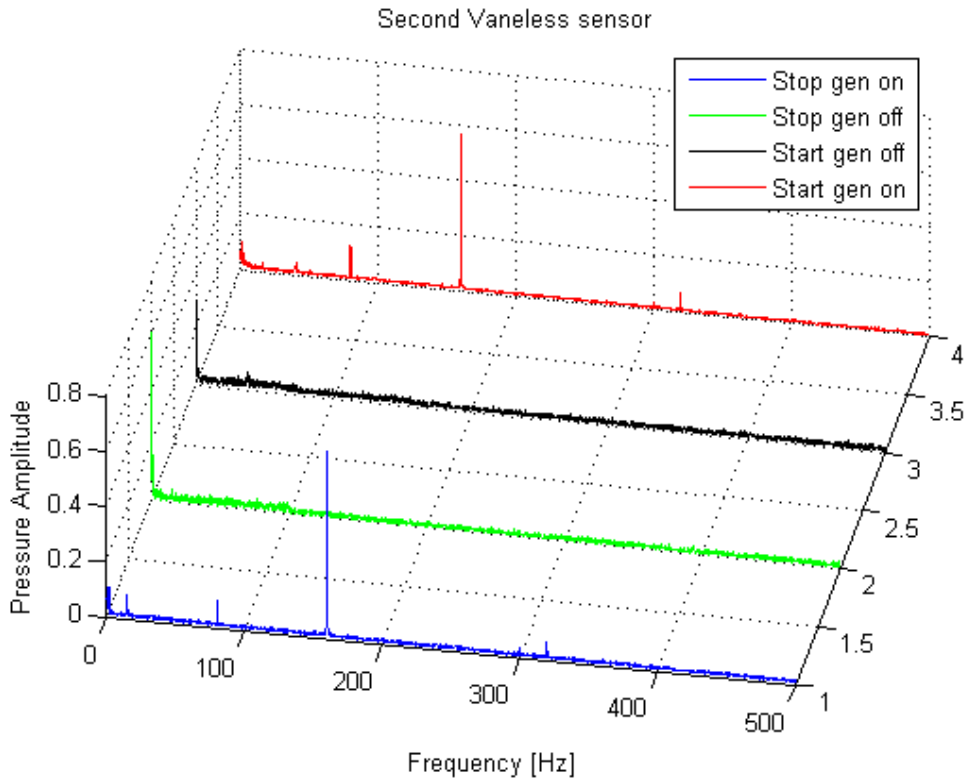


Figure 4.4.12: Frequency peaks at second vaneless transducers

4.4.3 Upper draft tube cone transducer

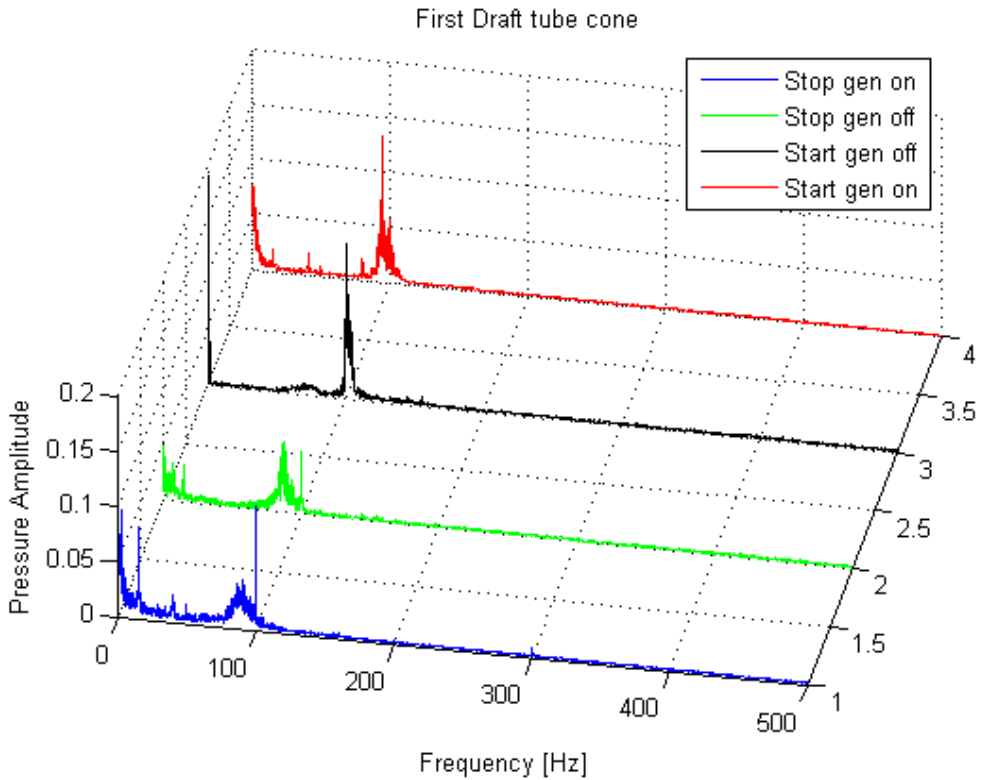


Figure 4.4.13: Frequency peaks at upper draft tube cone transducers

For the first sensor in the draft tube cone there were some different frequencies depending on the procedure. The frequencies at 14.7 Hz and at 39 Hz had peaks in both procedures, but only when the generator was on. The most dominant frequency at this sensor was located at 100 Hz for all procedures and the Rheingan frequency when generator was on. Frequency peaks at 49, 80, 160 and 300 Hz was experienced when the generator was on, while 86 Hz occurred during both stop procedures and 94 Hz during start procedure. These broaden peaks may be the cause of spectral leakage. A peak at 7.333 Hz occurred when the generator was off during the stop procedure.

4.4.4 Lower draft tube cone transducer

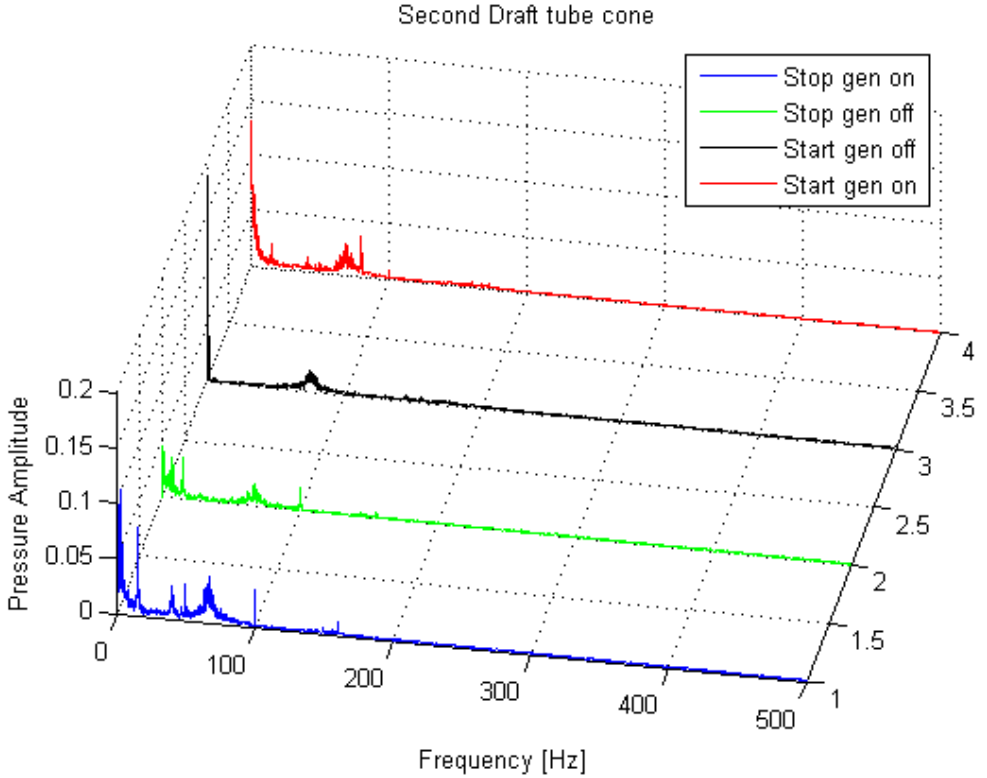


Figure 4.4.14: Frequency peaks at lower draft tube cone transducers

For the second sensor in the draft tube cone there were some different frequencies depending on the procedure. The frequencies at 14.7 Hz and at 39 Hz had peaks in both procedures, but only when the generator was on. The most dominant frequency at this sensor was the Rheingan frequency when generator was on. Frequency peaks at 49 and 160 was experienced when the generator was on. In addition peaks at 67 and 100 Hz was experienced for every procedure except start with the generator off which has a peak at 75 Hz. These broaden peaks may be the cause of spectral leakage. The same peak at 7.333 Hz was experienced when the generator was off during the stop procedure.

4.4.5 Downstream draft tube transducer

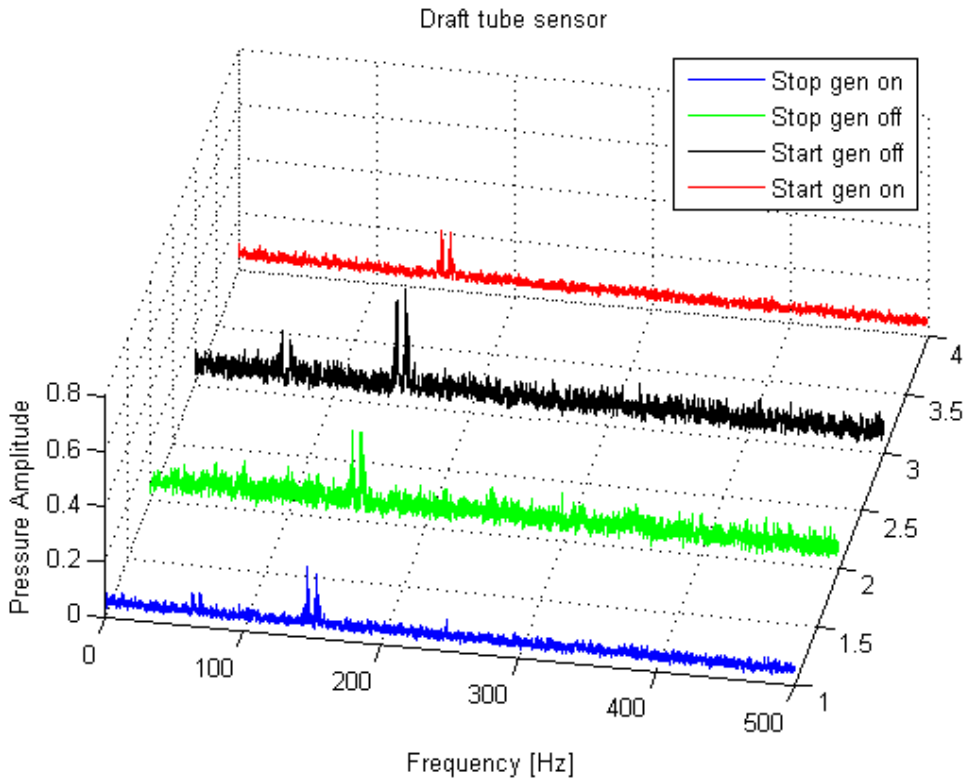


Figure 4.4.15: Frequency peaks at downstream draft tube transducers

This transducer showed issues related to interference, but there were some frequencies that were similar to the inlet transducer. The two frequency peaks found in every procedure and operation was found at 146.6 Hz & 152.7 Hz during the stop sequence and 147.1 Hz & 153.3 Hz during the startup sequence. Frequency peaks occurred at 68.6 and 63.1 Hz during all procedures except start with the generator on, while a peak at 96.6 Hz was experienced during stop when generator was off.

Chapter 5

Discussion

5.1 Post measurement experience

After the pressure measurements were proceeded there were some experiences and results that are worth mentioning regarding the uncertainties in the performed measurements. When the stop procedure was performed and the turbine settles to a standstill, the draft tube cone was emptied of water. This is because of the negative pressure in the draft tube surge tank and with the pump operating. The result of this was that the draft tube cone needed to be filled with water during the startup procedure when the turbine began to rotate. The guide vanes were at approximately 6° when the cone became completely filled with water. This may have had an effect on the pressure measurements from the draft tube cone transducers because of the time period the draft tube cone was not completely filled with water. This may also explain any different results for the start procedure compared to the stop procedure. One of the performed pressure measurements was filmed and some screenshots of this film are located in Appendix D.

There were some uncertainties regarding the chosen transducer placement on the Francis rig. The sensors were placed according to the IEC60193, but additional transducers should be calibrated and attached to the rig to verify results. By attaching more transducers in the draft tube cone it may intercept the pulsations occurring in the chaotic flow that was experience during the startup procedure. From the executed measurement it was experienced that the Druck transducers at the inlet and draft tube had individually two interference peaks with a large amplitude and these transducers should be replaced by transducers with a lower pressure range. These significant interference peaks were not found for the cone transducers which are designed for a lower pressure range. It should also be stated that the draft tube transducer experienced a lot of overall interference compared to the other transducers and it should be relocated to a more optimal place. It is believed that the main reason for this is because of transducer placement, and this should be reviewed to find a more suitable location to perform pressure measurements in the draft tube. Since the basement pump was constantly running during the start and stop procedure the inlet transducer may intercept the pump impeller rotation. It should be noted that if this transducer intercepts this frequency, it would occur for every procedure, and running with an open loop may remove this

interception. In section 3.1 the reason for choosing closed loop was explained, but further experimentation regarding open loop and pressure oscillations should be executed to compare the oscillations regarding both loops.

When analyzing the FFT results it was not surprising that when the generator was switched off the expected frequencies that are dependent on the runner rotation disappeared. Since the generator was turned off the rotational speed either increased or decreased, causing these frequencies to become higher or lower than the expected frequency. The runner also experiences a large speed variation in the transition between when the generator was switched off and the stabilization period. This is because when the generator is turned off the runner speed is increased due to the flow, but when continuing to close the guide vanes the flow is reduced before it is so little that the runner stops. The results did not show enhanced pressure amplitudes or interfering frequencies due to the speed variation in the explained transition. There were some issues when logging the turbine speed during the start and stop procedures and this was when the runner was under 100 rpm. These issues and a possible solution are located in appendix E.

5.2 Pressure oscillation frequencies

5.2.1 Expected frequencies

Runner vane frequency

The frequency with the highest pressure amplitude was the runner vane frequency at 160 Hz. The peaks of these frequencies are mainly found in the vaneless space, where the highest and most significant peak are found with the generator on. There were also experienced peaks at 80 and 320 Hz during the start and stop procedures. These frequencies are half and twice the runner vane frequency, resulting in the half and second harmonic frequency. The 80 Hz was also observed in the lower draft tube cone, but here it is most likely the second harmonic of the downstream water hammer frequency at around 40 Hz. The runner vane frequency was only seen when the generator was switched on, or else assumed small enough to be neglected or non-existing. An important observation is that the 160 Hz frequency was also found at the inlet, but the reason for this is due to the interference from the inlet pressure transducer. This is further explained in section 5.2.2.

Rheingan frequency

The Rheingan frequency showed a difference in pressure oscillations between the stop and start sequence. It was expected that the stop and start measurements would have fairly similar results, but the results regarding the stop procedure were approximately twice the size compared to the start measurements. The reason for this is believed to be a result of the emptied draft tube cone after turbine standstill,

explained in section 5.1. A evident visual swirl was not seen during the stop or start procedure.

Runner frequency

The FFT analysis showed a non-existing peaks regarding the runner frequency located at 5.33 Hz. It is beneficial that this frequency was low or approximately non-existing to ensure that the runner does not have any faults.

Guide vane frequency

The guide vane frequency at 149 Hz was similar to the runner frequency. The non-existing or low fluctuations at this frequency show that the guide vane frequency was hardly found by the transducers. Einar Kobro mentioned in his doctoral thesis that the guide vane frequency was not seen by the vaneless space transducers, but it was easily measured along the runner blades. This can be explained by the wake hitting the high and low pressure sides of the runner blades, illustrated in figure 5.2.1. It is therefore expected that the largest peaks of this frequency are located along the runner blades. This may explain why the measurements had no dominating peaks at this frequency and this need to be taken into consideration regarding further improvement of the instrumentation.

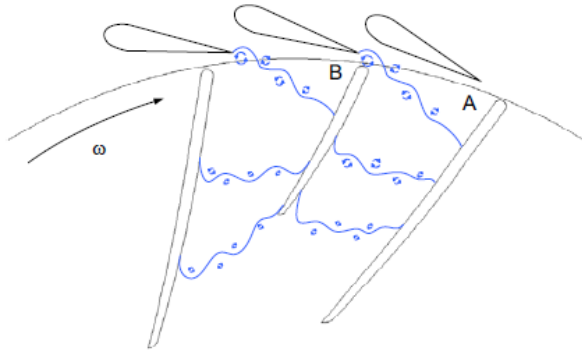


Figure 5.2.1: Wakes hitting the runner blades [23]

Water hammer frequencies

The frequencies experienced between 14.55 - 15.56 Hz and 33 - 41 Hz were the upstream and downstream water hammer frequency. These frequencies were caused by pressure waves traveling to the upstream pressure tank or draft tube surge tank. Both these frequencies have peak values either upstream or downstream of the turbine. The upstream water hammer frequency had the largest value at the inlet before gradually reducing in size through the turbine and to the draft tube. The downstream water hammer frequency was opposite with the largest values

in the draft tube cone and being reduced towards the inlet transducer. It was difficult to find a significant peak at the draft tube transducer due to the high interference in the FFT-analysis. The measurements showed the highest peak at the lower draft tube cone and the trend would indicate a similar or higher peak at the draft tube with a different transducer with little interference. Both water hammer frequencies showed an expected trend with the location of highest and lowest amplitudes upstream or downstream of the runner.

It is important to bear in mind that there are uncertainties regarding this frequency, mostly due to the assumption made in the calculations in section 4.1 and the varying water level in both upstream and downstream tanks. Since the variation of these water levels were not measured, a deviation regarding the frequency must be assumed. The water hammer frequencies were experienced in the expected frequency interval, but to get accurate frequency measures an analysis of the Francis rig and water level variation in the tanks should be executed to verify the used variables.

Mass oscillation frequency

The mass oscillation frequency was found in section 4.1 to be under 1 Hz. As explained earlier in section 4.4.1 this frequency is often under the influence of interference. Therefore the analysis of the frequency peak amplitudes are often neglected due to the high uncertainty regarding interference. The vaneless transducers were the only sensors that had frequency peaks between 0.17 - 0.27 Hz, and these peaks were only experienced during the stop procedures. The other transducers often measured peaks below and above the expected mass oscillation frequency which show the uncertainty regarding these low frequencies.

5.2.2 Unexpected frequencies

Transducer Interference

The pressure transducers located at the inlet and downstream draft tube are both Druck PTX1400 with a range from zero to ten bar gauge pressure. The measurements showed that these pressure transducers experienced interference during any turbine operation. The inlet transducer had two interference peaks at approximately 140 and 160 Hz, while the draft tube transducer had two interference peaks at approximately 147 and 153 Hz. Similar interference was not experienced on the other Druck transducers located in draft tube cone. A reason for this may be the lower pressure range, making them more optimal for pressure measurements under the performed start and stop conditions. No interference was found in the Kulite transducer measurements either.

300 Hz

The pressure oscillations at 300 Hz are a result of the three-phase rectifier that propagates through the generator and runner. The vaneless space transducers have the highest peaks at this frequency, which is because they are the transducers closest to the runner. Since this frequency is a result of the rectifier, the peaks only exist when the generator is on and disappear when the generator is stopped. The three-phase rectifier experiences six drops per signal period and results in fluctuations with six times of the 50 Hz grid frequency [22].

100 Hz

The 100 Hz frequency was observed in the draft tube cone during the pressure measurements. The upper transducer experienced this during every procedure, while lower transducer experienced this frequency for every procedure except startup with generator off. This frequency coincide with the third harmonics of the downstream water hammer frequency, approximately $3 \cdot 33$ Hz. This frequency can also interact with other observed frequencies and harmonics, and cause a higher pressure amplitude at 100 Hz. It should therefore be noted that this frequency is also the one-third harmonics to the three-phase rectifier and second harmonics of the grid frequency.

96 Hz

This peak occurred only at upper cone transducer during startup with the generator switched on. The reason for this peak coincide with the third harmonics of the downstream water hammer frequency, approximately 33 Hz. The 96 Hz peak may also be the result of a moved peak due to the close occurrence to the 100 Hz peak, which also occurs in the upper cone transducer. This may be caused by the chaotic flow in the draft tube cone during the startup procedure.

48 & 50 Hz

These frequencies were also experienced in the draft tube cone and were believed to be the half harmonic frequency of 96 and 100 Hz. The 50 Hz frequency is also related to the original grid frequency

63 – 68 Hz

The frequency interval between 63 and 68 Hz was occurring at the lower draft tube cone and is believed to be the second harmonics of the downstream water hammer frequency. This frequency was often affected by spectral leakage, causing a frequency interval and different peak amplitudes.

86 Hz

The 86 Hz frequency was found in the upper draft tube cone transducers during the

stop procedure. This frequency showed signs of spectral leakage and is believed to be a consequence of an overharmonic frequency of the downstream water hammer frequency. This is similar to the frequencies at 96 Hz, which occurred in the same transducer at startup.

7.333 Hz

The 7.333 Hz frequency was observed in both vaneless and cone transducers during the stop procedure when the generator was switched off. This frequency result in the half harmonic of the 14.6 Hz frequency, which is the upstream water hammer frequency. Since this half harmonic frequency was not experienced at the inlet the experienced frequency may also be related to the stabilization of the system, the speed reduction in the runner or irregularities regarding the flow.

21 & 26 Hz

There seems to be a relation between these frequencies at the inlet sensor. Peaks at 21 were highest when the generator is on, while the 26 Hz becomes dominant when the generator is off. A clear peak at 26 Hz also existed during the stop procedure when the generator was on. This frequency is believed to be in relation to the pump operating at constant rpm during the measurements. Equations (5.2.1) and (5.2.2) show the calculation of this frequency, which was located at 51.33 Hz frequency. Even though the given frequencies are not an exact harmonic frequency of the pump, it may be a cause of deviation due to the distance between the transducer and pump.

$$f_{pump} = \frac{n_{pump}}{60} \cdot Z_{impeller} \quad (5.2.1)$$

$$f_{pump} = \frac{440}{60} \cdot 7 = 51.33 \text{ Hz} \quad (5.2.2)$$

75 Hz

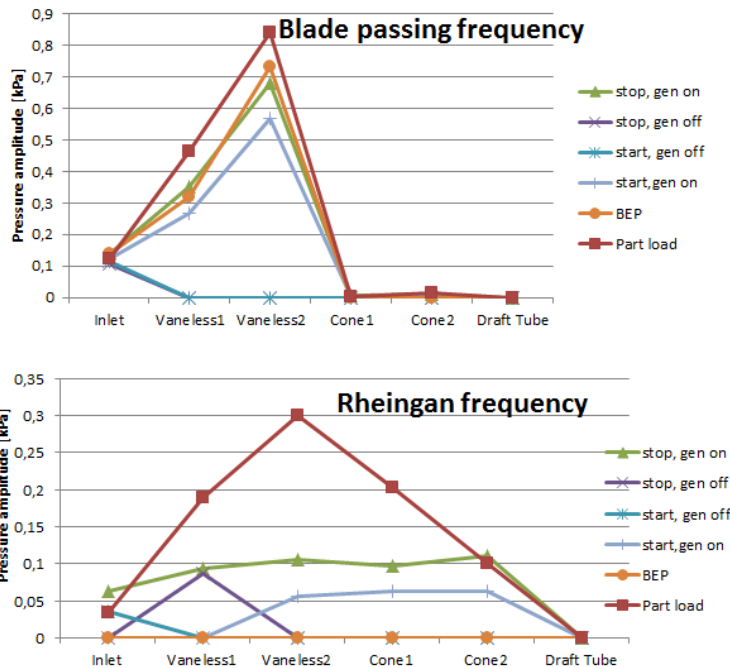
The inlet transducer experienced this frequency only when the generator was switched on. The reason for peaks at this frequency is believed to relate to the 25 Hz frequency since it is the third harmonics frequency. The 75 Hz frequency was also found in the cone transducer during startup procedure with generator off. This peak was a result of spectral leakage and a relocation of the 68 Hz frequency. A reason for this may be the chaotic flow in the draft tube cone during the start up procedure. It should also be mentioned that this frequency may also be determined as the half harmonic of the guide vane frequency, but since the guide vane frequency (149 Hz) was not experienced this is less likely.

56 Hz

The 56 Hz frequency was observed with small peaks at the inlet transducer for every procedure and may be due to the upstream water hammer frequency (14.67 Hz). Both these frequencies were experienced during every procedure, with the largest peaks located at the water hammer frequency. It is therefore believed that this is the fourth harmonic frequency of the water hammer frequency. There is also a possibility that this frequency relates to f_{pump} in equation (5.2.2)

5.2.3 Comparing different procedures and operational loads

The FFT results for the BEP operation is located in Appendix A.1.1. The reason to compare the different operational states with the start & stop procedures is to determine increases or decreases in pressure amplitudes. This may help to determine the dominating frequencies during turbine operation. The largest pressure amplitude measured in the FFT analysis was the runner vane frequency at 160 Hz. This runner vane frequency only existed when the generator was on and had the largest value at the second vaneless transducer. The startup operation had a slightly lower peak amplitude compared to the stop procedure at this transducer. This frequency was also experienced during BEP and part load operation, where the part load had the highest peak while BEP was approximately equal to the stop peak. During BEP operation the Rheingan frequency was not found, but part load operation experienced the highest peak compared to start and stop. The runner frequency and guide vane frequency was not found in BEP or part load operation, as for the different procedures during dynamic load. The upstream water hammer frequency occurred at every transducer during part load and BEP operation. The values of this frequency were approximately similar for the different procedures and steady state operations (BEP & part load). The downstream water hammer frequency was also approximately similar for the different procedures. This result shows how the steady state operations and the different procedures have approximately the same values and trends when looking at the water hammer frequencies, making them independent of the runner frequency. The FFT analysis of BEP and part load shows few or no peaks among the low frequencies, compared to the start and stop procedures which had sometimes the highest amplitudes among these low frequencies. The measurements showed that there were little occurrence of mass oscillations during BEP operation compared to some large peak amplitudes experienced during the start and stop procedures. Another benefit with no low frequencies is the lack of interference.



5.3 Suggested method of identification

When evaluating the used method for identifying pressure oscillations it is important to consider the results and uncertainty regarding this method. When analyzing the estimated curve compared to the pressure measurements it can be discussed how well these actually fit. Chapter 4.3 described the error of the estimated fit curve, but it should be noted that the main objective of this curve was to follow the gradient of the measured pressure fluctuations. An optimal result would be pressure fluctuations around a zero gradient line, often seen in pressure measurements during static load. When looking at the estimated fit curve and comparing it to the pressure measurements for the different procedures and transducers they mostly show a good fit. The exceptions were the cone transducers during the startup procedure. If the curve and measurements have a good fit they will result in a more reliable FFT analysis with reduced interference. The suggested method show mostly good FFT results with reliable peaks. There were some expectations that showed signs of spectral leakages, in addition to the downstream draft tube transducers which showed much interference. When the generator was turned off the transducers also experienced an increase in interference. This is an interesting observation and can be explained by the transducers measuring time varying signals with more irregularities in the pressure fluctuations. Since the FFT analysis showed mainly reliable peaks and fairly low interference for most of the transducers

the suggested method of identification must be evaluated to give reliable results during the start and stop measurements. It is important to know that the presented fit curves are based on values that are only valid for the proceeded pressure measurement. If new measurements are performed the equation for the 24 curves (dependent on the amount of transducers) need to be updated to fit the new measurement. It should also be noted that LabVIEW has an interpreted FFT analysis, and this function as a possible method should be analyzed further for a possible real time Fourier Transform.

5.4 Structural behavior of runner

To analyze the structural behavior of the runner during the start and stop procedures it is important to have the proper instrumentation and placement to get reliable results. The first experience of this was regarding the lack of instrumentation along the runner blade during the start and stop measurements. The chaotic flow in the draft tube cone during the startup sequence included a lot of air and water, and a change in flow direction. With instrumentation along the runner blades it is possible to analyze and measure the flow regarding the experienced chaotic flow as well as the dynamic load on the runner blades

One of the expected frequencies that the FFT analysis showed was the runner vane frequency, which is one of the high frequencies found in a rotating Francis turbine. Another frequency that is expected to have high peak values during operation is the guide vane frequency. These two vane frequencies are at part of the rotor stator interaction. This interaction is known to have high amplitudes during turbine operation, which is effecting the turbine lifetime regarding fatigue. When analyzing the peak amplitudes from these frequencies compared to other frequencies it may indicate enhanced stresses and the possibility for fatigue issues to occur. Due to the increase in issues regarding fatigue, it is important to perform runner measurements with respect to stress and pressure fluctuations during start and stop procedures, and operation outside BEP. The FFT results show that the largest peak was the runner vane frequency (blade passing frequency), opposed to the guide vane frequency which was not detected by the transducers. The reason for this is explained earlier and is a result of the lack of functioning transducers where this frequency is known to have its highest values, along the runner blade. From my measurements the transducers closest to the runner showed that the blade passing frequency was largest during the part load operation procedure, compared to the approximately equal start and stop procedures. The similarities in the measured frequencies may indicate that the transient load during start and stop procedures are approximately equal. To validate this statement further testing should be executed, especially along the runner blade since this is where the runner is expected to experience most load variation during the start and stop procedures. The runner frequency was also not detected, but this is beneficial due to the expected large values at this frequency. A large runner frequency peak often indicate issues or

damages to the runner, and it is a warning that maintenance or a change in operation is needed. The Rheingan frequency is caused by the flow direction from the runner blade outlet. A large Rheingan frequency peak would indicate that the flow has an effect on the runner and runner blades, because after the runner blades the flow induces a swirl rotation in the draft tube. The Rheingan frequency peaks also indicate operation outside of the ideal conditions, for example part load operation. This kind of operation often result in larger stresses on the runner blades and a higher chance of fatigue issues and reduced runner lifetime. By analyzing the proceeded pressure measurements it may indicate that part load operation result in the highest peaks of the expected frequencies, and therefore have a larger impact on the runner with respect to wear and tear, or fatigue. There are some uncertainties regarding this statement, mostly due to the lack of instrumentation at the actual runner, compared to before and after the runner. It is preferable to perform further measurements along the runner blade to verify this statement regarding part load operation.

A simple calculation was performed on the bending stresses acting on the hub and shroud during the start and stop procedure. This calculation was based on equations presented and derivated in the book *Konstruksjon av pumper og turbiner* by Hermod Brekke [7]. These equations are a simplified analytical approach to calculate the bending stresses acting on the blade at the hub or shroud T-joints and the bending stresses in the hub and shroud. The values from the performed start and stop measurements were used to calculate the estimated bending stresses during the performed measurements. This stress analysis has some elements of uncertainty due to the Francis model runner geometry and the difficulty of determining the load on the runner during the start and stop procedures. The graphical result of this calculation is presented in Appendix D. This calculation shows how the bending stresses were reduced with a smaller guide vane angle during the stop procedure, and peaked rapidly when the generator was switched off. The startup procedure shows a large peak when the guide vanes were opened, before the stresses are stabilized and increased as the guide vane angle increases. The overall calculated bending stresses were very low, with the largest stresses being experienced at the T-joints between blade and hub, and blade and shroud. The bending stresses on the hub and shroud are smaller in comparison to the T-joints. Since the observed bending stress values were small, under 1 MPa, they may be coherent with the statement regarding blade stiffness. This figure may be valuable when replacing the runner blade with rapid prototyped blades, but a further and more comprehensive calculation should be performed due to the uncertainty of these results.

A visual test was performed on the Francis runner three weeks after the performed pressure measurements, this is because of the runner being dissemble from the rig. This visual test is one of the non-destructive tests mentioned in chapter 2.3.2 and these tests are performed to detect cracks and other signs of fatigue. The visual test was the only non-destructive test that was performed on the runner during the time it was dissembled. There was not detected any visual cracks during the performed NDT, but this type of visual inspection has high uncertainty. This

uncertainty results in the need for further test methods and analysis to get a better identification of possible cracks. Chapters 2.2 & 2.3 mentions that there is a difference between model and prototype turbines regarding fatigue caused by load variation and cyclic stresses.

5.5 Runner blade replacement

Rapid prototyping is a technology with large area of application and projects within researching and development of this new technology are making it more applicable for scenarios involving high pressure. There are several benefits by replacing the material of the runner blades, but there are some uncertainties regarding this replacement. This is mainly because of the blade stiffness and how the material is reacting to the stresses and pressure fluctuations during turbine operation. Another master student (Kristoffer Rundhaug) at the Waterpower Laboratory who is writing a thesis on *Development of new mechanical design of model turbines*, spring 2014. His thesis involves rapid prototyping, how this can be applied as a runner material and producing a runner by using rapid prototyping. Figure 5.5.2 shows the structure of the Francis model at NTNU, where the hub and shroud are the same bronze material as mentioned in chapter 2.3.3. The current material for runner center is bronze, however according to rapid prototype technology it is desirable to replace this material with DuraForm HST.

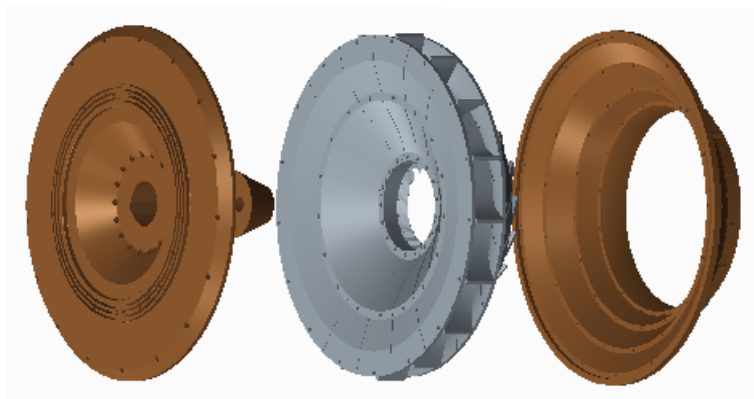


Figure 5.5.2: Rapid prototyped turbine model

To perform the strain gauge tests of the rapid prototyped runner vanes I was dependent on Rundhaug's progression in producing the runner or runner blades. Since this was not completed, the planned replacement and strain gauges tests on the runner blades were not performed. Even though these tests were not executed I attended material tests performed by Rundhaug, these tests were regarding how the hub and shroud should be attached to the DuraForm material. It is important

to ensure that the new runner material can withstand the fluctuating pressure and stress. The test objective was to measure the force needed to unloosen an attached vice from the plastic material. The test cube was made out of DuraForm HST and had six holes with three different hole diameters (7.5, 7.4 and 7.3 mm). Vices were placed in each hole in order to test and determine the maximum force for each diameter. The test results showed that a diameter of 7.4 millimeter proved to be sufficient, but there are some uncertainties regarding the performed test. These uncertainties are mainly due to a force of approximately 5000 N that could not unloosen the vice at 7.4 mm, and tests for 7.3 mm were not executed. Further tests should be done to validate and check these results.

5.6 Improving Instrumentation

5.6.1 Pressure transducers

By attaching more pressure transducers to the draft tube cone, especially the upper part, it may be possible to determine and analyze the chaotic flow that was experienced during the startup measurements. The result of this analysis could help to indicate the transient load on the runner during the startup procedure. There is also a need to place pressure transducers along the runner blades to be able to detect the fluctuating pressure in the runner. The runner blade is experiencing large stress, flow, and pressure variation during the start and stop procedures. The measurements performed on this turbine component are expected to give valuable information regarding fatigue issues on the runner. An important consideration regarding attaching pressure transducers along the runner blade is the guide vane frequency. As mentioned in 5.2.1 the guide vane frequency is expected to have dominating peaks along the runner blades. It is also possible that the runner frequency would have peak values around and along the runner blades.

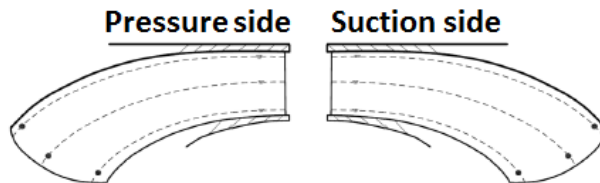


Figure 5.6.3: Pressure transducers located at runner blade [8]

Attaching pressure transducers along the runner blades have been proceeded earlier by Einar Kobro [23] in his Doctoral thesis in 2010. A total of six pressure transducers (transducer type Kulite LL-080) were located along the runner blade. Three of the transducers were on the blades pressure side, while the remaining transducers on the suction side of the blade (figure 5.6.3). Kobro discovered after his measurements that one of the transducers had failed, and later tests performed by

master students determined that more of the transducers started to fail [8]. These later tests showed that water and air leakage also occurred through the cable to the transducer. There are some difficulties of using pressure transducers along the blade. They are mostly related the ability to withstand the large dynamic forces occurring regarding the small size of the transducers.



Figure 5.6.4: Procedure to attach pressure transducers along the blade [23]

When applying pressure transducers along the blade it is important to maintain the blade smoothness for unaffected measurements. Figure 5.6.4 shows the finished transducer attachment (left sensor) and during installation (right sensor) from Einar Kobre's doctoral thesis [23]. The Kulite LL-080 transducers and cables were placed in milled notches and height adjusted with silicone adhesive. The transducers and cables were covered by epoxy and then curing the epoxy. The excessive epoxy was grinded off to smoothen the epoxy surface and the surface was coated to minimize the surface roughness.

There are some different methods regarding attaching new pressure transducers along the runner blade, either replacing the existing failed transducers or milling and attaching the new transducers on a new runner blade. After a discussion with the divisional engineer at the Waterpower laboratory, Joar Grilstad, he stated that replacing these pressure sensors with new functioning transducers is difficult due to the old epoxy filling that needed to be removed as well as the height of the notches. The new transducers must be analyzed regarding size, possible notch height and whether or not it is more beneficial to mill new notches on an unmodified blade. After speaking with Einar Kobre he mentioned that the problem was the transducer cables and not the actual transducer [21]. He stated that the transducers are good enough to perform pressure measurements under operational conditions and the problem was related to the surface material of the cables. These cables had the outer layer made out of Teflon which is a difficult to combine with other materials.

The result of this was that the Teflon and epoxy did not stick to each other. It is believed that water managed to come between the epoxy and Teflon during turbine operation, and travelling along the notch to the transducers. When water leaked into the transducers they became defect. A preventative method for this is to order new transducers of the same type, but modifying the transducer cables. This modification is mainly cutting the cable between 1 to 2 cm from the transducer and solder on a different type of cable. It is important that the new cable chosen is easily combined with epoxy, since this would minimize the possibility of gaps and leakage. PVC cables might be a possible solution, but a further analysis regarding ability to stick to epoxy and price should be exceeded. Kobro mentioned that removing the old epoxy to replace the transducers is possibly the easiest and preferable method compared to milling new notches in other runner blades. A further analysis regarding the most efficient procedure to install new transducers is needed.

5.6.2 Accelerometer

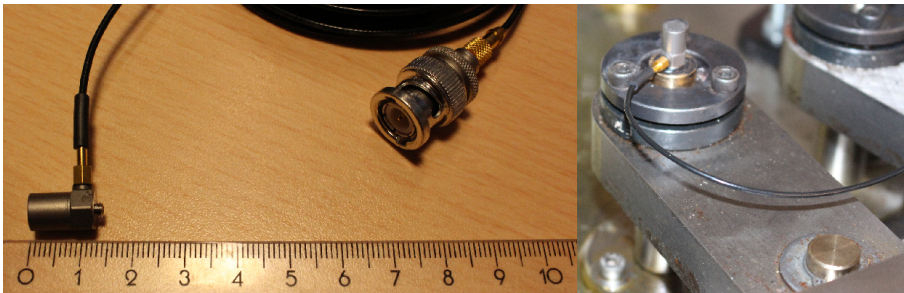


Figure 5.6.5: An example of an accelerometer and placement

An accelerometer can be attached on the guide vanes to detect vibration in the flow on the guide vanes. The reason for this is that vortices and cavitation bubbles that occur as a result of this fluid-structure interaction may be detected as vibration on the guide vanes. This guide vane vibration may be measured by using an accelerometer available in the laboratory, DeltaTron Type 4397. It is possible to perform these measurements by placing the accelerator on top of the guide vane trunnion, this placement is showed in the figure 5.6.5. By using an accelerometer to perform vibration measurements during start and stop procedures it may show how the vortices and cavitation bubbles affects the dynamic load of the runner.

During a startup the Francis runner experiences large stress fluctuations and Halvard Bjørndal presented a method that might reduce these large fluctuations [13]. If the guide vane angle is big during the startup procedure the water flows tangentially in the runner, resulting in large stress fluctuations. By reducing the guide vane angle the dynamic load would be reduced, this is because of a different direc-

tion and amount of flow. There are two disadvantages that may occur during this start procedure. The ball-bearings experience a larger wear and tear if the startup procedure is performed over a longer time period. The disadvantage is that interference with the natural frequencies may occur, causing more stress fluctuations with lower amplitude. By attaching an accelerometer to the ball-bearing it may be able to detect the vibration created by the stress fluctuations during the startup procedure. This accelerometer may be used to evaluate runner vibrations during normal and slow startup sequences.

5.6.3 Strain gauges

In order to measure the strains experienced on the runner during the start and stop procedures strain gauges may be placed on the runner. It is believed that strain gauges on the runner blades of the Francis model is a concern regarding the blade stiffness causing no considerable fluctuations and results. It could however be useful to check if this statement regarding blade stiffness is valid. A possibility is replacing the runner vanes with blades of another material with less stiffness. By attaching strain gauges and performing measurements on the new blades with less stiffness, the transient load can easier be detected. When attaching strain gauges it is important to maintain blade smoothness due to the cyclic stresses and not affecting flow. This is because an increase in smoothness may cause higher stresses and give false results. It is also possible to combine both pressure transducers and strain gauges. This combination could help to determine the stress and pressure fluctuations occurring during the start and stop procedures.

It is important to choose strain gauges accommodated to the planned measurements. After speaking with Einar Kobro a strain gauge that is often used on runner blades was the HBM LE11. The HBM LE11 is an encapsulated strain gauge that is waterproof and accommodated to use on runner blades. In addition to the mentioned stiffness there might be issues regarding strain gauge measurements and the design of the runner and runner blades [21]. These issues are the main reason for the statement that strain gauge measurements have no purpose. Kobro also stated that strains attached to the model would give different results compared to prototype measurements, and that they cannot be compared.

Chapter 6

Conclusion

The suggested method that was used to identify the pressure oscillations during the start and stop procedures consisted of finding curves that fit the performed pressure measurements. To simplify and reduce the FFT interference it was decided to divide the pressure measurements into four procedures; stop procedures with generator switched on and off and start procedures with generator switched off and on. By performing a FFT analysis on the pressure difference between the fit curve and divided pressure measurements, it resulted in reliable results with reduced interference.

There is always an occurrence of pressure oscillations, but large amplitudes of these pulsations may cause fatigue to occur. This is because of the many turbine rotations causing these pulsations to induce an increase in cyclic stresses. The results from the FFT analysis showed that the largest frequency experienced was the blade passing frequency and it was observed during the start and stop procedures. The guide vane frequency has its highest peaks along the runner blades, and since no functioning transducer was located in the runner blades this frequency was not observed. The runner frequency was not observed during the performed procedures. The Rheingan frequency had higher peak values during the stop sequence compared to startup. The reason for this is believed to be the chaotic flow pattern experienced in the draft tube cone during the startup sequence. The elastic oscillations were also experienced both upstream and downstream of the turbine, but there were some uncertainty regarding the mass oscillations coinciding with the low interference frequency.

To determine the structural behavior of the runner during the start and stop procedures proper instrumentation in the runner is needed. The large amplitude of the blade passing frequency is interesting regarding the cyclic stresses experienced by the runner. It was beneficial that the runner frequency was not observed because peaks at this frequency would indicate faults regarding the runner. The increase in pressure fluctuations during part load operation was an expected result, but the chaotic flow during startup needs to be measured further to determine how this affects the runner. This increase of pressure fluctuations in part load shows the unfavorable conditions the runner experiences during operation outside of BEP. Improved instrumentation at the runner is strongly advised to further analyze the structural behavior of the runner during the start and stop procedures.

By improving instrumentation on the Francis rig it is possible to perform transient load measurements on the runner during start and stop procedures. There is especially a need to perform measurements along the runner blades to further analyze the effect of the dynamic load on the runner. This can be done by replacing the current defect transducers in the runner blade with new transducers. By modifying the cables on the new transducers it is possible that they stick easier to epoxy, making them less exposed to leakage and failure. In addition to pressure transducers along the runner blades it is possible to locate more transducers at the upper draft tube cone. This is to perform more measurements on the chaotic mixture of air and water that was observed in the flow in the draft tube cone during the runner startup. The usage of accelerometers are suggested to determine the occurrence of vibration and cavitation. By installing the accelerometer on top of the guide vane trunnion it is possible to determine the wake and cavitation bubbles occurring from the guide vanes, and traveling into and affecting the runner. Another procedure is to attach an accelerometer on the ball-bearings to measure the wear on the ball-bearings while experimenting on how the guide vane angle during startup procedures effects the stress fluctuations on the runner. Strain gauges can also be used simultaneously with pressure transducers along the blade to determine both the pressure and strain occurring along the runner blades.

Chapter 7

Further Work

By analyzing and finding new procedures of optimizing the suggested method is beneficial. The reason for this is because of the existing method is performed by manually dividing the pressure measurements into different sections. After dividing into the mentioned sections, the Curve Fitting Toolbox application in MATLAB was used to find a curve that fit the measured pressure fluctuations. It is worth mentioning that LabVIEW has an interpreted FFT analysis, and by analyzing this function as a possible method due to the ability to perform a real time FFT analysis during the start and stop procedures.

The rapid prototyped runner blades and runner needs to be produced before it is possible to perform measurements on this new material. By doing simultaneous pressure and strain gauge measurements, it is possible to achieve knowledge of this new material. These measurements are useful regarding the idea of replacing model turbines with rapid prototyped turbines and determining how well this material works.

To improve the instrumentation on the Francis rig it is possible to measure the transient load on the runner more accurately during start and stop procedures. By installing the suggested instrumentation this would benefit in the understanding of the dynamic load experienced in the runner. The suggested instrumentation in this thesis consisted of pressure transducers along the runner blades and in draft tube cone, accelerometers on guide vane trunnion and ball-bearing, and possibly strain gauges on runner blades. With the proper instrumentation measuring the dynamic load on the runner it is easier to analyze the structural behavior of the runner with respect to fatigue. By knowing the frequency, vibration, and amplitude of the fluctuations affecting the runner it is easier to determine how the runner reacts to this dynamic load. Then a further analysis can be performed to safely determine the structural behavior of the runner.

A CFD analysis could be performed to simulate the structural behavior of the runner during the start and stop procedures. This CFD analysis may also include the dynamic change in pressure and stress on the runner to determine the expected dynamic load. By comparing this simulation with the performed measurements it may be possible to determine the structural behavior of the runner with respect to fatigue.

Bibliography

- [1] Sveisedagen Våren 1983. Sveiste konstruksjoner i vannturbiner ved Kværner Brug - Utviklingstendenser bestemt av forholdet materialkostnad/lønnskostnad.(Del 2). http://www.industrimuseum.no/filearchive/sveiste_konstruksjoner2-1.pdf, 2014. Modified picture, Accessed 2014-04-25.
- [2] 3Dsystems. DuraForm HST Composite. http://www.3dsystems.com/sites/www.3dsystems.com/files/DS_DuraForm_HST_XZdir_US.pdf, 2014. Accessed: 2014-05-21.
- [3] S. Prakash Akhilesh K. Chauhan, D.B. Goel. Solid particle erosion behaviour of 13Cr-4Ni and 21Cr-4Ni-N steels. *Journal of Alloys and Compounds 467 (2009)*, pages 459 - 464, 2007. Department of Metallurgical and Materials Engineering, Indian Institute of Technology Roorkee.
- [4] Arrk. Rapid prototyping - SLS: Selective Laser Sintering. http://www.spg-arrk.nl/site/index.php?option=com_content&view=article&id=35&Itemid=217&lang=en, 2014. Accessed: 2014-05-21.
- [5] M.M. Belsnes B.H Bakken, T. Bjørkvoll. *Start/stopp-kostnader for vannkraftverk*, pages 69-80. SINTEF Energiforskning, SINTEF, 2001.
- [6] Hermod Brekke. *Choice of materials for water turbines and the influences this has on the design manufacture, testing and operation*. NTH, NTH, 1984.
- [7] Hermod Brekke. *Konstruksjon av pumper og Turbiner*, pages 1-24 & 45-54. Vannkraftlaboratoriet NTNU, NTNU, 2008.
- [8] Ingeborg Lassen Bue. *Master thesis: Pressure pulsations and stress in a High head turbine - comparison between model and geometrically similar prototype*. NTNU, Spring 2013.
- [9] Stephen J. Chapman. *Electric Machinery Fundamentals*, pages 191-197. McGraw-Hill Education, 2012.
- [10] International Electrotechnical Commission. *International Standard IEC60193*, pages 379-410. International Electrotechnical Commission, 1999.
- [11] Dr. Andrew Greensted. Fade In and Out. <http://www.labbookpages.co.uk/audio/wavGenFunc.html>, 2014. Modified picture, Accessed: 2014-05-19.
- [12] Odd Guttormsen. *Vannkraftverk og vassdragsteknikk - Vassdragsteknikk II*, pages 172-190. NTNU - Institutt for vann- og miljøteknikk, NTNU, 2006.
- [13] Norconsult Halvard Bjørndal. Hva viser anleggsmålinger om variasjon av spenninger og belastning som funksjon av pådrag - Produksjons teknisk Konferanse 04.March 2014. http://www.energinorge.no/getfile.php/FILER/KALENDER/Foredrag%202014/PTK2014/0403_1A_10.30%20Bj%C3%B8rndal_Anleggsm%C3%A5linger%281%29.pdf, 2014. Accessed PTK:2014-03-04 & Accessed online: 2014-05-11.
- [14] Norconsult Halvard Bjørndal. Hva viser anleggsmålinger om variasjon av spenninger og belastning som funksjon av pådrag - Produksjons teknisk Konferanse 04.March 2014. http://www.energinorge.no/getfile.php/FILER/KALENDER/Foredrag%202014/PTK2014/0403_1A_10.30%20Bj%C3%B8rndal_Anleggsm%C3%A5linger%281%29.pdf, 2014. Modified picture. Accessed PTK:2014-03-04 & Accessed online: 2014-05-11.

- [15] Norconsult Halvard Bjørndal. Tilstandskontroll og vibrasjonsanalyse, 2013. NTNU Lecture in TEP4200: Mechanical Design, Operation and Maintenance of Hydraulic Machinery.
- [16] Kari Haugan. *Master thesis: Trykkpulsasjoner i Francisturbiner*, page 15. NTNU, June 2007. Modified picture.
- [17] Hans-Jörg Huth. *Doctoral thesis: Fatigue Design of Hydraulic Turbine Runners*. NTNU, February 2005.
- [18] Fridtjov Irgens. *Fasthetslære*, page 17. Tapir akademiske forlag, 2006.
- [19] Statkraft Jens Ragnvald Davidsen. Kjøremønsterrelaterte kostnader for vannkraftverkebl maskinteknisk forum 2008. <http://dok.ebl-kompetanse.no/Foredrag/2008/Liverpool/Davidsen.pdf>, 2014. Accessed online: 2014-05-16.
- [20] Arne Kjølle. *Mechanical Equipment*. NTNU, NTNU, 2001.
- [21] Einar Kobro. Phone conversation about blade transducers and strain gauges, 2014. Phone conversation: 2014-05-29, 14:29.
- [22] Einar Kobro. *Master thesis: Pressure pulsations in Francis turbines*. NTNU, Spring 2006.
- [23] Einar Kobro. *Doctoral thesis: Measurement of Pressure Pulsations in Francis turbines*. NTNU, Spring 2006.
- [24] Erwin Kreyszig. *Advanced Engineering Mathematics*, volume 9th edition, pages 518–528. John Wiley & Sons, inc, 2006.
- [25] Lagermetall. Materialsheet SS 5465-15 Cast tinbronze. <http://www.lagermetall.com/bronze/tennbron.asp>, 2014. Accessed: 2014-06-05.
- [26] I. Oftebro & A. Lønning. *Pressure oscillations in Francis Turbines*. Institution of Mechanical Engineers, 1966.
- [27] The University of Bolton Martin Tarr. S-N curve. http://www.ami.ac.uk/courses/topics/0124_seom/, 2014. Modified picture, Accessed: 2014-05-07.
- [28] MathWorks. Curve Fitting Toolbox Product Description. <http://www.mathworks.se/help/curvefit/product-description.html>, 2014. Accessed: 2014-05-10.
- [29] MathWorks. Evaluating Goodness of Fit. http://www.mathworks.se/help/curvefit/evaluating-goodness-of-fit.html#bq_5kwr-3, 2014. Accessed: 2014-05-10.
- [30] Torbjørn K. Nielsen. Fatigue, 2013. NTNU Lecture in TEP4200: Mechanical Design, Operation and Maintenance of Hydraulic Machinery.
- [31] Torbjørn K. Nielsen. Guide vanes in francis turbines, 2013. NTNU Lecture in TEP4200: Mechanical Design, Operation and Maintenance of Hydraulic Machinery.
- [32] Torbjørn K. Nielsen. Model tests, 2013. NTNU Lecture in TEP4200: Mechanical Design, Operation and Maintenance of Hydraulic Machinery.
- [33] Mirjam Sick Peter Dörfler and André Coutu. *Flow-Induced Pulsation and Vibration in Hydroelectric Machinery*, pages 120–125. Springer, NTNU, 2012.
- [34] Andrea Stranna. *Master thesis: Testing of RPT in pumping mode of operation*, page Appendix A. NTNU, Jan. 2013.
- [35] SINTEF Energi Thomas Welte. Endringer i kjøremønster - Hva sier driftshistorikken? - Produksjons teknisk Konferanse 04.March 2014. http://www.energinorge.no/getfile.php/FILER/KALENDER/Foredrag%202014/PTK2014/0403_1A_08.40%20Thomas%20Welte.pdf, 2014. Accessed PTK:2014-03-04 & Accessed online: 2014-05-11.
- [36] Anthony J. Wheeler and Ahmad R. Ganji. *Introduction to Engineering Experimentation*, pages 95–114. Pearson Education International, 2004.

- [37] Frank M. White. *Fluid Mechanics*, page 817. McGraw-Hill Education, 2009.
- [38] Jr William D. Callister. *Materials Science and Engineering an introduction*, pages 209 – 245. John Wiley & Sons, 2007.

Appendix A

Francis runner measurements

A.1 FFT analysis BEP and part load

A.1.1 BEP - Best efficiency point

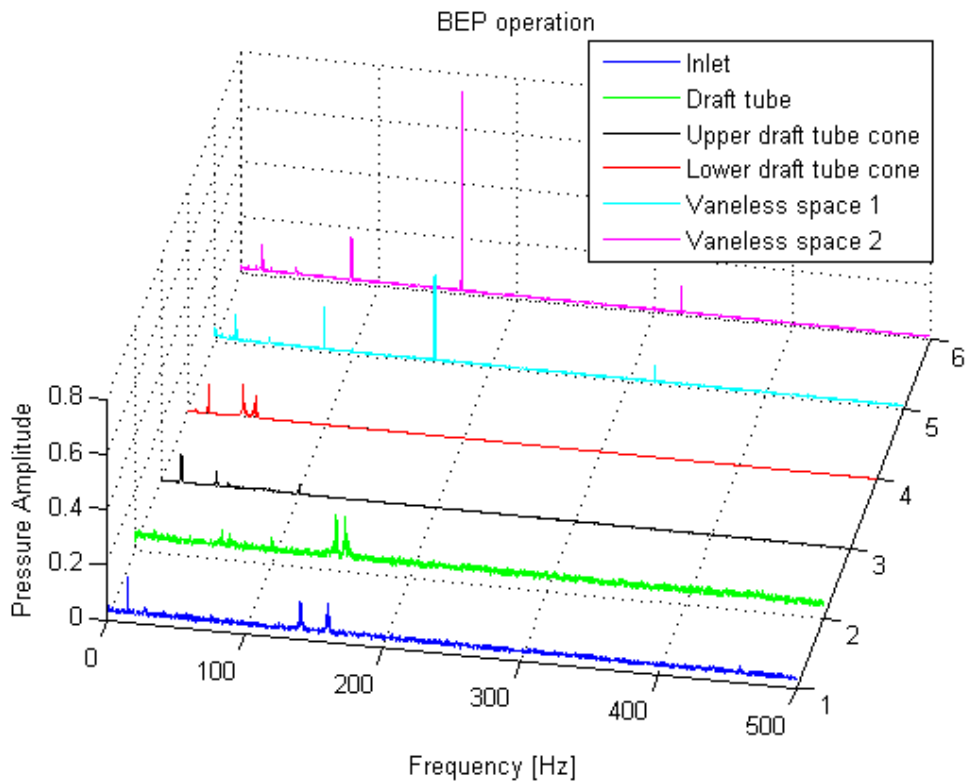


Figure A.1.1: Frequency peaks at BEP

A.1.2 Part load

Table A.1.1: Part load operation

Type	Value	Unit
Generator speed	320	rpm
Runner speed	320	rpm
Pump speed	440	rpm
n_{ED}	0.174	-
Q_{ED}	0.078	-
$\alpha_{guide\ vanes}$	4.878	°
H_{model}	11.7	m
$H_{prototype}$	457	m
Q_{model}	0.102	$\frac{m^3}{s}$
$Q_{prototype}$	18.1	$\frac{m^3}{s}$

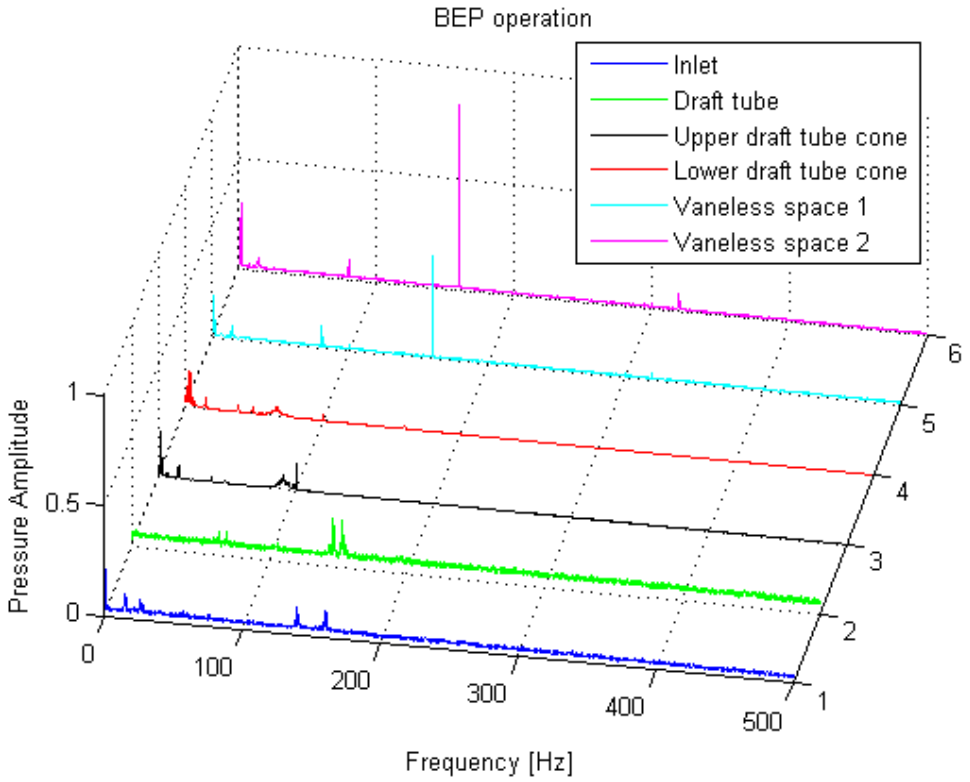
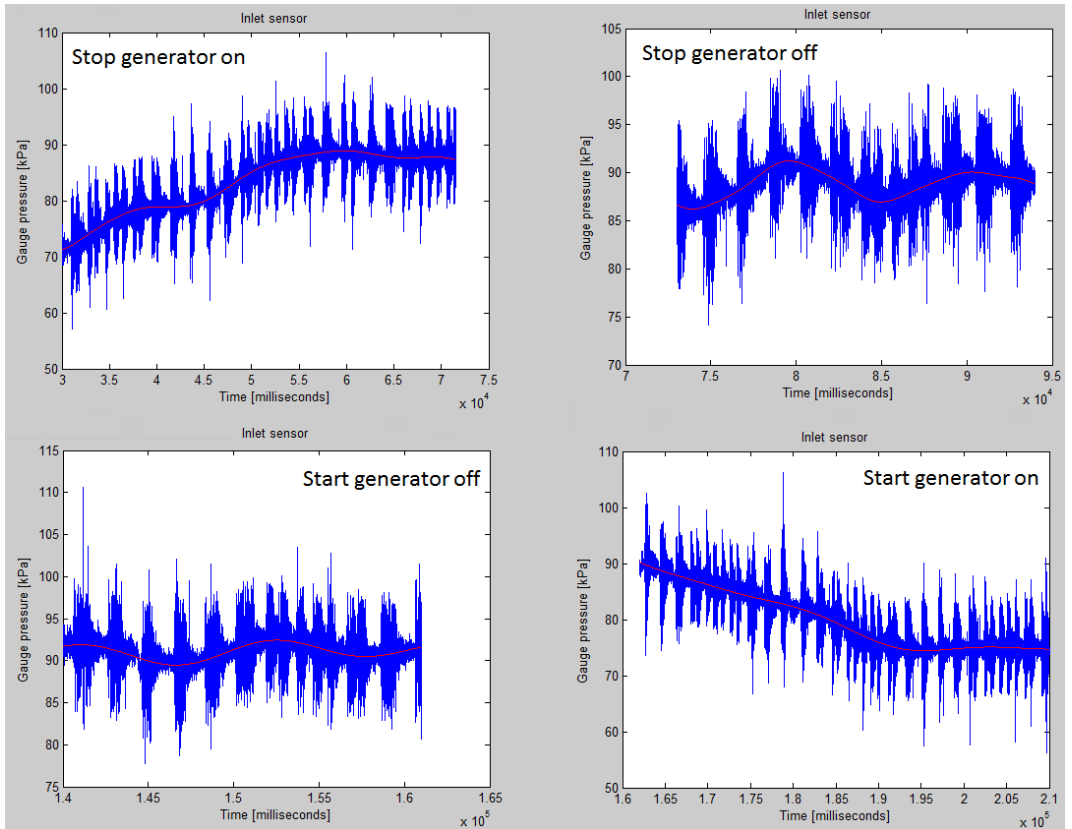


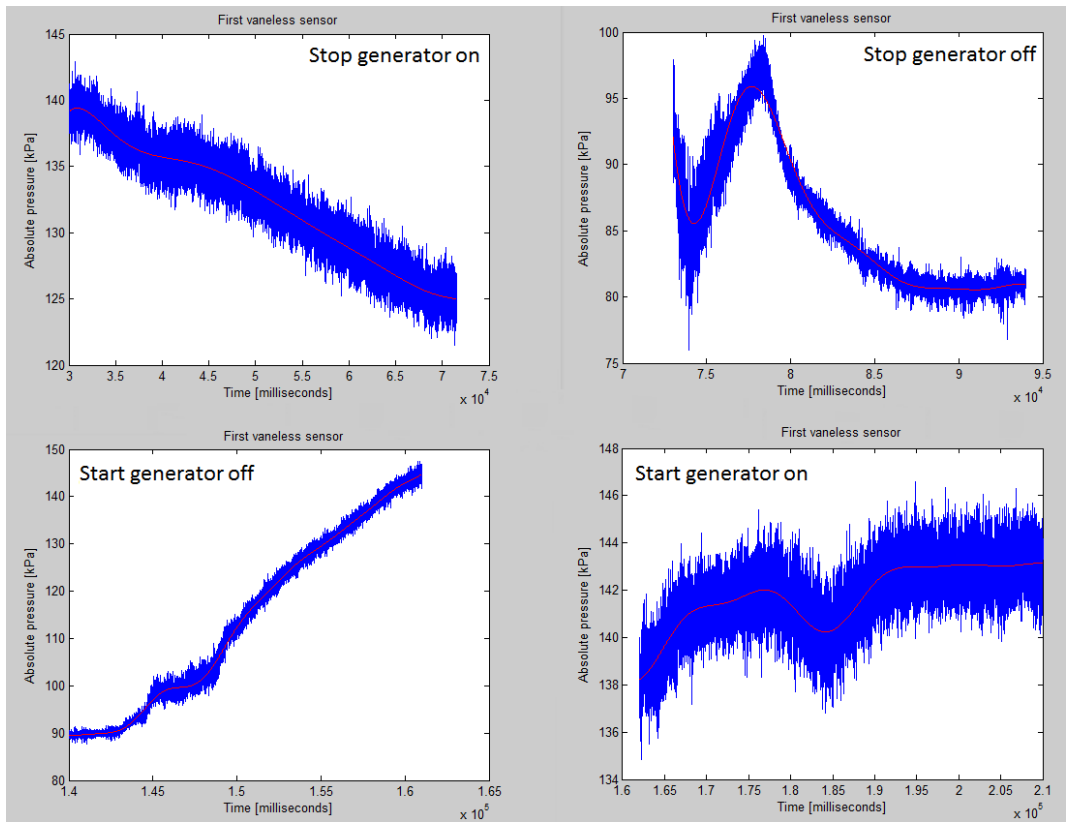
Figure A.1.2: Frequency peaks at Part load

A.2 Start & stop pressure measurements and pressure difference

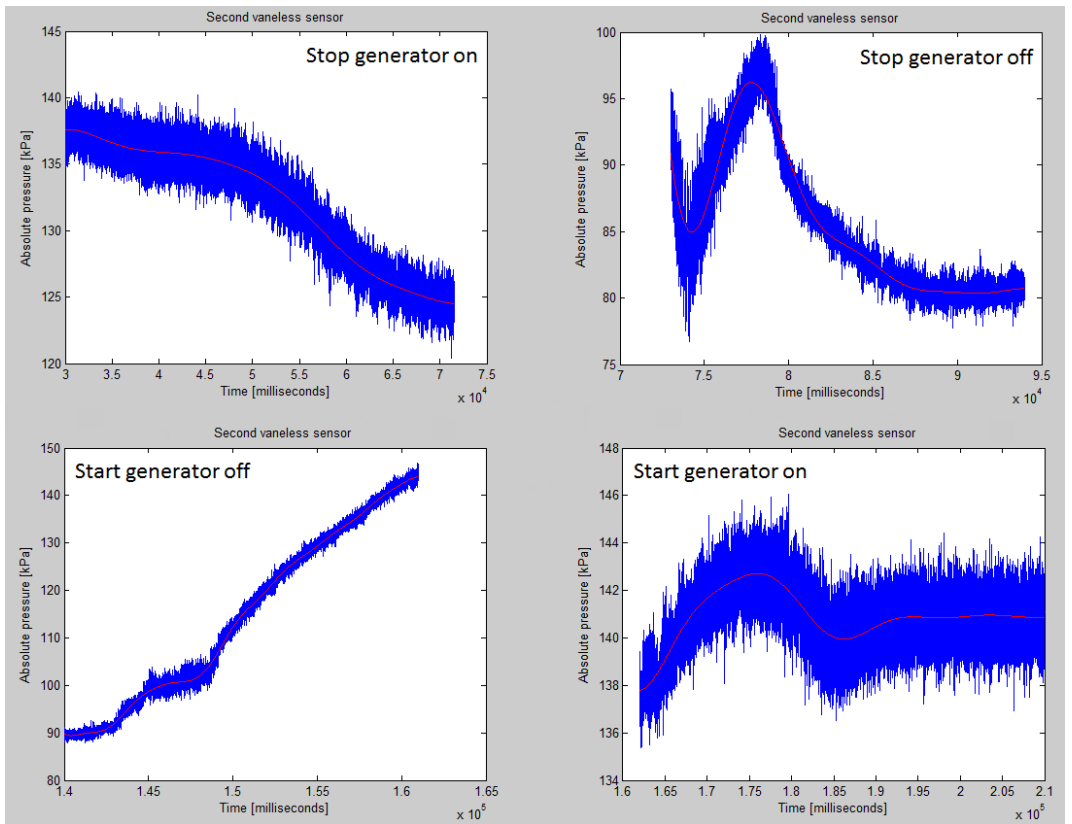
A.2.1 Inlet sensor



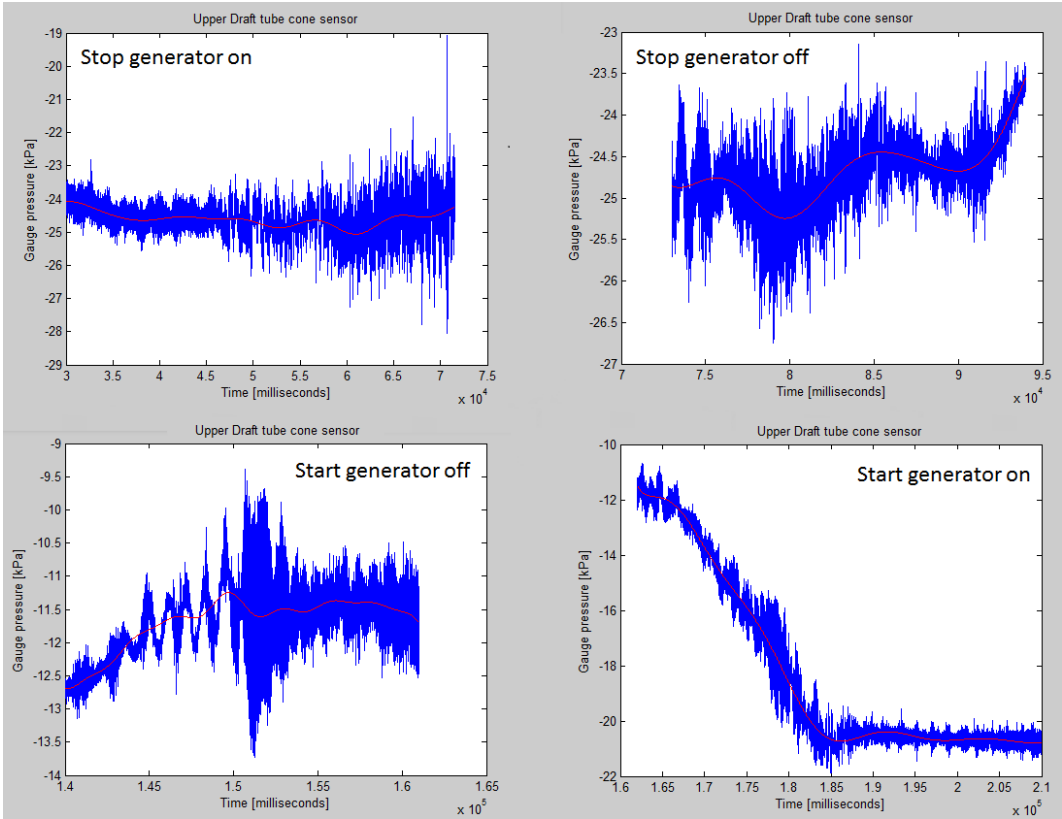
A.2.2 First Vaneless sensor



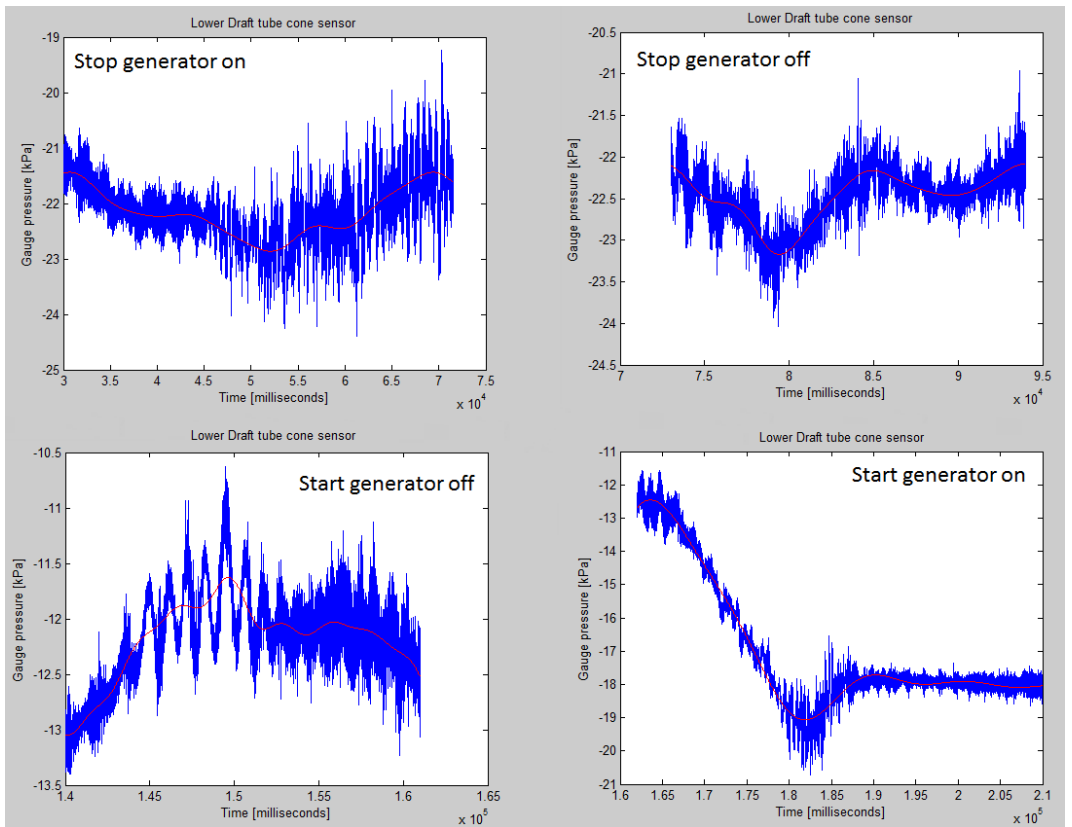
A.2.3 Second Vaneless sensor



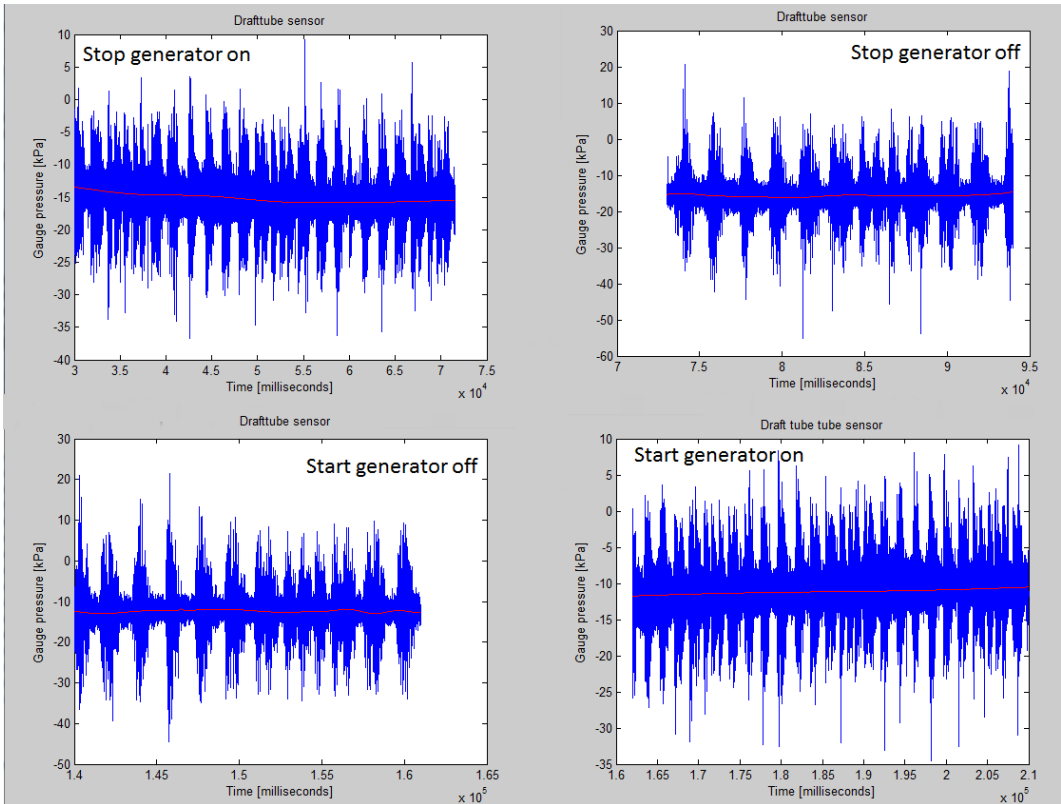
A.2.4 Upper draft tube cone sensor



A.2.5 Lower draft tube cone sensor

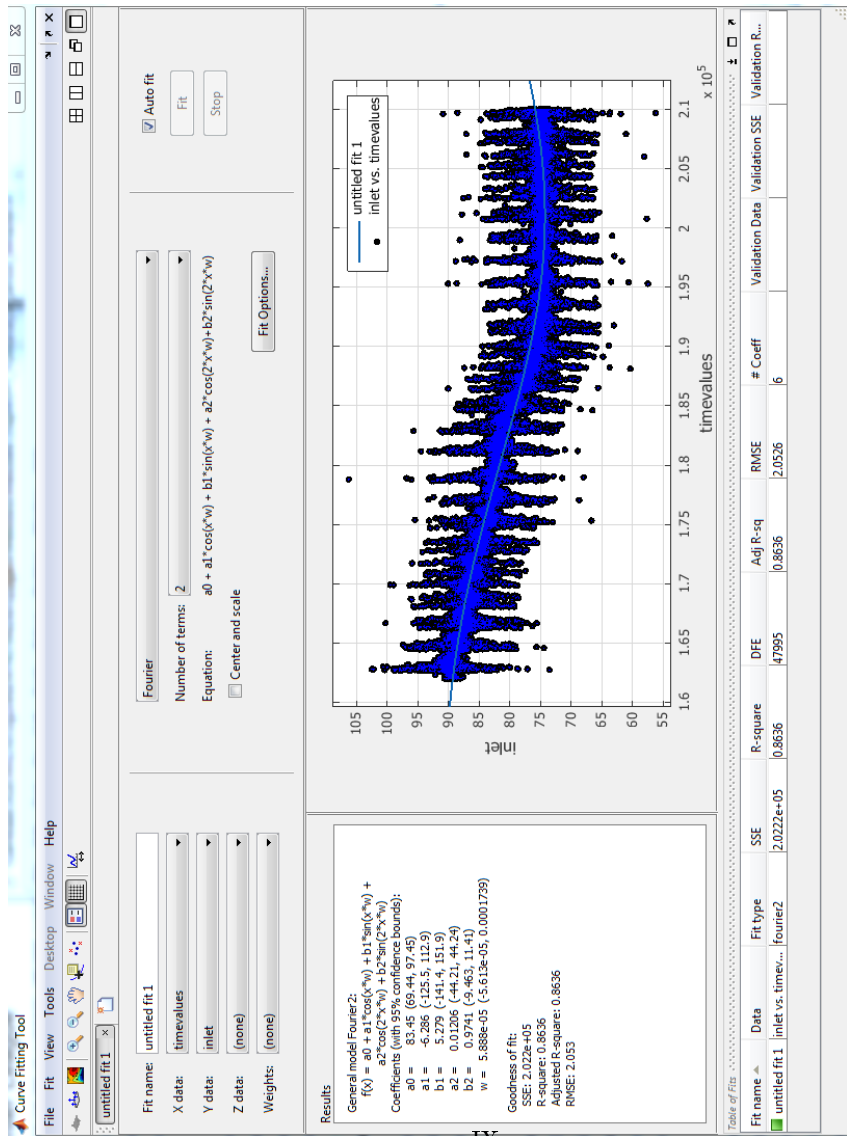


A.2.6 Downstream draft tube sensor



Appendix B

MATLAB application Curve Fitting Tool



Appendix **C**

Running the Francis rig

Procedure for Running the Francis turbine test rig

Closed Loop

This part of the procedure treats running the Francis turbine test rig with a closed loop, like the one seen in figure 1b. The water is directed through the pump, to the pressure tank, through the turbine to the draft tube tank and from there back to the pump. When going from an open loop to a closed loop, the loop needs to be filled before you can start running. A detailed procedure for this already exists, and can be found on the Waterpower Laboratory's server.

Start up

- 1. Turn on the power for the pumps**
This is done in the pump room in the basement. Turn the switch to *Start*, keep it there for a second and then let it go so that it stops at *1*.
- 2. Set the pipe loop**
From the control room, open/close the necessary valves in order to guide the water through an open loop as seen in figure 2b
- 3. Make an inspection round in the lab**
Walk through the lab and see that all drain tubes on the current pipe loop are closed.
- 4. Check for water on top of the turbine**
Water will leak up through the guide vanes and accumulate on top of the turbine when it is running. Check for water before starting. If there is water, use the water vacuum cleaner to remove it.
- 5. Turn on cooling water and hydraulics**
Always turn on the cooling water first, then the hydraulics. See figure 3b for hydraulics and figure 3c for the cooling water.
- 6. Open valve for priming water for the vacuum pump**
The valve can be seen in figure 3d.
- 7. Start the pump**
Start the pump at 100 rpm.
- 8. Start the generator**
Make sure the generator is in turbine mode, and the rpm is set to 100. Start the generator when the turbine has accelerated to around 90 rpm.
- 9. Run up pump and generator**
Increase head by increasing the speed of the pump. Always increase pump speed first, then follow with the generator. Do not exceed 30 meter head!

Shut down

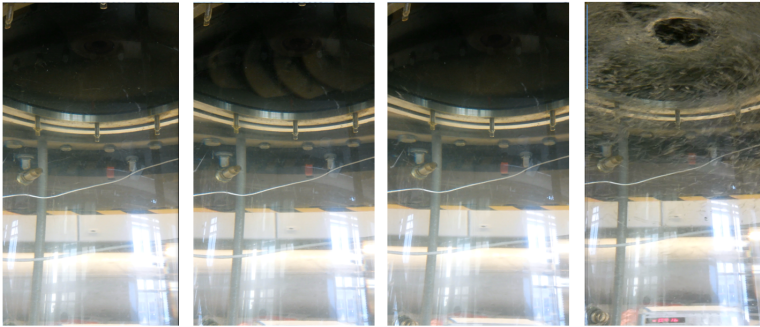
- 1. Slow down generator and pump**
Decrease the speed of the generator and the pump. Decrease generator speed first, then follow with the pump, step by step.
- 2. Stop the generator**
Stop the generator when both generator and pump are at 100 rpm.
- 3. Stop the pump**
- 4. Turn off cooling water and hydraulics for the Francis rig**
Make sure that the turbine has completely stopped spinning first.
- 5. Close valve for priming water for the vacuum pump**
- 6. Turn off the power for the pumps**
In the pump room in the basement. Turn the switch to *0*.

Appendix D

Draft tube cone during stop & start

Stop procedure

Start closing GV **Generator OFF** **GV closing** **GV closed**



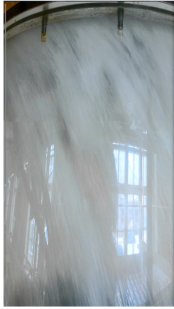
Water level in cone reducing

Turbine stopped

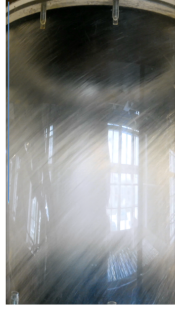
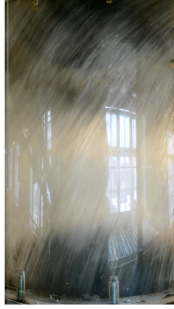


Start procedure

**Start
opening GV**



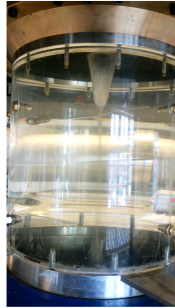
**Generator
ON**



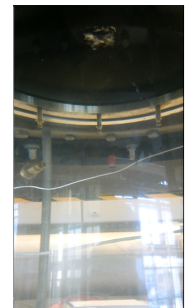
Continue opening of GV



Continue opening of GV



Close to BEP



Appendix E

Runner rotational speed measurements

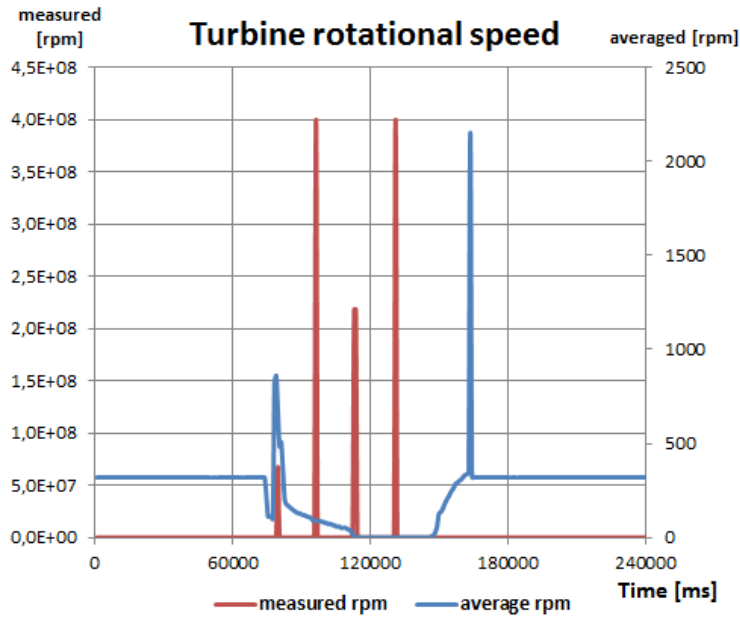


Figure E.0.1: Turbine rotational speed for measured rpm & averaged rpm

The rotational speed of the turbine is an important variable when performing the stop and start procedures, mainly to determine that the turbine has stopped. There were some issues with the rotational speed measurements during the start and stop procedures. The issue was occurring when the turbine obtained a rotational speed under 100 rpm. Under this speed the computer had difficulties recording the correct rotational speed, often unrealistically high peaks. Figure E.0.1 shows these high peaks for the measured rpm, while the averaged rpm only consists of two peaks in addition to being reduced in size. The first peak for both lines occurs when the generator is switched off causing in a rapid, but large increase in runner speed. While the averaged rpm peaks around 850 rpm the measured rpm is above $5.0 \cdot 10^7$ rpm. It is reasonable to expect some increase when switching off the generator,

but the size of the rpm increases makes these values too unrealistic. Further the measured rpm have multiple peaks above $2.0 \cdot 10^8$ rpm while the actual rpm was under 100 rpm which enhances the need to change the rotating shaft disc. The laboratory has two methods of measuring the runners rotational speed. The first method is a governor attached on top of the generator that reads and controls the rotational speed with the help from the frequency converter. This rotational speed is sent to the Francis rigs surveillance program in the control room (seen in figure3.1.1). This is currently the most accurate method of controlling the current rotational speed of the turbine.



Figure E.0.2: Disc installed at rig to measure rpm, 1 pulse per revolution

The second method is based on a pulse counter reading pulses created by the shaft disc rotating, figure E.0.2 shows the disc installed on the rig that has one pulse generation per revolution. This method is the one measured by the log program and the issues is a result of the program update time is varying between 600 and 800 milliseconds (ms). The experienced average values of the program update time was between 700 and 750 ms. When the rotational speed is low the disk does not exceed a revolution compared to the program update time resulting in the pulse counter misreading and showing too high turbine speeds. This is shown in figure E.0.3, where the number of rotations regarding program update time and turbine rotational speed is calculated. The red zones are areas where one revolution is under the update period causing problems reading the correct rotational speed. To remove this logging error the shaft disk can be replaced with a disk containing more pulse creations, a possible solution would be a disk that creates around 60 pulses per revolution. Compared to figure E.0.4 when inserting a disk with 60 pulses per revolution the problems with rotation under 100 rpm will be solved. The only red zones in this figure are due to the input of 0 rpm in equation (E.0.1). This equation calculates how many pulses that are created for each turbine revolution.

$$n_{puls} = \frac{(Turbin\ rpm) \cdot (pulse\ per\ revolution) \cdot (program\ update\ time)}{60} \quad (E.0.1)$$

Disk with 1 puls per revolution					
<i>Program update time</i>					
<i>Turbine rpm</i>	600 ms	650 ms	700 ms	750 ms	800 ms
100	1	1,083333	1,166667	1,25	1,333333
90	0,9	0,975	1,05	1,125	1,2
80	0,8	0,866667	0,933333	1	1,066667
70	0,7	0,758333	0,816667	0,875	0,933333
60	0,6	0,65	0,7	0,75	0,8
50	0,5	0,541667	0,583333	0,625	0,666667
40	0,4	0,433333	0,466667	0,5	0,533333
30	0,3	0,325	0,35	0,375	0,4
20	0,2	0,216667	0,233333	0,25	0,266667
10	0,1	0,108333	0,116667	0,125	0,133333
0	0	0	0	0	0

Figure E.0.3: Created pulse per revolution with used & installed disc

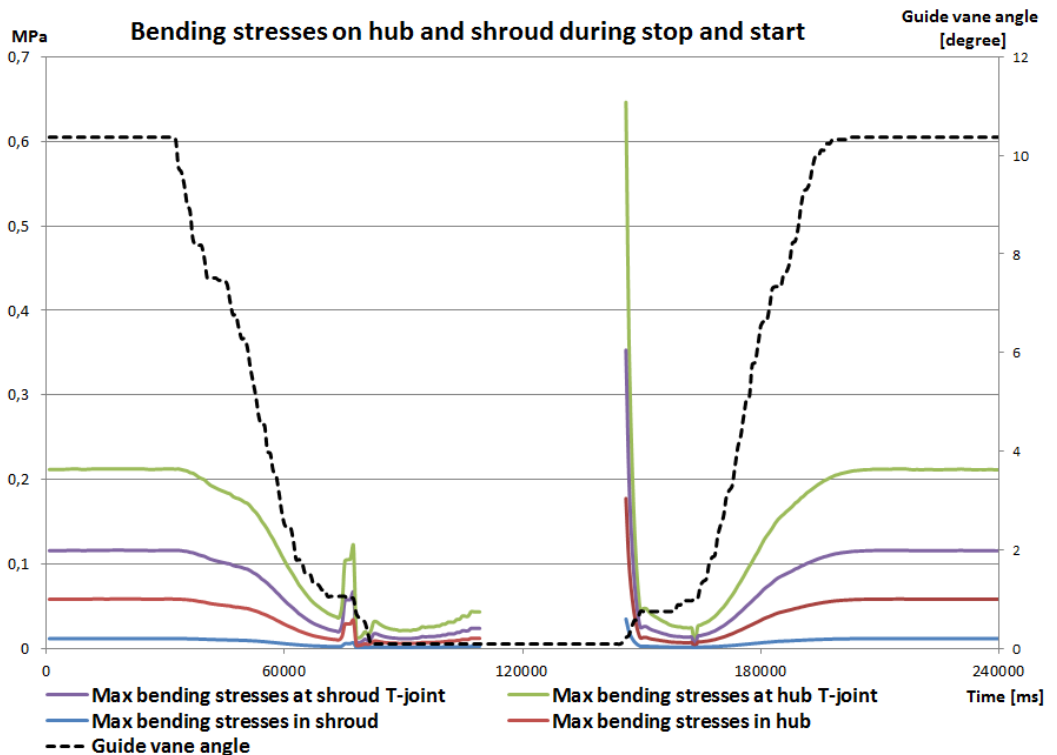
Disk with 60 pulses per revolution					
<i>Program update time</i>					
<i>Turbine rpm</i>	600 ms	650 ms	700 ms	750 ms	800 ms
100	60	65	70	75	80
90	54	58,5	63	67,5	72
80	48	52	56	60	64
70	42	45,5	49	52,5	56
60	36	39	42	45	48
50	30	32,5	35	37,5	40
40	24	26	28	30	32
30	18	19,5	21	22,5	24
20	12	13	14	15	16
10	6	6,5	7	7,5	8
0	0	0	0	0	0

Figure E.0.4: Created pulse per revolution with new & recommended disc

Appendix F

Calculation of bending stresses during the stop and start procedures

F.1 Graphical result of the calculated bending stresses



F.2 Equations to calculate the bending stresses

Maximum bending stresses at hub T-joint [7]

$$\sigma_{Blade-Hub} = k_{Hub} \cdot 6\Delta p \frac{b^2}{t_{Blade}^2} \quad (\text{F.2.1})$$

Maximum bending stresses in hub [7]

$$\sigma_{Hub} = k_{Hub} \cdot 3\Delta p \frac{b^2}{t_{Hub}^2} \quad (\text{F.2.2})$$

Maximum bending stresses at shroud T-joint [7]

$$\sigma_{Blade-Shroud} = k_{Shroud} \cdot 6\Delta p \frac{b^2}{t_{Blade}^2} \quad (\text{F.2.3})$$

Maximum bending stresses in shroud [7]

$$\sigma_{Shroud} = k_{Shroud} \cdot 3\Delta p \frac{b^2}{t_{Shroud}^2} \quad (\text{F.2.4})$$

Appendix **G**

Calibration

G.1 Pressure transducers attached on Francis rig

G.1.1 Pressure transducer Druck PTX1400 at inlet

CALIBRATION REPORT

CALIBRATION PROPERTIES

Calibrated by: Sigurd Haga
 Type/Producer: Druck PTX1400
 SN: Y21674/07
 Range: 0-10 bar g
 Unit: kPa

CALIBRATION SOURCE PROPERTIES

Type/Producer: Pressurements deadweight tester P3223-1
 SN: 66256
 Uncertainty [%]: 0,01

POLY FIT EQUATION:

$Y = -251.70683147E+0X^0 + 125.20071257E+0X^1$

CALIBRATION SUMMARY:

Max Uncertainty : Inf [%]
 Max Uncertainty : 0.041295 [kPa]
 RSQ : 1.000000
 Calibration points : 30

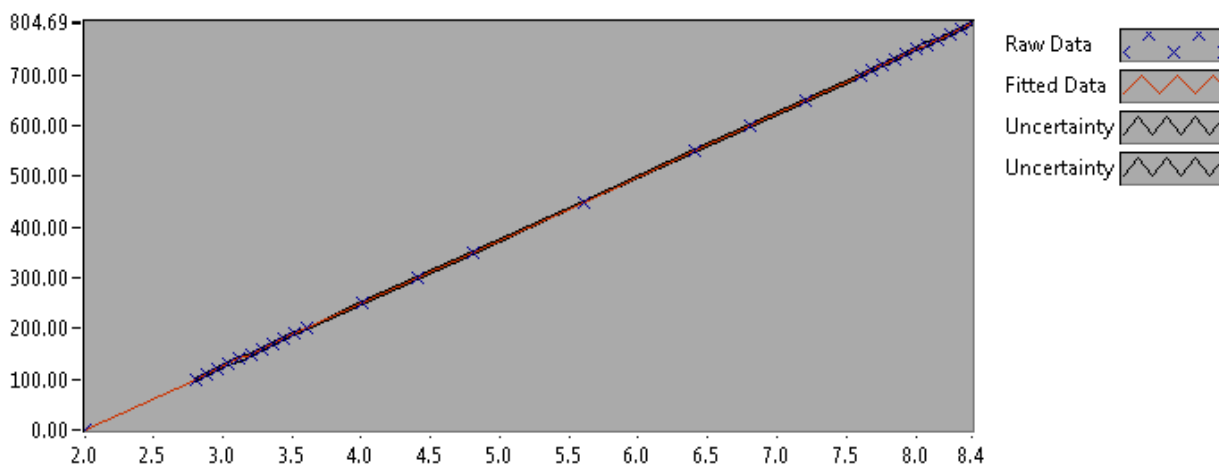


Figure 1 : Calibration chart (The uncertainty band is multiplied by 100)

Sigurd Haga

CALIBRATION VALUES

Value [kPa]	Voltage [V]	Best Poly Fit [kPa]	Deviation [kPa]	Uncertainty [%]	Uncertainty [kPa]
0.000000	2.011169	0.092931	-0.092931	Inf	NaN
99.415864	2.805229	99.509837	-0.093973	0.039400	0.039169
109.430971	2.885031	109.501155	-0.070184	0.035169	0.038486
119.446078	2.964944	119.506332	-0.060254	0.031654	0.037810
129.461185	3.044922	129.519614	-0.058429	0.028690	0.037143
139.476293	3.124689	139.506450	-0.030157	0.026160	0.036488
149.491400	3.204719	149.526257	-0.034858	0.023975	0.035841
159.506507	3.284417	159.504564	0.001942	0.022073	0.035207
169.521614	3.364449	169.524633	-0.003019	0.020400	0.034583
179.536721	3.444246	179.515229	0.021492	0.018923	0.033974
189.551828	3.524062	189.508202	0.043626	0.017609	0.033378
199.566935	3.603703	199.479328	0.087607	0.016435	0.032799
249.642471	4.003693	249.558330	0.084141	0.012059	0.030105
299.718006	4.403813	299.653673	0.064333	0.009300	0.027872
349.793541	4.803577	349.704463	0.089078	0.007500	0.026235
449.944612	5.602959	449.787613	0.156999	0.005587	0.025139
550.095683	6.403160	549.973410	0.122273	0.004935	0.027145
600.171219	6.803189	600.057219	0.114000	0.004857	0.029149
650.246754	7.203735	650.205901	0.040853	0.004871	0.031675
700.322290	7.604032	700.323337	-0.001048	0.004939	0.034587
710.337397	7.684037	710.340088	-0.002692	0.004958	0.035219
720.352504	7.764219	720.378959	-0.026456	0.004977	0.035854
730.367611	7.844151	730.386501	-0.018890	0.004997	0.036498
740.382718	7.924500	740.446277	-0.063559	0.005019	0.037159
750.397825	8.004477	750.459415	-0.061590	0.005041	0.037828
760.412932	8.084452	760.472328	-0.059396	0.005064	0.038506
770.428039	8.163878	770.416465	0.011574	0.005086	0.039181
780.443146	8.244222	780.475657	-0.032511	0.005109	0.039876
790.458254	8.324299	790.501372	-0.043118	0.005136	0.040595
800.473361	8.404625	800.558217	-0.084856	0.005159	0.041295

COMMENTS:

The uncertainty is calculated with 95% confidence. The uncertainty includes the randomness in the calibrated instrument during the calibration, systematic uncertainty in the instrument or property which the instrument under calibration is compared with (dead weight manometer, calibrated weights etc.), and due to regression analysis to fit the calibration points to a linear calibration equation. The calculated uncertainty can be used as the total systematic uncertainty of the calibrated instrument with the given calibration equation.

G.1.2 Pressure transducer PTX1400 in upper draft tube cone

CALIBRATION REPORT

CALIBRATION PROPERTIES

Calibrated by: Sigurd Haga
 Type/Producer: Druck PTX1400
 SN: Z00227/07
 Range: 0-4 bar g
 Unit: kPa

CALIBRATION SOURCE PROPERTIES

Type/Producer: Pressurements deadweight tester P3223-1
 SN: 66256
 Uncertainty [%]: 0,01

POLY FIT EQUATION:

$Y = -100.41820358E+0X^0 + 49.96688477E+0X^1$

CALIBRATION SUMMARY:

Max Uncertainty : Inf [%]
 Max Uncertainty : 0.044186 [kPa]
 RSQ : 1.000000
 Calibration points : 24

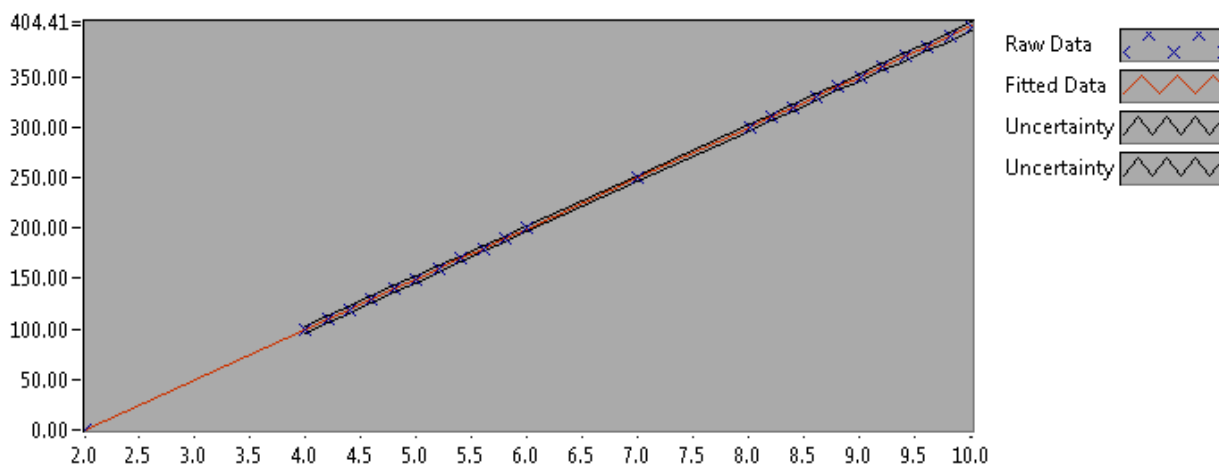


Figure 1 : Calibration chart (The uncertainty band is multiplied by 100)

Sigurd Haga

CALIBRATION VALUES

Value [kPa]	Voltage [V]	Best Poly Fit [kPa]	Deviation [kPa]	Uncertainty [%]	Uncertainty [kPa]
0.000000	2.012470	0.138675	-0.138675	Inf	NaN
99.415864	3.999243	99.411494	0.004370	0.040645	0.040408
109.430971	4.200290	109.457181	-0.026210	0.035337	0.038669
119.446078	4.401184	119.495226	-0.049148	0.030966	0.036988
129.461185	4.601059	129.482380	-0.021195	0.027329	0.035380
139.476293	4.801165	139.481032	-0.004739	0.024265	0.033844
149.491400	5.000907	149.461528	0.029871	0.021669	0.032393
159.506507	5.201620	159.490552	0.015955	0.019455	0.031031
169.521614	5.402217	169.513742	0.007872	0.017568	0.029781
179.536721	5.602288	179.510661	0.026060	0.015962	0.028657
189.551828	5.801537	189.466505	0.085323	0.014599	0.027673
199.566935	6.001874	199.476747	0.090188	0.013448	0.026838
249.642471	7.004300	249.564850	0.077620	0.010177	0.025406
299.718006	8.006613	299.647304	0.070702	0.009585	0.028729
309.733113	8.207218	309.670897	0.062216	0.009642	0.029865
319.748220	8.407960	319.701378	0.046842	0.009735	0.031128
329.763327	8.608415	329.717492	0.045835	0.009854	0.032495
339.778434	8.809336	339.756860	0.021575	0.009995	0.033962
349.793541	9.010762	349.821523	-0.027982	0.010153	0.035514
359.808649	9.210883	359.820914	-0.012266	0.010319	0.037127
369.823756	9.411952	369.867704	-0.043949	0.010496	0.038815
379.838863	9.612487	379.887836	-0.048973	0.010677	0.040556
389.853970	9.813714	389.942494	-0.088524	0.010863	0.042350
399.869077	10.014834	399.991847	-0.122770	0.011050	0.044186

COMMENTS:

The uncertainty is calculated with 95% confidence. The uncertainty includes the randomness in the calibrated instrument during the calibration, systematic uncertainty in the instrument or property which the instrument under calibration is compared with (dead weight manometer, calibrated weights etc.), and due to regression analysis to fit the calibration points to a linear calibration equation. The calculated uncertainty can be used as the total systematic uncertainty of the calibrated instrument with the given calibration equation.

G.1.3 Pressure transducer PTX1400 in lower draft tube cone

CALIBRATION REPORT

CALIBRATION PROPERTIES

Calibrated by: Sigurd Haga
 Type/Producer: Druck PTX1400
 SN: Z00580/02
 Range: 0-2,5 bar g
 Unit: kPa

CALIBRATION SOURCE PROPERTIES

Type/Producer: Pressurements deadweight tester P3223-1
 SN: 66256
 Uncertainty [%]: 0,01

POLY FIT EQUATION:

$Y = -62.94281179E+0X^0 + 31.34806609E+0X^1$

CALIBRATION SUMMARY:

Max Uncertainty : Inf [%]
 Max Uncertainty : 0.016306 [kPa]
 RSQ : 1.000000
 Calibration points : 17

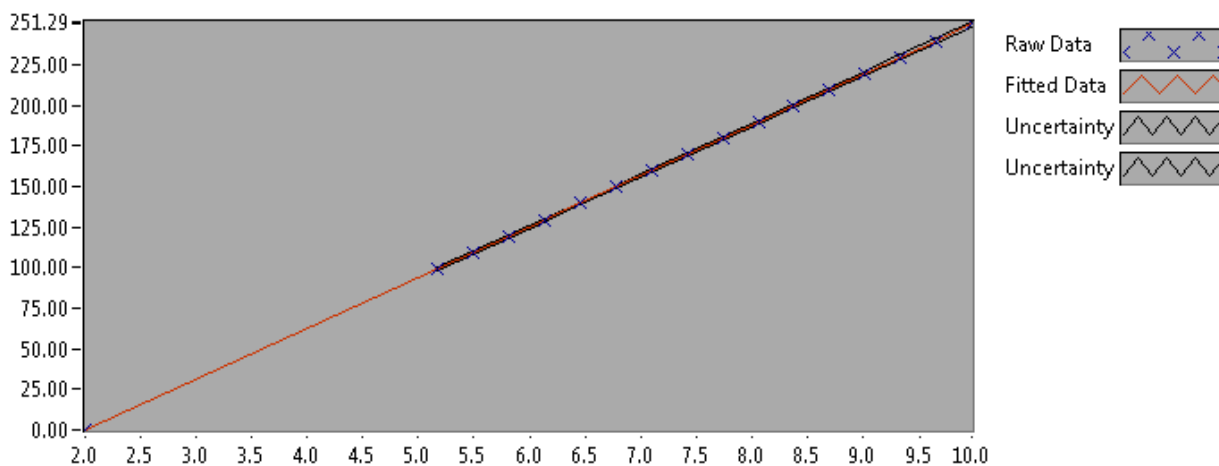


Figure 1 : Calibration chart (The uncertainty band is multiplied by 100)

Sigurd Haga

CALIBRATION VALUES

Value [kPa]	Voltage [V]	Best Poly Fit [kPa]	Deviation [kPa]	Uncertainty [%]	Uncertainty [kPa]
0.000000	2.009170	0.040768	-0.040768	Inf	NaN
99.415864	5.179483	99.423951	-0.008087	0.013903	0.013822
109.430971	5.498190	109.414805	0.016166	0.011636	0.012734
119.446078	5.817696	119.430701	0.015378	0.009834	0.011747
129.461185	6.137583	129.458531	0.002654	0.008414	0.010893
139.476293	6.456885	139.468040	0.008252	0.007321	0.010211
149.491400	6.775547	149.457469	0.033931	0.006509	0.009731
159.506507	7.095612	159.490895	0.015611	0.005946	0.009484
169.521614	7.415071	169.505309	0.016305	0.005598	0.009490
179.536721	7.734466	179.517728	0.018993	0.005429	0.009747
189.551828	8.054542	189.551501	0.000327	0.005402	0.010240
199.566935	8.373961	199.564681	0.002254	0.005478	0.010931
209.582042	8.693828	209.591877	-0.009835	0.005628	0.011796
219.597149	9.013899	219.625484	-0.028334	0.005824	0.012789
229.612256	9.333073	229.630978	-0.018721	0.006046	0.013883
239.627363	9.652167	239.633960	-0.006596	0.006285	0.015060
249.642471	9.971997	249.660001	-0.017530	0.006532	0.016306

COMMENTS:

The uncertainty is calculated with 95% confidence. The uncertainty includes the randomness in the calibrated instrument during the calibration, systematic uncertainty in the instrument or property which the instrument under calibration is compared with (dead weight manometer, calibrated weights etc.), and due to regression analysis to fit the calibration points to a linear calibration equation. The calculated uncertainty can be used as the total systematic uncertainty of the calibrated instrument with the given calibration equation.

G.1.4 Pressure transducer PTX1400 at downstream draft tube

CALIBRATION REPORT

CALIBRATION PROPERTIES

Calibrated by: Sigurd Haga
Type/Producer: Druck PTX1400
SN: D20661/04/2011
Range: 0-10 bar g
Unit: kPa

CALIBRATION SOURCE PROPERTIES

Type/Producer: Pressurements deadweight tester P3223-1
SN: 66256
Uncertainty [%]: 0,01

POLY FIT EQUATION:

$Y = -250.91547257E+0X^0 + 125.18474835E+0X^1$

CALIBRATION SUMMARY:

Max Uncertainty : Inf [%]
Max Uncertainty : 0.036732 [kPa]
RSQ : 1.000000
Calibration points : 30

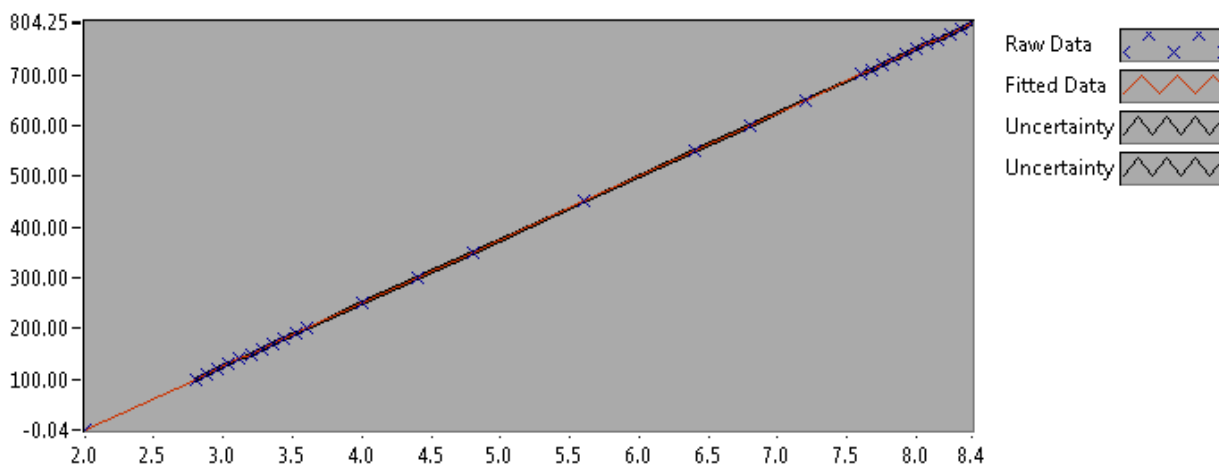


Figure 1 : Calibration chart (The uncertainty band is multiplied by 100)

Sigurd Haga

CALIBRATION VALUES

Value [kPa]	Voltage [V]	Best Poly Fit [kPa]	Deviation [kPa]	Uncertainty [%]	Uncertainty [kPa]
0.000000	2.004067	-0.036839	0.036839	Inf	NaN
99.415864	2.797695	99.313294	0.102570	0.035048	0.034844
109.430971	2.878049	109.372396	0.058575	0.031281	0.034232
119.446078	2.958511	119.444976	0.001102	0.028153	0.033628
129.461185	3.038730	129.487224	-0.026039	0.025516	0.033033
139.476293	3.118577	139.482812	-0.006519	0.023266	0.032450
149.491400	3.198913	149.539687	-0.048287	0.021321	0.031874
159.506507	3.278927	159.556150	-0.049643	0.019627	0.031307
169.521614	3.359178	169.602432	-0.080819	0.018140	0.030751
179.536721	3.439146	179.613178	-0.076457	0.016825	0.030207
189.551828	3.519165	189.630271	-0.078443	0.015655	0.029675
199.566935	3.598926	199.615207	-0.048272	0.014609	0.029155
249.642471	3.998583	249.646179	-0.003709	0.010721	0.026765
299.718006	4.398473	299.706296	0.011710	0.008270	0.024786
349.793541	4.797999	349.720871	0.072670	0.006670	0.023331
449.944612	5.597755	449.838134	0.106479	0.004969	0.022359
550.095683	6.398159	550.036443	0.059240	0.004390	0.024146
600.171219	6.797914	600.079637	0.091582	0.004320	0.025926
650.246754	7.198177	650.186546	0.060208	0.004331	0.028160
700.322290	7.598640	700.318362	0.003928	0.004393	0.030763
710.337397	7.678699	710.340535	-0.003138	0.004410	0.031325
720.352504	7.758745	720.361007	-0.008503	0.004427	0.031890
730.367611	7.838548	730.351140	0.016471	0.004444	0.032454
740.382718	7.918889	740.408616	-0.025898	0.004463	0.033047
750.397825	7.997820	750.289668	0.108157	0.004481	0.033626
760.412932	8.078768	760.423119	-0.010186	0.004503	0.034238
770.428039	8.158853	770.448531	-0.020492	0.004524	0.034851
780.443146	8.239067	780.489997	-0.046850	0.004545	0.035467
790.458254	8.319413	790.548207	-0.089953	0.004568	0.036109
800.473361	8.399547	800.579684	-0.106323	0.004589	0.036732

COMMENTS:

The uncertainty is calculated with 95% confidence. The uncertainty includes the randomness in the calibrated instrument during the calibration, systematic uncertainty in the instrument or property which the instrument under calibration is compared with (dead weight manometer, calibrated weights etc.), and due to regression analysis to fit the calibration points to a linear calibration equation. The calculated uncertainty can be used as the total systematic uncertainty of the calibrated instrument with the given calibration equation.

G.1.5 First pressure transducer Kuliter XTL-190-7BARA in vaneless space

CALIBRATION REPORT

CALIBRATION PROPERTIES

Calibrated by: Sigurd Haga
 Type/Producer: Kulite XTL-190M
 SN: V4537-34
 Range: 0-7 bar abs
 Unit: kPa

CALIBRATION SOURCE PROPERTIES

Type/Producer: Pressurements deadweight tester P3223-1
 SN: 66256
 Uncertainty [%]: 0,01

POLY FIT EQUATION:

$Y = + 92.68619459E+0X^0 - 70.72386673E+0X^1$

CALIBRATION SUMMARY:

Max Uncertainty : 0.118965 [%]
 Max Uncertainty : 0.120765 [kPa]
 RSQ : 0.999999
 Calibration points : 28

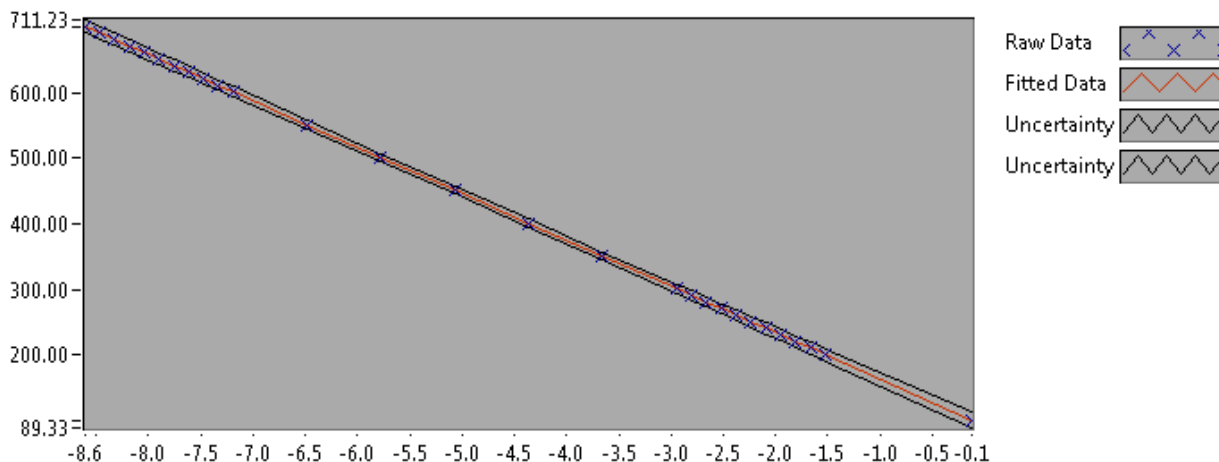


Figure 1 : Calibration chart (The uncertainty band is multiplied by 100)

Sigurd Haga

CALIBRATION VALUES

Value [kPa]	Voltage [V]	Best Poly Fit [kPa]	Deviation [kPa]	Uncertainty [%]	Uncertainty [kPa]
101.513126	-0.123252	101.403060	0.110066	0.118965	0.120765
200.928990	-1.528589	200.793953	0.135037	0.046653	0.093739
210.934082	-1.669567	210.764432	0.169649	0.043267	0.091265
220.949189	-1.811563	220.806961	0.142228	0.040160	0.088733
230.964296	-1.953644	230.855434	0.108862	0.037417	0.086420
240.979403	-2.095628	240.897092	0.082311	0.034948	0.084217
250.994510	-2.239450	251.068734	-0.074224	0.032665	0.081986
261.009617	-2.380289	261.029449	-0.019832	0.030603	0.079877
271.024724	-2.522025	271.053570	-0.028846	0.028715	0.077825
281.039831	-2.663851	281.084056	-0.044225	0.026980	0.075824
291.044923	-2.805688	291.115330	-0.070406	0.025424	0.073995
301.060030	-2.947466	301.142407	-0.082377	0.023957	0.072126
351.135566	-3.656630	351.297188	-0.161622	0.018356	0.064453
401.201086	-4.365497	401.431055	-0.229969	0.014907	0.059807
451.276622	-5.073456	451.500646	-0.224024	0.013035	0.058822
501.342142	-5.781257	501.559053	-0.216911	0.012312	0.061723
551.417677	-6.488607	551.585551	-0.167873	0.012326	0.067970
601.493213	-7.194344	601.497996	-0.004783	0.012757	0.076733
611.498305	-7.336260	611.534841	-0.036536	0.012867	0.078683
621.513412	-7.477995	621.558897	-0.045485	0.012995	0.080766
631.528519	-7.618288	631.480958	0.047561	0.013120	0.082857
641.543626	-7.759356	641.457873	0.085753	0.013251	0.085012
651.558733	-7.902752	651.599351	-0.040617	0.013382	0.087192
661.563825	-8.040629	661.350600	0.213226	0.013514	0.089401
671.578932	-8.181430	671.308549	0.270383	0.013664	0.091762
681.594039	-8.331349	681.911433	-0.317394	0.013818	0.094182
691.609147	-8.466824	691.492731	0.116415	0.013949	0.096471
701.624254	-8.606068	701.340620	0.283633	0.014088	0.098844

COMMENTS:

The uncertainty is calculated with 95% confidence. The uncertainty includes the randomness in the calibrated instrument during the calibration, systematic uncertainty in the instrument or property which the instrument under calibration is compared with (dead weight manometer, calibrated weights etc.), and due to regression analysis to fit the calibration points to a linear calibration equation. The calculated uncertainty can be used as the total systematic uncertainty of the calibrated instrument with the given calibration equation.

**G.1.6 Second pressure transducer Kuliter XTL-190-3.5BARA
in vaneless space**

CALIBRATION REPORT

CALIBRATION PROPERTIES

Calibrated by: Sigurd Haga
 Type/Producer: Kulite XTL-190M
 SN: V4537-33
 Range: 0-3.5 bar abs
 Unit: kPa

CALIBRATION SOURCE PROPERTIES

Type/Producer: Pressurements deadweight tester P3223-1
 SN: 66256
 Uncertainty [%]: 0,01

POLY FIT EQUATION:

$Y = + 8.06160398E+0X^0 - 79.61615924E+0X^1$

CALIBRATION SUMMARY:

Max Uncertainty : 0.178622 [%]
 Max Uncertainty : 0.181396 [kPa]
 RSQ : 0.999996
 Calibration points : 17

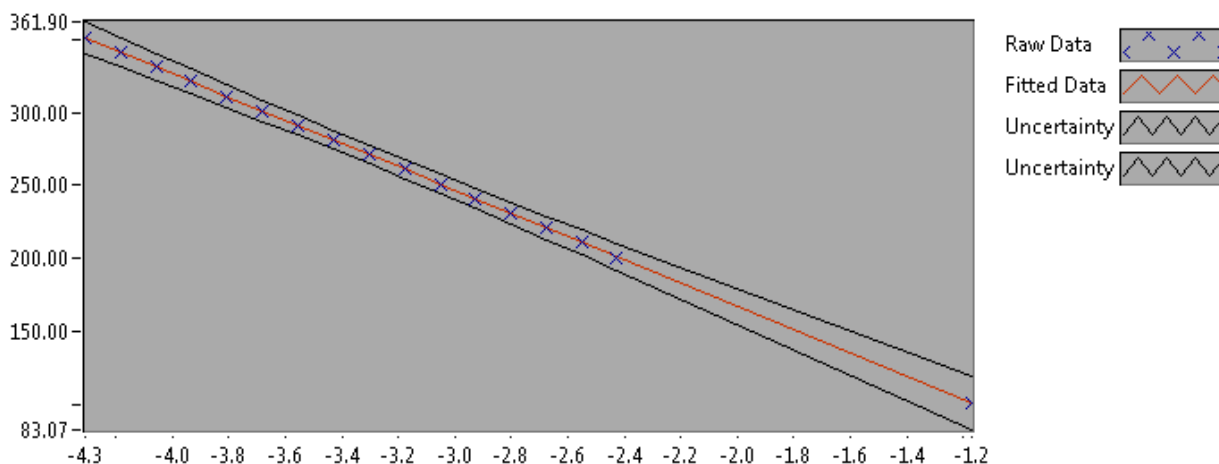


Figure 1 : Calibration chart (The uncertainty band is multiplied by 100)

Sigurd Haga

CALIBRATION VALUES

Value [kPa]	Voltage [V]	Best Poly Fit [kPa]	Deviation [kPa]	Uncertainty [%]	Uncertainty [kPa]
101.553186	-1.169910	101.205350	0.347836	0.178622	0.181396
200.969050	-2.426168	201.223777	-0.254727	0.045624	0.091690
210.984157	-2.550665	211.135779	-0.151622	0.040058	0.084517
220.999264	-2.675776	221.096647	-0.097382	0.035297	0.078006
231.004356	-2.801404	231.098595	-0.094239	0.031322	0.072356
241.019463	-2.927003	241.098359	-0.078896	0.028141	0.067824
251.034570	-3.051805	251.034634	-0.000064	0.025755	0.064655
261.049678	-3.177858	261.070484	-0.020806	0.024139	0.063015
271.064785	-3.303612	271.082530	-0.017745	0.023264	0.063060
281.079892	-3.429160	281.078124	0.001768	0.023046	0.064778
291.094999	-3.554588	291.064251	0.030748	0.023372	0.068034
301.110106	-3.680280	301.071367	0.038739	0.024122	0.072635
311.125213	-3.805596	311.048569	0.076644	0.025174	0.078322
321.130305	-3.932369	321.141706	-0.011401	0.026459	0.084967
331.145412	-4.057422	331.097957	0.047455	0.027847	0.092213
341.160519	-4.182763	341.077091	0.083428	0.029315	0.100012
351.175626	-4.308343	351.075362	0.100264	0.030825	0.108248

COMMENTS:

The uncertainty is calculated with 95% confidence. The uncertainty includes the randomness in the calibrated instrument during the calibration, systematic uncertainty in the instrument or property which the instrument under calibration is compared with (dead weight manometer, calibrated weights etc.), and due to regression analysis to fit the calibration points to a linear calibration equation. The calculated uncertainty can be used as the total systematic uncertainty of the calibrated instrument with the given calibration equation.

G.2 Internal pressure transducers in Francis rig

Calibration of inlet pressure

CALIBRATION REPORT

CALIBRATION PROPERTIES

Calibrated by: Sigurd Haga
 Type/Producer: FHCW36W1-ACKAY / Fuji Electric
 SN: N3M7766T
 Range: -50 - 50 bar
 Unit: kPa

CALIBRATION SOURCE PROPERTIES

Type/Producer: Pressurements deadweight tester P3223-1
 SN: 66256
 Uncertainty [%]: 0,01

POLY FIT EQUATION:

$$Y = -123.4925116E+3X^0 + 62.6940117E+3X^1$$

CALIBRATION SUMMARY:

Max Uncertainty : Inf [%]
 Max Uncertainty : 0.11945150 [kPa]
 RSQ : 1.000000
 Calibration points : 31

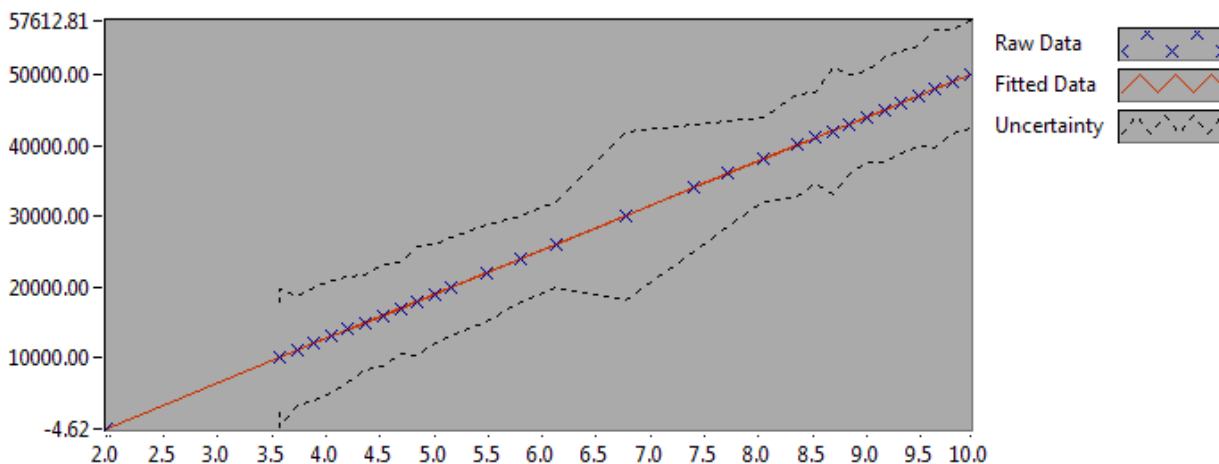


Figure 1 : Calibration chart (The uncertainty band is multiplied by 1000)

Sigurd Haga

CALIBRATION VALUES

Value [kPa]	Voltage [V]	Best Poly Fit [kPa]	Deviation [kPa]	Uncertainty [%]	Uncertainty [kPa]
100.15107096	3.568514	100.23194381	-0.08087286	0.078017	0.07813460
110.16617805	3.728806	110.28131534	-0.11513728	0.069667	0.07674990
120.18128515	3.887419	120.22538384	-0.04409870	0.065701	0.07896064
130.19639224	4.047206	130.24307170	-0.04667946	0.061127	0.07958517
140.21149934	4.205739	140.18214229	0.02935705	0.053951	0.07564578
150.22660644	4.366537	150.26323251	-0.03662607	0.044391	0.06668730
160.24171353	4.525215	160.21139279	0.03032074	0.044800	0.07178866
170.25682063	4.684813	170.21719787	0.03962276	0.038009	0.06471346
180.27192772	4.846488	180.35327244	-0.08134472	0.042415	0.07646212
190.28703482	5.004530	190.26156363	0.02547118	0.036347	0.06916286
200.30214191	5.162530	200.16722868	0.13491323	0.034843	0.06979034
220.33235611	5.481835	220.18572320	0.14663291	0.030977	0.06825306
240.36257030	5.801508	240.22732202	0.13524828	0.025258	0.06070966
260.39278449	6.121151	260.26701631	0.12576818	0.023296	0.06066156
300.45321287	6.764796	300.61967074	-0.16645787	0.039757	0.11945150
340.51364125	7.399644	340.42084282	0.09279843	0.026285	0.08950298
360.54385545	7.721100	360.57421222	-0.03035677	0.020555	0.07411008
380.57406964	8.037890	380.43508505	0.13898458	0.015876	0.06041961
400.60428383	8.360698	400.67320123	-0.06891740	0.018127	0.07261675
410.61939092	8.518145	410.54415357	0.07523735	0.015897	0.06527732
420.63449802	8.681732	420.80006677	-0.16556876	0.021281	0.08951393
430.64960511	8.838419	430.62340630	0.02619882	0.016469	0.07092244
440.66471221	8.998681	440.67090756	-0.00619535	0.014683	0.06470099
450.67981931	9.158291	450.67751380	0.00230551	0.016641	0.07499894
460.69492640	9.317464	460.65669249	0.03823391	0.015766	0.07263225
470.71003350	9.477423	470.68515556	0.02487793	0.014922	0.07023966
480.72514059	9.636606	480.66498479	0.06015581	0.017254	0.08294249
490.74024769	9.798846	490.83644408	-0.09619639	0.014973	0.07347674
500.75535478	9.958927	500.87256862	-0.11721383	0.015028	0.07525550
100.15107096	3.569086	100.26777774	-0.11670679	0.096805	0.09695141
0.000000	1.969028	-0.04624555	0.04624555	Inf	NaN

COMMENTS:

The uncertainty is calculated with 95% confidence. The uncertainty includes the randomness in the calibrated instrument during the calibration, systematic uncertainty in the instrument or property which the instrument under calibration is compared with (dead weight manometer, calibrated weights etc.), and due to regression analysis to fit the calibration points to a linear calibration equation. The calculated uncertainty can be used as the total systematic uncertainty of the calibrated instrument with the given calibration equation.

Calibration of differential pressure

CALIBRATION REPORT

CALIBRATION PROPERTIES

Calibrated by: Sigurd Haga
 Type/Producer: FHCW36W1-ACKAY / Fuji Electric
 SN: N3M7762T
 Range: -50 - 50 bar
 Unit: kPa

CALIBRATION SOURCE PROPERTIES

Type/Producer: Pressurements deadweight tester P3223-1
 SN: 66256
 Uncertainty [%]: 0,01

POLY FIT EQUATION:

$Y = -123.4029305E+3X^0 + 62.6675364E+3X^1$

CALIBRATION SUMMARY:

Max Uncertainty : Inf [%]
 Max Uncertainty : 0.08238731 [kPa]
 RSQ : 1.000000
 Calibration points : 30

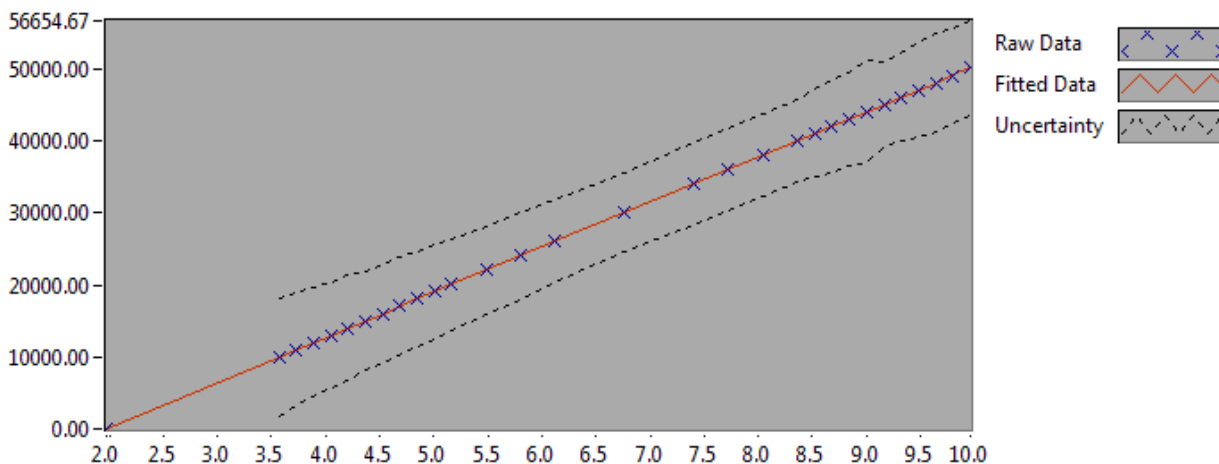


Figure 1 : Calibration chart (The uncertainty band is multiplied by 1000)

Sigurd Haga

CALIBRATION VALUES

Value [kPa]	Voltage [V]	Best Poly Fit [kPa]	Deviation [kPa]	Uncertainty [%]	Uncertainty [kPa]
0.000000	1.975083	0.37065083	-0.37065083	Inf	NaN
100.15107096	3.567598	100.16962074	-0.01854979	0.082263	0.08238731
110.16617805	3.727182	110.17040291	-0.00422486	0.070363	0.07751579
120.18128515	3.886257	120.13919505	0.04209010	0.062481	0.07509030
130.19639224	4.046721	130.19510559	0.00128665	0.056863	0.07403338
140.21149934	4.206555	140.21148661	0.00001273	0.052981	0.07428499
150.22660644	4.366058	150.20719170	0.01941474	0.045691	0.06864049
160.24171353	4.525651	160.20846578	0.03324775	0.043076	0.06902508
170.25682063	4.685033	170.19656377	0.06025686	0.040731	0.06934736
180.27192772	4.845520	180.25386611	0.01806161	0.036399	0.06561766
190.28703482	5.004610	190.22364069	0.06339413	0.034469	0.06558975
200.30214191	5.164502	200.24369873	0.05844319	0.031441	0.06297703
220.33235611	5.483303	220.22213608	0.11022002	0.027966	0.06161770
240.36257030	5.803237	240.27164610	0.09092420	0.025286	0.06077768
260.39278449	6.123783	260.35943944	0.03334505	0.021861	0.05692380
300.45321287	6.762144	300.36398327	0.08922960	0.018367	0.05518412
340.51364125	7.402044	340.46492528	0.04871597	0.016989	0.05785083
360.54385545	7.721382	360.47705527	0.06680018	0.016125	0.05813864
380.57406964	8.041240	380.52176449	0.05230514	0.015111	0.05750792
400.60428383	8.361462	400.58928744	0.01499639	0.014245	0.05706766
410.61939092	8.521777	410.63581110	-0.01642018	0.014788	0.06072124
420.63449802	8.681091	420.61963846	0.01485956	0.015406	0.06480335
430.64960511	8.841386	430.66493558	-0.01533047	0.014914	0.06422514
440.66471221	9.000692	440.64825390	0.01645831	0.015969	0.07036982
450.67981931	9.161257	450.71049160	-0.03067230	0.013138	0.05921241
460.69492640	9.321747	460.76797292	-0.07304652	0.013339	0.06145330
470.71003350	9.480984	470.74696393	-0.03693044	0.013958	0.06570405
480.72514059	9.641579	480.81105685	-0.08591626	0.014141	0.06797985
490.74024769	9.801412	490.82744223	-0.08719454	0.013352	0.06552514
500.75535478	9.961352	500.85048081	-0.09512602	0.013119	0.06569623

COMMENTS:

The uncertainty is calculated with 95% confidence. The uncertainty includes the randomness in the calibrated instrument during the calibration, systematic uncertainty in the instrument or property which the instrument under calibration is compared with (dead weight manometer, calibrated weights etc.), and due to regression analysis to fit the calibration points to a linear calibration equation. The calculated uncertainty can be used as the total systematic uncertainty of the calibrated instrument with the given calibration equation.

G.3 Weighing tank



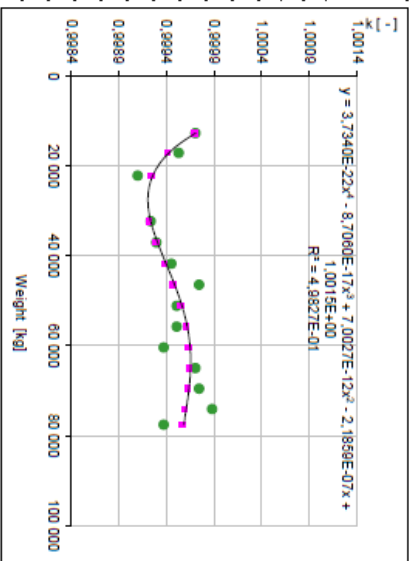
WATERPOWER LABORATORY		Date:
Calibration Sheet		30.09.2013
Calibration of weighing tank load cells		Operator:
		Masterstudentene

W_L 5126,075 [kg]


Unit: Weighing tank load cells, reg. nr. 4331-5/07

Comments:
The flow controlled via the left storage tanks.
Indicated Q= ca.200 l/s ->time of filling->30s
"Valve 1" 200% open

Manual Observation Weights off [kg]	Manual Observation Weights on [kg]	Displayed load increase ΔW [kg]	$k = \frac{W_L}{\Delta W}$ [-]	Weight midpoint [kg]	Estimated correction factor k [-]	Difference in real k and estimated k Δk [-]	Δk [%]
10096	16223,6	6127,6	0,9997	12659,8	0,99969	-0,00001	0,001
14489,8	19618,3	5128,5	0,9995	17054,1	0,99941	-0,00012	0,012
19689,2	24719,9	5130,7	0,9991	22154,6	0,99924	0,00014	0,014
29710,4	34940,4	5130	0,9992	32275,4	0,99922	-0,00002	0,002
34446,6	39676,3	5129,7	0,9993	37011,5	0,99929	0,00000	0,000
39164,7	44293,6	5128,9	0,9994	41729,2	0,99938	-0,00007	0,007
43980	48997,4	5127,4	0,9997	46423,7	0,99947	-0,00027	0,027
49632,1	53660,7	5128,6	0,9995	51096,4	0,99954	0,00004	0,004
53182,2	58310,8	5128,6	0,9995	55746,5	0,99960	0,00009	0,009
57805,7	62995	5129,3	0,9994	60370,4	0,99963	0,00026	0,026
62412	67539,6	5127,6	0,9997	64975,8	0,99963	-0,00007	0,007
66999,6	72127	5127,4	0,9997	69683,3	0,99962	-0,00012	0,012
71600,3	76697	5126,7	0,9999	74123,7	0,99959	-0,00029	0,029
74999,2	80125,5	5129,3	0,9994	77590,9	0,99956	0,00019	0,019



G.4 Flowmeter



WATERPOWER LABORATORY

Calibration Sheet

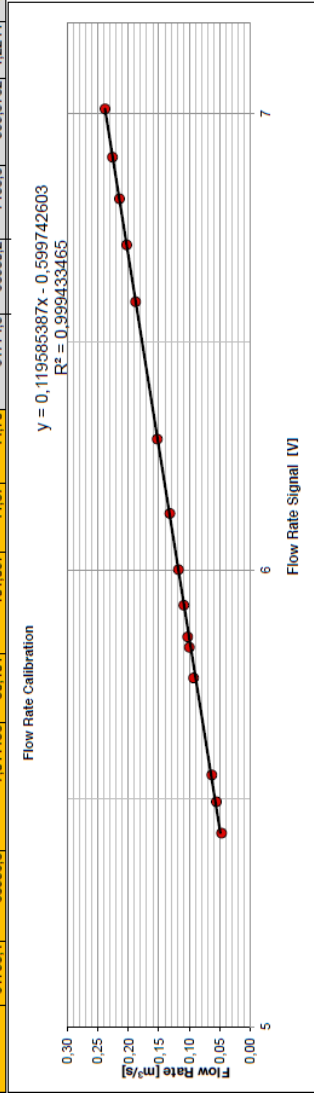
Calibration of flow meter

Date: 28.01.2014

Operator: **Sigurd Haga**

Calibrator: Weighing tank system Unit: Flowmeter, reg nr. 4624-7 (A03 36133)

Date	Manual Observation before Weight [kg]	Manual Observation after Weight [kg]	Manual Observation Voltage [V]	Time [s]	Ambient pressure P _{amb} [kPa]	Water temp T _w [°C]	Air temp T _a [°C]	Calculated value		Density of water [kg/m ³]	Density of air [kg/m ³]	Differential volume [m ³]	Calculated Flow Rate Q [m ³ /s]	Estimate Q [m ³ /s]	Deviation [%]
								before Weight [kg]	after Weight [kg]						
28.01.2014	22127.8	26789.8	5.424157	100.088	100.995	11.71	15.79	22127.9	26786.2	999.5964	1.2185	4.66587	0.0466130	0.04891	4.69115
	26789.8	32329.8	5.492908	100.089	101.007	11.72	15.82	26786.2	32321.8	999.5953	1.2184	5.54456	0.0563907	0.05713	3.04259
	32329.8	37453.4	5.551698	80.101	101.034	11.76	15.90	32321.8	37341.6	999.5907	1.2185	5.02904	0.0627712	0.06415	2.14360
	37453.4	43663.0	5.764079	70.101	101.055	11.79	15.27	37341.6	43847.1	999.5873	1.2215	6.51606	0.0929523	0.08956	-3.79140
	43663.0	49353.4	5.831967	95.102	101.052	11.72	15.19	43847.1	49334.6	999.5963	1.2218	5.49643	0.0987502	0.09760	-2.19919
	49353.4	54479.4	5.854269	101.050	101.044	11.73	15.04	49334.6	54458.3	999.5941	1.2221	5.13207	0.1024325	0.10034	-2.08298
	54479.4	59835.5	5.923835	40.101	101.044	11.73	15.04	54458.3	58812.7	999.5941	1.2224	4.36149	0.1087626	0.10866	-0.09306
	59835.5	63553.4	6.001593	40.102	101.039	11.73	15.00	58812.7	63528.8	999.5941	1.2224	4.72385	0.1177960	0.11796	0.13925
	63553.4	68831.6	6.124743	40.101	101.045	11.74	14.88	63528.8	68805.1	999.5930	1.2230	5.28487	0.1317889	0.13269	0.67698
	68831.6	74922.5	6.287605	35.102	101.083	11.80	14.83	68805.1	74904.4	999.5862	1.2237	5.34970	0.1524087	0.15216	-0.16144
	74922.5	81792.5	6.589692	30.102	101.086	11.80	14.80	74904.4	81768.8	999.5862	1.2238	6.66366	0.1881491	0.18817	0.00977
	81792.5	89675.5	6.713098	30.101	101.101	11.79	14.79	81768.8	89652.3	999.5873	1.2240	6.10359	0.2027703	0.20305	0.13378
	89675.5	96121.9	6.814321	30.101	101.096	11.83	14.76	89652.3	96096.4	999.5828	1.2241	6.45463	0.2144325	0.21515	0.33378
	96121.9	102798.4	6.905254	30.101	101.092	11.83	14.74	96096.4	102770.9	999.5828	1.2242	6.80578	0.2266980	0.22602	-0.03235
	102798.4	110113.8	7.011138	30.101	101.097	11.87	14.70	102770.9	110109.2	999.5782	1.2244	7.16756	0.2381171	0.23889	0.23877



G.5 Friction torque

CALIBRATION REPORT

CALIBRATION PROPERTIES

Calibrated by: Sigurd Haga

Type/Producer:

SN: V4331-9

Range: 0-X kg

Unit: kg

CALIBRATION SOURCE PROPERTIES

Type/Producer: Calibrated weights from the Norwegian Metrology Service

SN: -

Uncertainty [%]: -

POLY FIT EQUATION:

$$Y = + 4.94233453E+0X^0 + 3.56050316E+0X^1$$

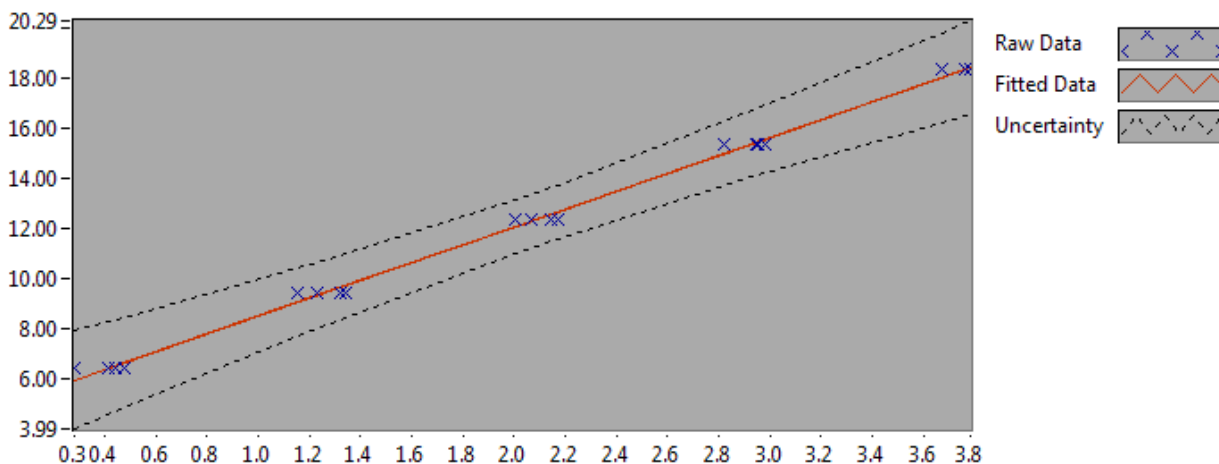
CALIBRATION SUMMARY:

Max Uncertainty : 3.050197 [%]

Max Uncertainty : 0.195622 [Nm]

RSQ : 0.996974

Calibration points : 20



Sigurd Haga

CALIBRATION VALUES

Value [Nm]	Voltage [V]	Best Poly Fit [Nm]	Deviation [Nm]	Uncertainty [%]	Uncertainty [Nm]
6.413417	0.282346	5.947627	0.465790	3.050197	0.195622
9.392601	1.156561	9.060273	0.332328	1.451454	0.136329
12.371785	2.004324	12.078738	0.293048	0.868079	0.107397
15.350969	2.823888	14.996796	0.354174	0.822492	0.126261
18.330154	3.671944	18.016302	0.313852	0.977586	0.179193
18.330154	3.759031	18.326378	0.003776	1.012307	0.185557
15.350969	2.950999	15.449377	-0.098408	0.864223	0.132667
12.371785	2.143939	12.575837	-0.204052	0.866651	0.107220
9.392601	1.319573	9.640678	-0.248077	1.359450	0.127688
6.413417	0.444982	6.526693	-0.113276	2.859470	0.183390
6.413417	0.414234	6.417216	-0.003800	2.894625	0.185644
9.392601	1.233979	9.335922	0.056679	1.406125	0.132072
12.371785	2.065743	12.297419	0.074366	0.865852	0.107121
15.350969	2.945771	15.430761	-0.079791	0.862500	0.132402
18.330154	3.762655	18.339281	-0.009128	1.013819	0.185835
18.330154	3.783015	18.411773	-0.081619	1.022025	0.187339
15.350969	2.980893	15.555812	-0.204843	0.874880	0.134302
12.371785	2.170794	12.671452	-0.299667	0.867867	0.107371
9.392601	1.342211	9.721281	-0.328680	1.347812	0.126595
6.413417	0.475706	6.636088	-0.222671	2.824769	0.181164

COMMENTS:

The uncertainty is calculated with 95% confidence. The uncertainty includes the randomness in the calibrated instrument during the calibration, systematic uncertainty in the instrument or property which the instrument under calibration is compared with (dead weight manometer, calibrated weights etc.), and due to regression analysis to fit the calibration points to a linear calibration equation. The calculated uncertainty can be used as the total systematic uncertainty of the calibrated instrument with the given calibration equation.

G.6 Generator torque

CALIBRATION REPORT

CALIBRATION PROPERTIES

Calibrated by: Sigurd Haga
 Type/Producer: HBM Z6FC3
 SN: V4536-4
 Range: 50-500 kg
 Unit: kg

CALIBRATION SOURCE PROPERTIES

Type/Producer: Calibrated weights from the Norwegian Metrology Service
 SN:
 Uncertainty [%]:

POLY FIT EQUATION:

$Y = -194.76444248E+0X^0 + 483.04451254E+0X^1$

CALIBRATION SUMMARY:

Max Uncertainty : Inf [%]
 Max Uncertainty : 8.452808 [Nm]
 RSQ : 0.999220
 Calibration points : 62

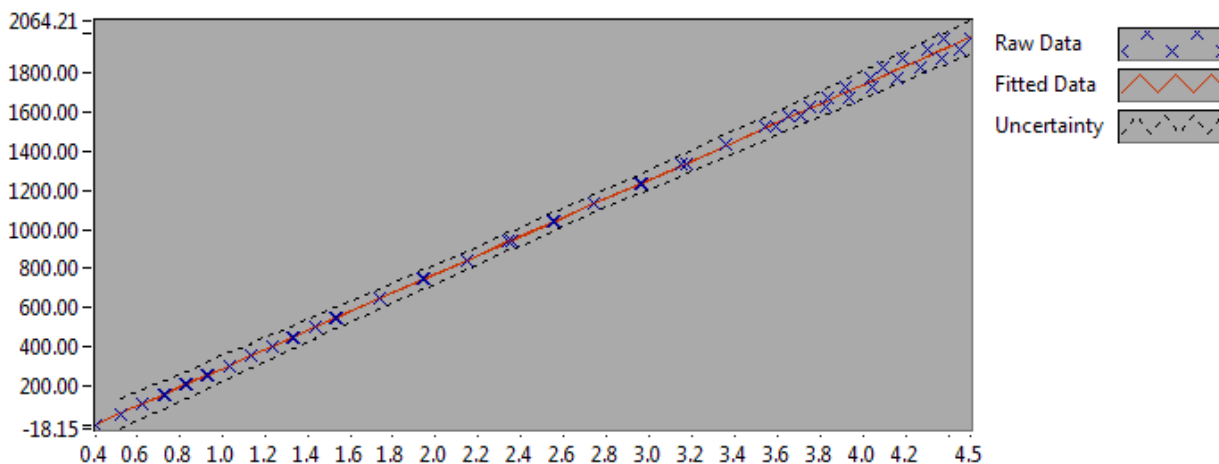


Figure 1 : Calibration chart (The uncertainty band is multiplied by 10)

Sigurd Haga

CALIBRATION VALUES

Value [kPa]	Voltage [V]	Best Poly Fit [kPa]	Deviation [kPa]	Uncertainty [%]	Uncertainty [kPa]
0.000000	0.410646	3.595961	-3.595961	Inf	NaN
58.977897	0.529835	61.169460	-2.191563	13.407204	7.907287
107.986952	0.630283	109.690456	-1.703504	7.065710	7.630045
156.996987	0.731147	158.412290	-1.415303	4.686240	7.357256
206.005258	0.831619	206.944393	-0.939135	3.442486	7.091701
255.009020	0.931386	255.136282	-0.127262	2.680214	6.834787
304.021113	1.035067	305.219148	-1.198036	2.163003	6.575986
353.033010	1.132356	352.213670	0.819340	1.796264	6.341404
402.048337	1.234668	401.635295	0.413043	1.518360	6.104540
451.058372	1.330344	447.850784	3.207589	1.306529	5.893210
500.073406	1.438344	500.019922	0.053484	1.133380	5.667731
549.086381	1.540121	549.182498	-0.096117	0.996124	5.469582
647.103020	1.741200	646.312688	0.790332	0.791997	5.125040
745.123188	1.947096	745.769782	-0.646594	0.650646	4.848113
843.139827	2.147145	842.402091	0.737737	0.553365	4.665645
941.118242	2.351661	941.192738	-0.074495	0.486476	4.578313
1039.116945	2.549372	1036.695846	2.421099	0.442080	4.593730
1137.101731	2.743416	1130.427749	6.673981	0.413694	4.704121
1235.089555	2.957853	1234.010046	1.079508	0.399043	4.928538
1333.069734	3.145622	1324.710785	8.358948	0.390189	5.201493
1431.046384	3.360490	1428.501789	2.544595	0.390509	5.588360
1529.024113	3.537953	1514.224575	14.799538	0.389636	5.957631
1578.014741	3.648419	1567.584175	10.430566	0.393305	6.206415
1627.003606	3.746582	1615.001447	12.002159	0.395663	6.437445
1676.002075	3.831716	1656.124927	19.877148	0.396516	6.645617
1724.989959	3.917986	1697.797167	27.192792	0.397820	6.862360
1773.978824	4.034160	1753.914646	20.064177	0.403788	7.163105
1822.975039	4.094789	1783.200834	39.774205	0.401768	7.324121
1871.970372	4.186937	1827.712680	44.257691	0.404472	7.571590
1920.963255	4.302142	1883.361417	37.601838	0.410692	7.889244
1969.964566	4.372498	1917.346524	52.618042	0.410464	8.085992
1969.964566	4.501549	1979.683916	-9.719350	0.429084	8.452808
1920.963255	4.454698	1957.052856	-36.089602	0.433041	8.318562
1871.970372	4.369423	1915.861315	-43.890944	0.431475	8.077078
1822.975039	4.268232	1866.981609	-44.006571	0.427579	7.794661
1773.978824	4.160712	1815.044851	-41.066028	0.422810	7.500555
1724.989959	4.041867	1757.637047	-32.647088	0.416415	7.183124
1676.002075	3.935476	1706.245864	-30.243789	0.412111	6.906994

1627.003606	3.826877	1653.787511	-26.783906	0.407718	6.633594
1578.014741	3.710861	1597.746685	-19.731943	0.402565	6.352529
1529.024113	3.594883	1541.724191	-12.700078	0.397910	6.084138
1431.046384	3.360998	1428.747314	2.299070	0.390595	5.589589
1333.069734	3.172108	1337.504695	-4.434962	0.393563	5.246471
1235.089555	2.962215	1236.117039	-1.027484	0.399524	4.934475
1137.101731	2.743054	1130.252505	6.849226	0.413676	4.703912
1039.116945	2.554077	1038.968350	0.148595	0.442248	4.595473
941.118242	2.342820	936.921971	4.196271	0.486619	4.579664
843.139827	2.146877	842.272629	0.867198	0.553446	4.666323
745.123188	1.938783	741.754240	3.368948	0.651995	4.858169
647.103020	1.740374	645.913790	1.189230	0.792226	5.126518
549.086381	1.532850	545.670511	3.415870	0.998672	5.483572
500.073406	1.437283	499.507236	0.566170	1.133871	5.670186
451.058372	1.336905	451.020188	0.038184	1.303406	5.879120
402.048337	1.238649	403.558265	-1.509928	1.516153	6.095670
353.033010	1.135234	353.604171	-0.571162	1.794362	6.334690
304.021113	1.034678	305.030905	-1.009792	2.163314	6.576931
255.009020	0.934020	256.408576	-1.399556	2.677605	6.828135
206.005258	0.832455	207.348429	-1.343171	3.441409	7.089483
156.996987	0.733303	159.453756	-2.456769	4.682537	7.351442
107.986952	0.628319	108.741471	-0.754519	7.070680	7.635411
58.977897	0.529357	60.938394	-1.960497	13.409473	7.908625
0.000000	0.410078	3.321469	-3.321469	Inf	NaN

COMMENTS:

The uncertainty is calculated with 95% confidence. The uncertainty includes the randomness in the calibrated instrument during the calibration, systematic uncertainty in the instrument or property which the instrument under calibration is compared with (dead weight manometer, calibrated weights etc.), and due to regression analysis to fit the calibration points to a linear calibration equation. The calculated uncertainty can be used as the total systematic uncertainty of the calibrated instrument with the given calibration equation.

Appendix H

Risk Assessment

The risk assessment was done with help from Bård Brandstø at the Waterpower Laboratory. This assessment is written in Norwegian and it should be noted that no incidents occurred during the performed measurements in the laboratory.



Risikovurderingsrapport

Francisrigg; Reversibel Pumpeturbin(RPT)

Prosjekttittel	Generell operasjon av Francis-riggen ved VKL
Prosjektleder	Torbjørn Nielsen
Enhet	NTNU
HMS-koordinator	Morten Grønli
Linjeleder	Olav Bolland
Riggnavn	Francis turbin/pumpeturbin-rigg ved VKL
Plassering	Vannkraftlab
Romnummer	42
Riggansvarlig	Bård Aslak Brandåstrø
Risikovurdering utført av	Bård Aslak Brandåstrø

INNHALDSFORTEGNELSE

1	INNLEDNING	1
2	ORGANISERING.....	1
3	RISIKOSTYRING AV PROSJEKTET	1
4	TEGNINGER, FOTO, BESKRIVELSER AV FORSØKSOPPSETT	1
5	EVAKUERING FRA FORSØKSOPPSETNINGEN.....	1
6	VARSLING.....	2
6.1	Før forsøkskjøring.....	2
6.2	Ved uønskede hendelser	2
7	VURDERING AV TEKNISK SIKKERHET	3
7.1	Fareidentifikasjon, HAZOP.....	3
7.2	Brannfarlig, reaksjonsfarlig og trykksatt stoff og gass	3
7.3	Trykkpåkjent utstyr	3
7.4	Påvirkning av ytre miljø (utslipp til luft/vann, støy, temperatur, rystelser, lukt)	4
7.5	Stråling.....	4
7.6	Bruk og behandling av kjemikalier	4
7.7	El sikkerhet (behov for å avvike fra gjeldende forskrifter og normer).....	4
8	VURDERING AV OPERASJONELL SIKKERHET.....	4
8.1	Prosedyre HAZOP	4
8.2	Drifts og nødstopps prosedyre.....	4
8.3	Opplæring av operatører.....	5
8.4	Tekniske modifikasjoner	5
8.5	Personlig verneutstyr	5
8.6	Generelt.....	5
8.7	Sikkerhetsutrustning	5
8.8	Spesielle tiltak.....	5
9	TALLFESTING AV RESTRISIKO – RISIKOMATRISSE	5
10	KONKLUSJON	5
11	LOVER FORSKRIFTER OG PÅLEGG SOM GJELDER	7
12	VEDLEGG.....	8
13	DOKUMENTASJON.....	9
14	VEILEDNING TIL RAPPORTMAL.....	10

1 INNLEDNING

Riggen står i hovedrommet til vannkraftlaboratoriet. Formålet med riggen er å gjøre modelltester på løpehjul av typen Francis eller pumpeturbin. Riggen har vært i bruk i lang tid. De aktuelle målingene skal kunne vise virkningsgradsdiagram og karakteristikker for turbiner.

2 ORGANISERING

Rolle	NTNU	Sintef
Lab Ansvarlig:	Morten Grønli	Harald Mæhlum
Linjeleder:	Olav Bolland	Mona J. Mølnvik
HMS ansvarlig:	Olav Bolland	Mona J. Mølnvik
HMS koordinator	Morten Grønli	Harald Mæhlum
HMS koordinator	Per Bjørnås	
Romansvarlig:	Bård Brandåstrø	
Prosjekt leder:	Torbjørn Nielsen	
Ansvarlig riggoperatører:	Bård Brandåstrø, Joar Grilstad, Ole dahlhaug	

3 RISIKOSTYRING AV PROSJEKTET

Hovedaktiviteter risikostyring	Nødvendige tiltak, dokumentasjon	DTG
Prosjekt initiering	Prosjekt initiering mal	
Veiledningsmøte	Skjema for Veiledningsmøte med pre-risikovurdering	X
Innledende risikovurdering	Fareidentifikasjon – HAZID Skjema grovanalyse	X
Vurdering av teknisk sikkerhet	Prosess-HAZOP Tekniske dokumentasjoner	X
Vurdering av operasjonell sikkerhet	Prosedyre-HAZOP Opplæringsplan for operatører	X
Sluttvurdering, kvalitetssikring	Uavhengig kontroll Utstedelse av apparaturkort Utstedelse av forsøk pågår kort	X

4 TEGNINGER, FOTO, BESKRIVELSER AV FORSØKSOPPSETT

Vedlegg:

Prosess og Instrumenterings Diagram, (PID)

Komponentliste med spesifikasjoner

Tegninger og bilder som beskriver forsøksoppsetningen.

5 EVAKUERING FRA FORSØKSOPPSETNINGEN

Se kapittel 14 "Veiledning til rapport mal.

Evakuering skjer på signal fra alarmklokker eller lokale gassalarmstasjon med egen lokal varsling med lyd og lys utenfor aktuelle rom, se 6.2

Evakuering fra rigg området foregår igjennom merkede nødutganger.

6 VARSLING

6.1 Før forsøkskjøring

Varsling per e-post, med opplysning om forsøkskjøringens varighet og involverte til:

- HMS koordinator NTNU/SINTEF
HaraldStein.S.Mahlum@sintef.no
Erik.langorgen@ntnu.no
Baard.brandaastro@ntnu.no
- *Prosjektledere på naborigger varsles for avklaring rundt bruk av avtrekksanlegget uten fare eller forstyrrelser av noen art, se rigg matrise.*

All forsøkskjøringen skal planlegges og legges inn i aktivitetskalender for lab. Forsøksleder må få bekreftelse på at forsøkene er klarert med øvrig labdrift før forsøk kan iverksettes.

6.2 Ved uønskede hendelser

BRANN

Ved brann en ikke selv er i stand til å slukke med rimelige lokalt tilgjengelige slukkemidler, skal nærmeste brannalarm utløses og arealet evakueres raskest mulig. En skal så være tilgjengelig for brannvesen/bygningsvaktmester for å påvise brannsted.

Om mulig varsles så:

NTNU	SINTEF
Labsjef Morten Grønli, tlf: 918 97 515	
HMS: Morten Grønli, tlf: 91897515	
Instituttleder: Olav Bolland: 91897209	

GASSALARM

Ved gassalarm skal gassflasker stenges umiddelbart og området ventileres. Klarer man ikke innen rimelig tid å få ned nivået på gasskonsentrasjonen så utløses brannalarm og laben evakueres. Dedikert personell og eller brannvesen sjekker så lekkasjested for å fastslå om det er mulig å tette lekkasje og lufte ut området på en forsvarlig måte.

Varslingsrekkefølge som i overstående punkt.

PERSONSKADE

- Førstehjelpsutstyr i Brann/førstehjelpsstasjoner,
- Rop på hjelp,
- Start livreddende førstehjelp
- **Ring 113** hvis det er eller det er tvil om det er alvorlig skade.

ANDRE UØNSKEDE HENDELSER (AVVIK)

NTNU:

Rapporteringsskjema for uønskede hendelser på

http://www.ntnu.no/hms/2007_Nettsider/HMSRV0401_avvik.doc

SINTEF:

Synergi

7 VURDERING AV TEKNISK SIKKERHET

7.1 Fareidentifikasjon, HAZOP

Se kapittel 14 "Veiledning til rapport mal.

Forsøksoppsetningen deles inn i følgende noder:

Node 1	Rørsystem med pumpe
Node 2	Roterende turbin
Node 3	Hydraulikkanlegg
Node 4	Energidreper

Vedlegg, skjema: Hazop_mal

Vurdering:

Node1:

-Overtrykksventil som slår ut dersom trykket i systemet blir for høyt.

-Rørelementer er eksternt levert og godkjent for aktuelt trykk.

Node2:

-Roterende utstyr står utilgjengelig for folk. Dvs det er innkapslet eller man må klatre for å nå opp til det.

Node3:

-Trykk i slanger og rør(olje vann) Hydraulikkslanger er ikke egenprodusert

-Trykksatt utstyr er sertifisert og kjøpt inn av eksterne leverandører

Node4:

-Fare for støy.

7.2 Brannfarlig, reaksjonsfarlig og trykksatt stoff og gass

Se kapittel 14 "Veiledning til rapport mal.

Inneholder forsøkene brannfarlig, reaksjonsfarlig og trykksatt stoff

Ja	Trykksatt hydraulikkolje, trykksatt vann
----	--

Vedlegg Ex-sonkart:

Vurdering: Arbeidsmedium er vann. Alle rør er levert av eksternt firma med prøvesertifikat

Hydraulikk til hydrostatisk lager. Hylleware komponenter, de er dermed ikke egenprodusert.

7.3 Trykkpåkjent utstyr

Inneholder forsøksoppsetningen trykkpåkjent utstyr:

JA	Utstyret trykktestes i henhold til norm og dokumenteres
----	---

Trykkutsatt utstyr skal trykktestes med driftstrykk gange faktor 1.4, for utstyr som har usertifiserte sveiser er faktoren 1.8. Trykktesten skal dokumenteres skriftlig hvor fremgangsmåte framgår.

Vedlegg: Prøvesertifikat for trykktesting finnes i Lab.perm.

Vurdering:

7.4 Påvirkning av ytre miljø (utslipp til luft/vann, støy, temperatur, rystelser, lukt)

Se kapittel 14 "Veiledning til rapport mal..

NEI	
------------	--

Vurdering: Det blir ingen utslipp til ytre miljø.

7.5 Stråling

Se kapittel 14 "Veiledning til rapport mal.

NEI	
------------	--

Vedlegg:

Vurdering: Ingen strålekilder.

7.6 Bruk og behandling av kjemikalier

Se kapittel 14 "Veiledning til rapport mal.

Ja	
-----------	--

Vedlegg:

Vurdering: Hydraulikkolje, mineralsk olje. Datablad er vedlagt

7.7 El sikkerhet (behov for å avvike fra gjeldende forskrifter og normer)

NEI	
------------	--

Her forstås montasje og bruk i forhold til normer og forskrifter med tanke på berøringsfare

Vedlegg:

Vurdering: Alt elektrisk utstyr er forsvarlig montert og står slik permanent.

8 VURDERING AV OPERASJONELL SIKKERHET

Sikrer at etablerte prosedyrer dekker alle identifiserte risikoforhold som må håndteres gjennom operasjonelle barrierer og at operatører og teknisk utførende har tilstrekkelig kompetanse.

8.1 Prosedyre HAZOP

Se kapittel 14 "Veiledning til rapport mal.

Metoden er en undersøkelse av operasjonsprosedyrer, og identifiserer årsaker og farekilder for operasjonelle problemer.

Vedlegg: HAZOP_MAL_Pro prosedyre

Vurdering: Operatør har et eget rom for å kjøre riggen.

8.2 Drifts og nødstopps prosedyre

Se kapittel 14 "Veiledning til rapport mal.

Nødstopp koordineres med labpersonell, for å unngå at man må ta en omvei via labben for nødstopp ved evakuering.

Vedlegg "Procedure for running experiments"

8.3 Opplæring av operatører

Dokument som viser Opplæringsplan for operatører utarbeides for alle forøksoppsetninger.

- *Kjøring av pumpesystem.*

Vedlegg: Opplæringsplan for operatører

8.4 Tekniske modifikasjoner

Vurdering: Modifikasjoner gjøres i samråd med Torbjørn Nielsen/Bård Brandåstrø

8.5 Personlig verneutstyr

- *Det er påbudt med vernebriller i sonen anlegget er plassert i.*

Vurdering: Vernebriller viktig, pga vann og hydraulikkolje under trykk.

8.6 Generelt

Vurdering: Alle forsøk kjøres med operatør til stede.

8.7 Sikkerhetsutrustning

- *Vernebriller*

8.8 Spesielle tiltak

9 TALLFESTING AV RESTRISIKO – RISIKOMATRISJE

Se kapittel 14 "Veiledning til rapportmal.

Risikomatrissen vil gi en visualisering og en samlet oversikt over aktivitetens risikoforhold slik at ledelse og brukere får et mest mulig komplett bilde av risikoforhold.

IDnr	Aktivitet-hendelse	Frekv-Sans	Kons	RV
1	<i>Lekkasje i Hydraulikk,</i>	1	A	A1
2	<i>Fremmedlegemer i vannet</i>	1	A	A1
3	<i>Rørbrudd</i>	1	A	A1
4	<i>Roterende Aksling</i>	1	B	B1

Vurdering restrisiko: *Det er liten restrisiko ved forsøkene, foruten at trykksatt vann og olje fordrer bruk av vernebriller. Fremmedlegemer i vannet gir liten risiko for personskade, men kan føre til store skader på maskineri.*

10 KONKLUSJON

Riggen er bygget til god laboratorium praksis (GLP).

Hvilke tekniske endringer eller endringer av driftsparametere vil kreve ny risikovurdering: Ingen

Apparaturkortet får en gyldighet på **4 måneder**
Forsøk pågår kort får en gyldighet på **4 måneder**

11 LOVER FORSKRIFTER OG PÅLEGG SOM GJELDER

Se <http://www.arbeidstilsynet.no/regelverk/index.html>

- Lov om tilsyn med elektriske anlegg og elektrisk utstyr (1929)
- Arbeidsmiljøloven
- Forskrift om systematisk helse-, miljø- og sikkerhetsarbeid (HMS Internkontrollforskrift)
- Forskrift om sikkerhet ved arbeid og drift av elektriske anlegg (FSE 2006)
- Forskrift om elektriske forsyningsanlegg (FEF 2006)
- Forskrift om utstyr og sikkerhetssystem til bruk i eksplosjonsfarlig område NEK 420
- Forskrift om håndtering av brannfarlig, reaksjonsfarlig og trykksatt stoff samt utstyr og anlegg som benyttes ved håndteringen
- Forskrift om Håndtering av eksplosjonsfarlig stoff
- Forskrift om bruk av arbeidsutstyr.
- Forskrift om Arbeidsplasser og arbeidslokaler
- Forskrift om Bruk av personlig verneutstyr på arbeidsplassen
- Forskrift om Helse og sikkerhet i eksplosjonsfarlige atmosfærer
- Forskrift om Høytrykksspyling
- Forskrift om Maskiner
- Forskrift om Sikkerhetsskilting og signalgivning på arbeidsplassen
- Forskrift om Stillaser, stiger og arbeid på tak m.m.
- Forskrift om Sveising, termisk skjæring, termisk sprøyting, kullbuemeisling, lodding og sliping (varmt arbeid)
- Forskrift om Tekniske innretninger
- Forskrift om Tungt og ensformig arbeid
- Forskrift om Vern mot eksponering for kjemikalier på arbeidsplassen (Kjemikalieforskriften)
- Forskrift om Vern mot kunstig optisk stråling på arbeidsplassen
- Forskrift om Vern mot mekaniske vibrasjoner
- Forskrift om Vern mot støy på arbeidsplassen

Veiledninger fra arbeidstilsynet

se: <http://www.arbeidstilsynet.no/regelverk/veiledninger.html>

12 VEDLEGG

13 DOKUMENTASJON

- Tegninger, foto, beskrivelser av forsøksoppsetningen
- Hazop_mal
- Sertifikat for trykkpåkjent utstyr
- Håndtering avfall i NTNU
- Sikker bruk av LASERE, retningslinje
- HAZOP_MAL_Prosedyre
- Forsøksprosedyre
- Opplæringsplan for operatører
- Skjema for sikker jobb analyse, (SJA)
- Apparatorkortet
- Forsøk pågår kort

14 VEILEDNING TIL RAPPORTMAL

Kap 5 Evakuering fra forsøksoppsetningen

Beskriv i hvilken tilstand riggen skal forlates ved en evakuerings situasjon.

Kap 7 Vurdering av teknisk sikkerhet

Sikre at design av apparatur er optimalisert i forhold til teknisk sikkerhet.

Identifisere risikoforhold knyttet til valgt design, og eventuelt å initiere re-design for å sikre at størst mulig andel av risiko elimineres gjennom teknisk sikkerhet.

Punktene skal beskrive hva forsøksoppsetningen faktisk er i stand til å tåle og aksept for utslipp.

7.1 Fareidentifikasjon, HAZOP

Forsøksoppsetningen deles inn i noder: (eks *Motorenhhet, pumpeenhet, turbinenhet.*)

Ved hjelp av ledeord identifiseres årsak, konsekvens og sikkerhetstiltak. Konkluderes det med at tiltak er nødvendig anbefales disse på bakgrunn av dette. Tiltakene lukkes når de er utført og Hazop sluttføres.

(eks "No flow", årsak: rør er deformert, konsekvens: pumpe går varm, sikkerhetsforanstaltning: måling av flow med kobling opp mot nødstoppe eller hvis konsekvensen ikke er kritisk benyttes manuell overvåkning og punktet legges inn i den operasjonelle prosedyren.)

7.2 Brannfarlig, reaksjonsfarlig og trykksatt stoff.

I henhold til Forskrift om håndtering av brannfarlig, reaksjonsfarlig og trykksatt stoff samt utstyr og anlegg som benyttes ved håndteringen

Brannfarlig stoff: Fast, flytende eller gassformig stoff, stoffblanding, samt stoff som forekommer i kombinasjoner av slike tilstander, som i kraft av sitt flammepunkt, kontakt med andre stoffer, trykk, temperatur eller andre kjemiske egenskaper representerer en fare for brann.

Reaksjonsfarlig stoff: Fast, flytende, eller gassformig stoff, stoffblanding, samt stoff som forekommer i kombinasjoner av slike tilstander, som ved kontakt med vann, ved sitt trykk, temperatur eller andre kjemiske forhold, representerer en fare for farlig reaksjon, eksplosjon eller utslipp av farlig gass, damp, støv eller tåke.

Trykksatt stoff: Annet fast, flytende eller gassformig stoff eller stoffblanding enn brann- eller reaksjonsfarlig stoff, som er under trykk, og som derved kan representere en fare ved ukontrollert utslipp.

Nærmere kriterier for klassifisering av brannfarlig, reaksjonsfarlig og trykksatt stoff er fastsatt i vedlegg 1 i veiledningen til forskriften "Brannfarlig, reaksjonsfarlig og trykksatt stoff"

<http://www.dsb.no/Global/Publikasjoner/2009/Veiledning/Generell%20veiledning.pdf>

http://www.dsb.no/Global/Publikasjoner/2010/Tema/Temaveiledning_bruk_av_farlig_stoff_Del_1.pdf

Rigg og areal skal gjennomgås med hensyn på vurdering av Ex sone

- Sone 0: Alltid eksplosiv atmosfære, for eksempel inne i tanker med gass, brennbar væske.
- Sone 1: Primær sone, tidvis eksplosiv atmosfære for eksempel et fyllerapparat
- Sone 2: Sekundært utslippssted, kan få eksplosiv atmosfære ved uhell, for eksempel ved flenser, ventiler og koblingspunkt

7.4 Påvirkning av ytre miljø

Med forurensning forstås: tilførsel av fast stoff, væske eller gass til luft, vann eller i grunnen støy og rystelser påvirkning av temperaturen som er eller kan være til skade eller ulempe for miljøet.

Regelverk: <http://www.lovdatabasen.no/all/hl-19810313-006.html#6>

NTNU retningslinjer for avfall se: <http://www.ntnu.no/hms/retningslinjer/HMSR18B.pdf>

7.5 Stråling

Stråling defineres som

Ioniserende stråling: Elektromagnetisk stråling (i strålevernsammenheng med bølgelengde <100 nm) eller hurtige atomære partikler (f.eks alfa- og beta-partikler) som har evne til å ionisere atomer eller molekyler
Ikke-ioniserende stråling: Elektromagnetisk stråling (bølgelengde >100 nm), og ultralyd ¹ , som har liten eller ingen evne til å ionisere.
Strålekilder: Alle ioniserende og sterke ikke-ioniserende strålekilder.
Ioniserende strålekilder: Kilder som avgir ioniserende stråling, f.eks alle typer radioaktive kilder, røntgenapparater, elektronmikroskop
Sterke ikke-ioniserende strålekilder: Kilder som avgir sterk ikke-ioniserende stråling som kan skade helse og/eller ytre miljø, f.eks laser klasse 3B og 4, MR2-systemer, UVC3-kilder, kraftige IR-kilder ⁴
¹ Ultralyd er akustisk stråling ("lyd") over det hørbare frekvensområdet (>20 kHz). I strålevernforskriften er ultralyd omtalt sammen med elektromagnetisk ikke-ioniserende stråling. ² MR (eg. NMR) - kjernemagnetisk resonans, metode som nyttes til å «avbilde» indre strukturer i ulike materialer. ³ UVC er elektromagnetisk stråling i bølgelengdeområdet 100-280 nm. ⁴ IR er elektromagnetisk stråling i bølgelengdeområdet 700 nm – 1 mm.

For hver laser skal det finnes en informasjonsperm(HMSRV3404B) som skal inneholde:

- Generell informasjon
- Navn på instrumentansvarlig og stedfortreder, og lokal strålevernskoordinator
- Sentrale data om apparaturen
- Instrumentspesifikk dokumentasjon
- Referanser til (evt kopier av) datablader, strålevernbestemmelser, o.l.
- Vurderinger av risikomomenter
- Instruks for brukere
- Instruks for praktisk bruk; oppstart, drift, avstenging, sikkerhetsforholdsregler, loggføring, avlåsning, evt. bruk av strålingsmåler, osv.
- Nødprosedyrer

Se ellers retningslinjen til NTNU for laser: <http://www.ntnu.no/hms/retningslinjer/HMSR34B.pdf>

7.6 Bruk og behandling av kjemikalier.

Her forstås kjemikalier som grunnstoff som kan utgjøre en fare for arbeidstakers sikkerhet og helse.

Se ellers: <http://www.lovdatabasen.no/cgi-wifit/ldles?doc=/sf/sf/sf-20010430-0443.html>

Sikkerhetsdatablar skal være i forøkenes HMS perm og kjemikaliene registrert i Stoffkartoteket.

Kap 8 Vurdering av operasjonell sikkerhet

Sikrer at etablerte prosedyrer dekker alle identifiserte risikoforhold som må håndteres gjennom operasjonelle barrierer og at operatører og teknisk utførende har tilstrekkelig kompetanse.

8.1 Prosedyre Hazop

Prosedyre-HAZOP gjennomføres som en systematisk gjennomgang av den aktuelle prosedyren ved hjelp av fastlagt HAZOP-metodikk og definerte ledeord. Prosedyren brytes ned i enkeltstående arbeidsoperasjoner (noder) og analyseres ved hjelp av ledeordene for å avdekke mulige avvik, uklarheter eller kilder til mangelfull gjennomføring og feil.

8.2 Drifts og nødstopps prosedyrer

Utarbeides for alle forsøksoppsetninger.

Driftsprosedyren skal stegvis beskrive gjennomføringen av et forsøk, inndelt i oppstart, under drift og avslutning. Prosedyren skal beskrive forutsetninger og tilstand for start, driftsparametere med hvor store avvik som tillates før forsøket avbrytes og hvilken tilstand riggen skal forlates.

Nødstopps-prosedyre beskriver hvordan en nødstopps skal skje, (utført av uinnvidde), hva som skjer, (strøm/gass tilførsel) og hvilke hendelser som skal aktivere nødstopps, (brannalarm, lekkasje).

Kap 9 Risikomatrixe

9 Tallfesting av restrisiko, Risikomatriksen

For å synliggjøre samlet risiko, jevnfør skjema for risikovurdering, plottes hver enkelt aktivitets verdi for sannsynlighet og konsekvens inn i risikomatriksen. Bruk aktivitetens IDnr.

Eksempel: Hvis aktivitet med IDnr. 1 har fått en risikoverdi D3 (sannsynlighet 3 x konsekvens D) settes aktivitetens IDnr i risikomatriksens felt for 3D. Slik settes alle aktivitetenes risikoverdier (IDnr) inn i risikomatriksen.

I risikomatriksen er ulike grader av risiko merket med rød, gul eller grønn. Når en aktivitets risiko havner på rød (= uakseptabel risiko), skal risikoreduserende tiltak gjennomføres. Ny vurdering gjennomføres etter at tiltak er iverksatt for å se om risikoverdien er kommet ned på akseptabelt nivå.

KONSEKVENNS	Svært alvorlig	E1	E2	E3	E4	E5
	Alvorlig	D1	D2	D3	D4	D5
	Moderat	C1	C2	C3	C4	C5
	Liten	B1	B2	B3	B4	B5
	Svært liten	A1	A2	A3	A4	A5
		Svært liten	Liten	Middels	Stor	Svært Stor
SANSYNLIGHET						

Prinsipp over akseptkriterium. Forklaring av fargene som er brukt i risikomatriksen.

Farge	Beskrivelse
Rød	Uakseptabel risiko. Tiltak skal gjennomføres for å redusere risikoen.
Gul	Vurderingsområde. Tiltak skal vurderes.
Grønn	Akseptabel risiko. Tiltak kan vurderes ut fra andre hensyn.

